MINISTRY OF EDUCATION, RESEARCH, YOUTH AND SPORT

THE ANNALS OF "DUNAREA DE JOS" UNIVERSITY OF GALATI

Fascicle IX
METALLURGY AND MATERIALS SCIENCE

YEAR XXIX (XXXIV),
June 2011, no. 2

ISSN 1453-083X

2011
GALATI UNIVERSITY PRESS

EDITORIAL BOARD

PRESIDENT OF HONOUR

Prof. Olga MITOSERIU - ''Dunarea de Jos'' University of Galati, Romania

EDITOR-IN-CHIEF

Prof. Nicolae CANANAU - ''Dunarea de Jos'' University of Galati, Romania

EXECUTIVE EDITOR

Prof. Marian BORDEI - ''Dunarea de Jos'' University of Galati, Romania

SCIENTIFIC ADVISORY COMMITTEE

Prof. Lidia BENEA – ''Dunarea de Jos'' University of Galati, Romania
Acad. Prof. Ion BOSTAN - Technical University of Moldova, Moldova Republic
Prof. Francisco Manuel BRAZ FERNANDES - New University of Lisbon Caparica, Portugal
Acad. Prof. Valeriu CANTSER - Academy of Moldova Republic, Moldova Republic
Prof. Jean Pierre CELIS - Katholieke Universiteit Leuven, Belgium
Prof. Anisoara CIOCAN - ''Dunarea de Jos'' University of Galati, Romania
Prof. Alexandru CHIRIAC - ''Dunarea de Jos'' University of Galati, Romania
Assoc. Prof. Stela CONSTANTINESCU - ''Dunarea de Jos'' University of Galati, Romania
Prof. Elena DRUGESCU - ''Dunarea de Jos'' University of Galati, Romania
Prof. Valeriu DULGHERU - Technical University of Moldova, Moldova Republic
Prof. Jean Bernard GUILLOT – École Centrale Paris, France
Assoc. Prof. Gheorghe GURAU - ''Dunarea de Jos'' University of Galati, Romania
Prof. Iulian IONITA – ''Gheorghe Asachi'' Technical University Iasi, Romania
Prof. Philippe MARCUS - École Nationale Supérieure de Chimie de Paris, France
Prof. Vasile MARINA - Technical University of Moldova, Moldova Republic
Prof. Rodrigo MARTINS–NOVA University of Lisbon, Portugal
Prof. Strul MOISA - Ben Gurion University of the Negev, Israel
Prof. Daniel MUNTEANU - Transilvania University of Brasov, Romania
Prof. Viorel MUNTEANU - ''Dunarea de Jos'' University of Galati, Romania
Prof. Viorica MUSAT - ''Dunarea de Jos'' University of Galati, Romania
Prof. Maria NICOLAE - Politehnica University Bucuresti, Romania
Prof. Petre Stelian NITA - ''Dunarea de Jos'' University of Galati, Romania
Prof. Pierre PONTHIAUX – École Centrale Paris, France
Prof. Florentina POTECASU - ''Dunarea de Jos'' University of Galati, Romania
Assoc. Prof. Octavian POTECASU - ''Dunarea de Jos'' University of Galati, Romania
Prof. Cristian PREDESCU - Politehnica University Bucuresti, Romania
Prof. Iulian RIPOSAN - Politehnica University Bucuresti, Romania
Prof. Rami SABAN - Politehnica University Bucuresti, Romania
Prof. Antonio de SAJA - University of Valladolid, Spain
Prof. Wolfgang SAND - Duisburg-Essen University Duisburg Germany
Prof. Ion SANDU – ''Al. I. Cuza'' University of Iasi
Prof. Georgios SAVAIDIS - Aristotle University of Thessaloniki, Greece
Prof. Ioan VIDA-SIMITI - Technical University of Cluj Napoca, Romania
Prof. Mircea Horia TIEREAN - Transilvania University of Brasov, Romania
Assoc. Prof. Petrica VIZUREANU – ''Gheorghe Asachi'' Technical University Iasi, Romania
Prof. Maria VLAD - ''Dunarea de Jos'' University of Galati, Romania
Prof. François WENGER – École Centrale Paris, France

THE ANNALS OF "DUNAREA DE JOS" UNIVERSITY OF GALATI.
FASCICLE IX. METALLURGY AND MATERIALS SCIENCE
N^0. 2 – 2011, ISSN 1453 – 083X

Table of Content

THE ANNALS OF "DUNAREA DE JOS" UNIVERSITY OF GALATI.
FASCICLE IX. METALLURGY AND MATERIALS SCIENCE
N^0. 2 – 2011, ISSN 1453 – 083X

VERSATILITY OF NICKEL-ALUMINIUM BRONZES AS WEAR RESISTING MATERIALS

Anisoara CIOCAN
„Dunarea de Jos" University of Galati
email: aciocan@ugal.ro

ABSTRACT

The paper presents the results of experimental research regarding the establishing of some chemical positions of the nickel-aluminium bronzes used as monoblock and bimetallic bearings. The areas of the applications are discussed with reference to the working property required of these alloys. Normally a combination of several properties finally governs the selection of a particular material. The correlations between chemical compositions, structures and properties are analysed with a view to selecting the material for certain application. The wear resistance and the corrosion behavior into seawater of the nickel-aluminium bronzes with variable content of iron and manganese are studied.

KEYWORDS: nickel-aluminum bronzes, alloying elements, bimetal, wear applications, seawater corrosion

1. Introduction

The nickel-aluminum bronzes comprise a wide range of compositions by alloying with some specifically chosen elements (iron and manganese). Consequently there is a family of copper-based alloys with complex metallurgical structures that offer a combination of mechanical and chemical properties unmatched by any other alloy series.

This feature often makes nickel-aluminum bronzes the first choice (and sometimes the only logical choice) for applications. These attributes are: excellent strength, similar to that of low alloy steels; excellent corrosion resistance, especially in seawater and similar environments, where the alloys often outperform many stainless steels; favorable high temperature properties, for short or long term usage; good resistance to fatigue, ensuring a long service life; good resistance to creep, making the alloys useful at elevated temperatures; oxidation resistance, for exposure at elevated temperatures and in oxidizing environments; ease of casting and fabrication, when compared to many materials used for similar purposes; high hardness and wear resistance, providing excellent bearing properties in arduous applications; ductility, which, like that for all copper alloys, is not diminished at low temperatures; good weldability, making fabrication economical; readily machined, when compared with other high-duty alloys; low magnetic susceptibility, useful for many special applications; ready availability in cast or wrought forms [1, 2, 3].

The nickel-aluminum bronzes can be considered a versatile material. By selecting the elements content and their controlled added it can modify the properties. This is easier as than redesigning parts and modification of their fabrication technology. But for this it is necessary to correct knowledge of the working conditions for demanding applications. This is the most important criterion to follow when making a good material selection. This paper presents the results of several experimental studies for an optimum selection of the composition, the thermal treatment and the manufacturing method of the nickel-aluminium bronzes alloyed with iron and manganese, used as wear resisting materials. For each industrial application the material selection was based on the requirements for working conditions: friction conditions, forces and pressures, lubrication, corrosion conditions etc.

2. Constitution of nickel-aluminium bronze alloys and its influence on the properties

The nickel-aluminium copper alloys are a range of copper-based alloys in which aluminium is the primary alloying element (up to 14-15%). For obtaining the aluminium bronzes with excellent properties especially for marine applications the

addition of nickel is important. Besides Ni and Al, the main alloying elements of the bronzes analysed include Mn and Fe that could also be added into nickel-aluminium bronzes to improve their properties. The content of each element added has an important influence on the structure and, as a result, on the properties [4, 5].

The microstructure of these bronzes is quite complicated, not only because of its multiple alloying elements, but also because several phase transformations could take place during their preparation (Figure 1)

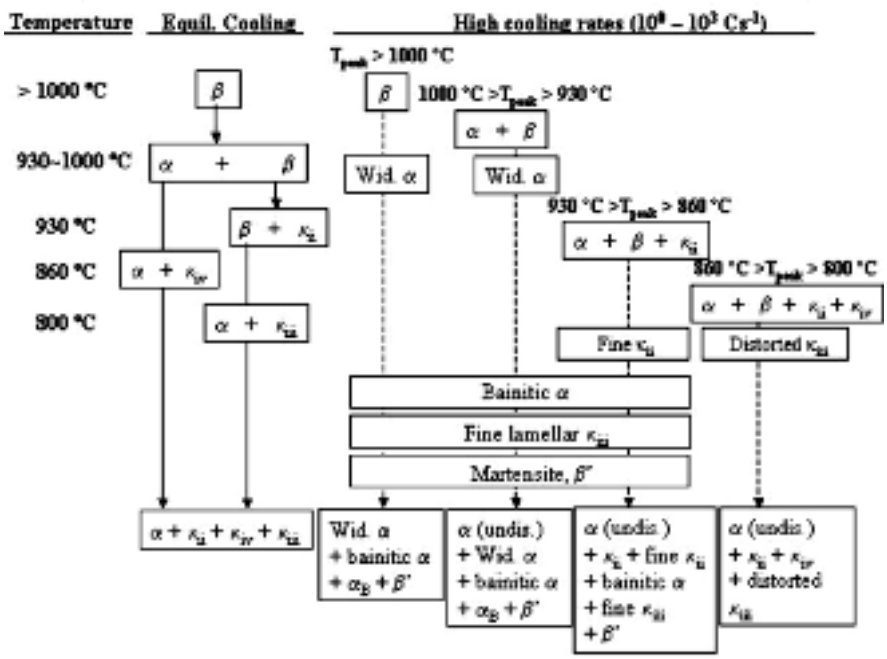

Fig. 1. *Transformation products of nickel-aluminium bronzes during cooling [6].*

Binary Cu-Al alloys (Figure 2a) containing less than 9.4 wt. % Al are single phase α alloys. The solidification commences with the formation of α dendrites.

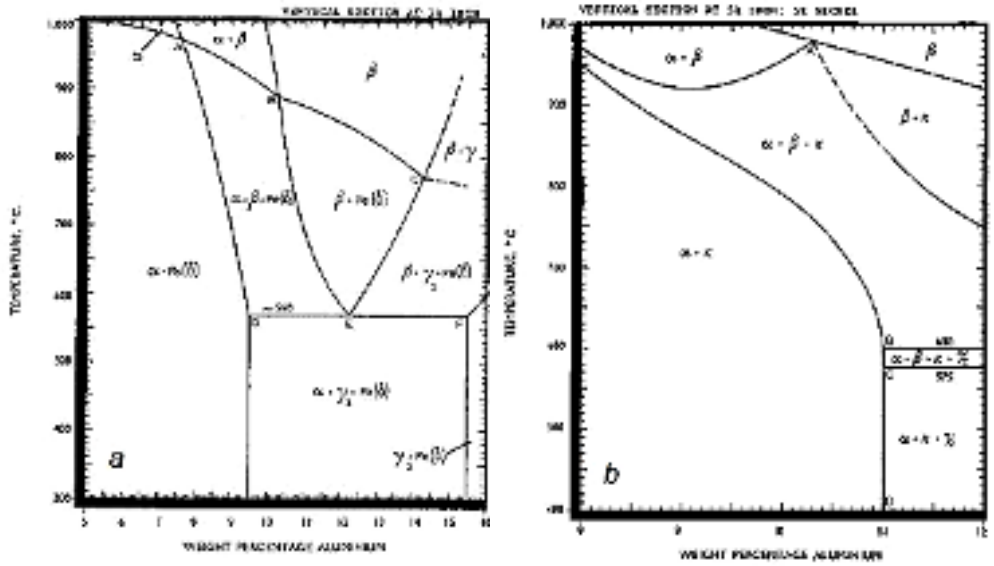

Fig. 2. *Equilibrium diagram of Cu-Al system (a) and a cross section of CuAlFeNiMn diagram at 5% Fe and 5%Ni (b). [2]*

The freezing range is short and so segregation is not pronounced and the alloy solidifies as a single phase.

Copper-aluminum alloys containing more that 9.4 wt. % Al solidify as a single-phase bcc β; under slow-cooling conditions, fcc α gradually forms from the β until the remaining β transforms to α + γ in a eutectoid reaction at about 570ºC. The γ phase corrodes preferentially due to its high Al content and its presence is thus deleterious.

Even greater strength and hardness is developed in alloys containing more than 10% Al. Such alloys are favored for specialized applications that require superior wear resistance. Other alloying elements also modify the structure and thereby increase strength and corrosion resistance: iron improves tensile strength and acts as a grain refiner; nickel improves yield stress and corrosion resistance and has a beneficial stabilizing effect on the metallurgical structure; manganese also performs a stabilizing function [7].

The addition of nickel and iron to copper-aluminum alloys extends the α phase field while effectively suppressing γ phase formation (Figure 2b) [2].

The mechanical properties of aluminum bronze depend primarily on the aluminum content and also on the varying proportions of secondary additions. The Ni and Fe additions have been found to considerably increase the mechanical properties of aluminium bronzes (especially give higher strength) through the formation, from both the α and the β, of complex intermetallic κ phases [8].

The alloy remains fully β upon cooling to about 1000ºC. Below this temperature α phase precipitates from the β with Widmanstätten morphology, followed by the nucleation of globular κ, which is nominally Fe_3Al, in the β. This phase is apparent in the micrograph of the cast alloy (Figure 3) and is often termed κ_{ii}. In Cu-Al-Ni-Fe alloys containing ≥ 5 wt. % Fe, an Fe_3Al phase forms with a dendrite morphology, which is usually termed κ_i. At about 850ºC, the solubility of Fe in the α is exceeded and fine κ precipitates begin to form; these fine precipitates are also nominally Fe_3Al and are usually termed κ_{iv}. Finally, at about 580ºC, a nickel-rich κ phase, κ_{iii}, forms from β. The α phase is an fcc equilibrium terminal solid solution with a lattice parameter a = 3.64 a eutectoid reaction giving lamellar α + κ. Proeutectoid κ may exhibit a globular morphology. The α phase is an fcc equilibrium terminal solid solution with a lattice parameter a = 3.64Å [15]. The Fe_3Al phases (κ_i, κ_{ii} and κ_{iv}) have a DO_3 structure; the lattice parameter of κ_{ii} is 5.71Å while that of κ_{iv} is 5.77Å. The NiAl (κ_{iii}) phase exhibits a B_2 structure with a lattice parameter of 2.88 Å. Thus, fully ordered Fe_3Al (κ_i, κ_{ii} and κ_{iv}) and NiAl (κ_{iii}) phases will have inter-atom spacing that differ by less than one percent.

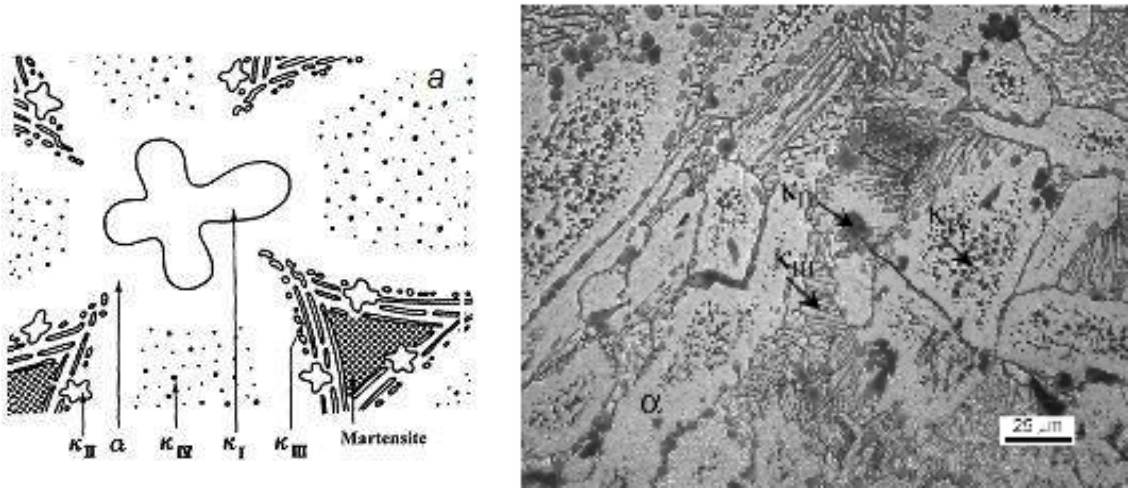

Fig.3. *Microstructure of NAB specimens: a) schematic representation; b) optical micrograph of as-cast aluminium bronze (etched with ferric chloride and hydrochloric acid in ethanol) [8, 9].*

Iron acts as a grain refiner both during solidification and during slow cooling, and increases resistance and hardness: every Fe percentage in a bronze with aluminium leads to an increase of the mechanical resistance of the alloys with 2.8 daN/mm^2. The addition of nickel increases the mechanical characteristics, the antifriction and anticorrosion properties.

The nickel addition also increases compactness and high temperature resistance. The manganese increases resistance, plasticity and antifriction properties, but significantly decreases fluidity. In comparison with iron, manganese behaves as a stabilizer. It is dissolved in the solid solution and it doesn't provoke structural changes [8, 10].

3. Experimental research and industrial applications

In cast and wrought forms the literature recommends the nickel-aluminum bronzes for their excellent wear resistance. Metal-sprayed or welded overlay deposits of aluminum bronze on steel also provide effective wear-resistant surfaces. As a result these alloys can be used as bearing materials. They thrive on heavy loads, shocks and harsh working environments. In rotating applications, best results are usually achieved when running aluminum bronzes against hardened surfaces. When lubrication of sliding surfaces is less than ideal, aluminum bronzes are superior to ferrous materials [7, 11].

The research summarized in this paper were focused on the establishing of the optimum compositions of the bronzes as wear resisting materials for monoblock and bimetallic parts.

These were tested as bearing at the following industrial applications: steel mill, presses in rubber industry, manufacturing of the ferrites, offshore drilling equipments, and the parts for machine - building industry. Also the corrosion behaviour into marine media for the bimetals was analysed.

The experiments were based on the correlations between the chemical composition, structure, properties and manufacturing methods in accordance with a thorough knowledge of the working conditions for each application.

The conventional materials that were used to cast the steel mill bearings studied (Figure 4a) are tin bronzes (10 - 14 %Sn sometimes with Pb additions) [12, 13]. For their substitution a copper alloy of around 6% - 10% of aluminium with addition of nickel, iron and manganese was tested. After experimental study the following ranges of chemical compositions were tested for this application: 6.5 - 7.5 %Al; 1-1.5 %Ni, 1-1.5 %Fe%; 1 - 1.5 %Mn, Cu balance.

These ensure an optimum structure in accordance with required mechanical properties and specific working conditions (wear conditions and lubrication, forces, specific pressure, environmental media etc.). There are single phase α alloys. The solid solution α is the soft base and it ensures the plasticity of the mill bearing. The other alloying elements involved the development of the complex intermetallic κ phases.

These are incorporated and uniformly distributed as hard compounds in the soft base (solid solution α). A like structure ensures the properties for a good behavior in practical applications. Figure 4b show the microstructure of the aluminium bronze with 7.2 %Al, 1.2 %Ni, 1.2 %Fe, 1.32 %Mn, and Cu balance.

A crucible graphite furnace was used to make the alloy. Argon was blown into the melting bath to produce degasification: 0.2 Nm^3 at 0.3 – 0.5 daN/cm^2. Also charcoal as protective flux and respectively phosphor copper as deoxidizer were used. The alloy was casted at maximum 1150 ^{0}C [14, 15].

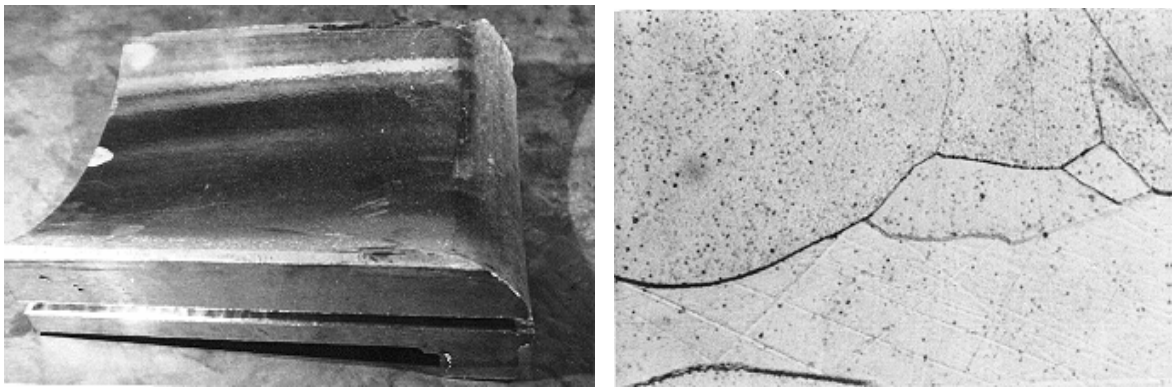

a. b.

Fig. 4. *Mill bearing (400x600mm) (a) and optical micrograph of aluminium bronze alloyed with nickel, iron and manganese (b)*

The rubber industry is other industrial domain whe the utilization of the nickel-aluminium bronzes as wear resisting material was studied. The castings which were assembled into presses for tire vulcanization are exposed at clamping forces variable into range of 200-546x10^3 daN.

The composition of the experimental material is given in table 1 [16].

Table 1. *Composition (wt. %) of experimental bronzes for the rubber industry*

Al	Ni	Fe	Mn	Sn	Pb	Cu
7.90	2.50	5.84	1.50	-	-	bal.
5.58	1.30	4.60	1.50	-	-	bal.
10.00	1.20	5.24	2.10	-	-	bal.
8.85	4.00	5.6	1.5	-	-	bal.

The castings were heat-treated through annealing. The following parameters were recommended: heating rate ≤80^{0}C/h; tempering temperature 600^{0}C, treatment time 5 minute/mm; cooling in air. This treatment controls the coarseness of the κ precipitates and improves the mechanical properties.

For machine - building industry systems aboard ships and offshore platforms the unstandardized aluminium bronzes were casted as bars with diameters from 70 to 600 mm and machine worked to obtain parts used as bushings or bearings.

In other applications the nickel-aluminium bronzes were used to obtain bimetals because, most often than not, a single material cannot satisfy all of the working requirements in special conditions. For these applications the bimetals are recommended because they satisfy working conditions impossible for a single metallic material. In the cases analyzed the bimetals were obtained by deposition of bronze layers on steel support by a welding process. The high resistance to corrosion of the aluminium bronzes with nickel, manganese and iron, combined with their ability to carry heavy loads under friction conditions without excessive wear, makes them suitable for antifriction layers deposited on steel for bearings constructions.

This paper presents the results of the experimental research carried out to establish the corresponding chemical composition of the bronze and the cladding technology in accordance with a specific industrial application.

The first experimental bimetal obtained was subjected to high contact pressures. The parts named PATINA TPA 45 and CAMA 45 were components that were used into ferrites presses [17], characterized by a high hardness necessary for special working conditions: a good wear resistance at a specific contact pressure of min. 200 daN/mm^2 and a working speed of 60 m/min, high corrosion and abrasion resistance, a minimum wear loss at the end of the working time. Bronzes with variable compositions (Table 2) were deposed as multilayers on steel support (C≤0.25%). These are casted as bars with diameters of 4mm.

Table 2. *Bronzes with variable compositions and their adequate hardness*

Samples	Chemical composition (%wt)					Hardness (HB)
	Al	Ni	Fe	Mn	Cu	
1	7.8	-	3.5	-	bal.	178
2	9.5	4.5	4.6	0.8	bal.	214
3	10.6	3.7	4.2	0.9	bal.	230
4	11.2	4.6	4.8	1.0	bal.	275
5	14.7	4.1	4.4	1.1	bal.	338

Argon shielded arc welding (WIG welding) with the following parameters was the method applied: 20-30l/min for the inert gas flow; 200-250A for the welding current. It is seldom necessary to preheat the steel samples to higher than 150-200°C. Excessive preheat can lead to the heat-affected zone being excessive, with a greater volume of metal at risk of hot cracking and distortion problems. [7, 18].

In accordance with the properties required by the working conditions the following composition range was recommended: 11-12%Al, 4-5%Ni, 4-5%Fe, 0.8-1.2%Mn, Cu balance. In other applications the nickel-aluminium bronzes were tested as wear resistant material deposed on the cones for the drilling pipes used by petroleum exploitation industry (Figure 5). The cones were made by steel with ≤0.25%C, ~0.3%Mo and ~3.5%Ni [19, 20]. An important problem that arises is the service endurance of the bearings. The cones are usually subjected to high variable contact pressures on the sliding surface and to wear under improper lubrication. The nickel-aluminium bronze was tested for the substitution of the classical antifriction material AgMn15. The silver alloy is very expensive. The same welding method for cladded bronze was used. Only the welding current was different (120-150A). For selecting the material more factors were taken into consideration: the properties, the results of wear tests, the economical aspects (in this case the antifriction material AgMn15 is very expensive), etc.

Also the rules imposed for parts manufacturing were taken in consideration.

Fig. 5. *Steel cone of drilling rod and its section as support for bronze deposition.*

For the steel cones it is compulsory to apply the heat treatments after antifriction layers deposition: carbonitriding (at 950°C), double quenching (at 860^{0}C and 760 ^{0}C), and stress relieving (at 180^{0}C).

In order the microstructure of the antifriction material is highly influenced and the properties and the wear behaviour are modified. The behaviour to wear was tested on an Amsler stand.

As counter-sample the hard steel thermal treated to obtained 43HRC hardness was used. The wear results are given in Table 3.

Table 3. *Results of wear behaviour tested on Amsler stand*

Antifriction material	**Working time**	**Friction coefficient**	**Working temperature**	**Wear of sample radius**
	[h]		[^{0}C]	[mm]
Nickel-aluminium bronze alloyed with iron and manganese	83	0.07-0.12	125-140	0.33

The heat affected zone and a transition zone are developed in the bimetal at steel-bronze interface. These were analized from the structural and the chemical composition points of view (Figure 6).

In other applications the nickel-aluminum bronzes work in marine environments. When exposed to sea water, aluminium bronze with controlled composition and structure shows a high corrosion resistance together with good resistance to heavy loads and friction conditions.

The electrolyte is not aggressive for the individual alloy [5, 10].

When the bronze and the steel as dissimilar alloys are in contact in the presence of an electrolyte (which may not be aggressive for individual metals when they are not coupled), an additional corrosion (named bimetallic corrosion) occurs (if the difference in the electrode potential is sufficiently large) [21-25]. Galvanic corrosion results from differences in composition or structure of the weld bronze and the parent steel. This may occur in the transition zone formed between the two alloys. In the case studied, the multilayer welding technology, and its parameters, may adversely affect corrosion resistance.

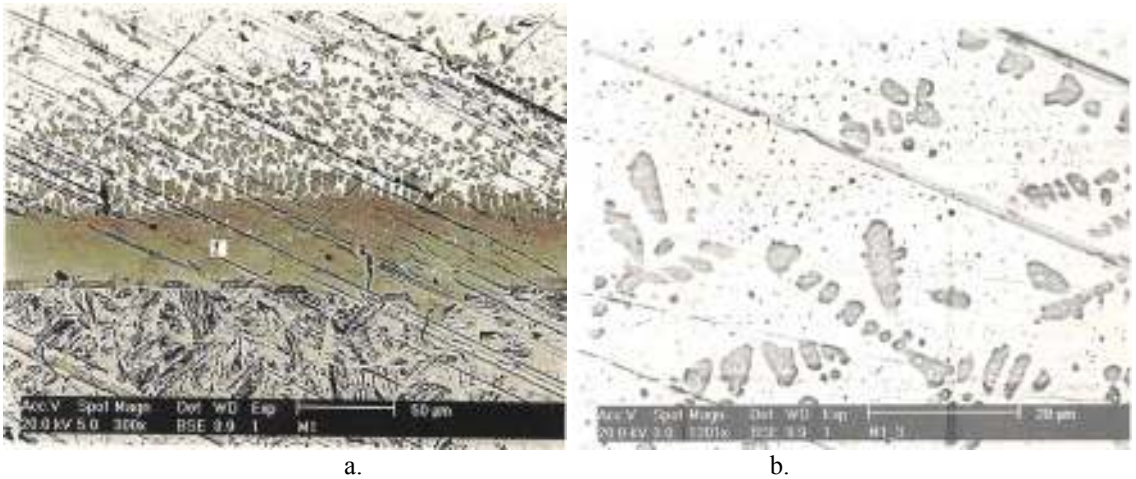

a. b.

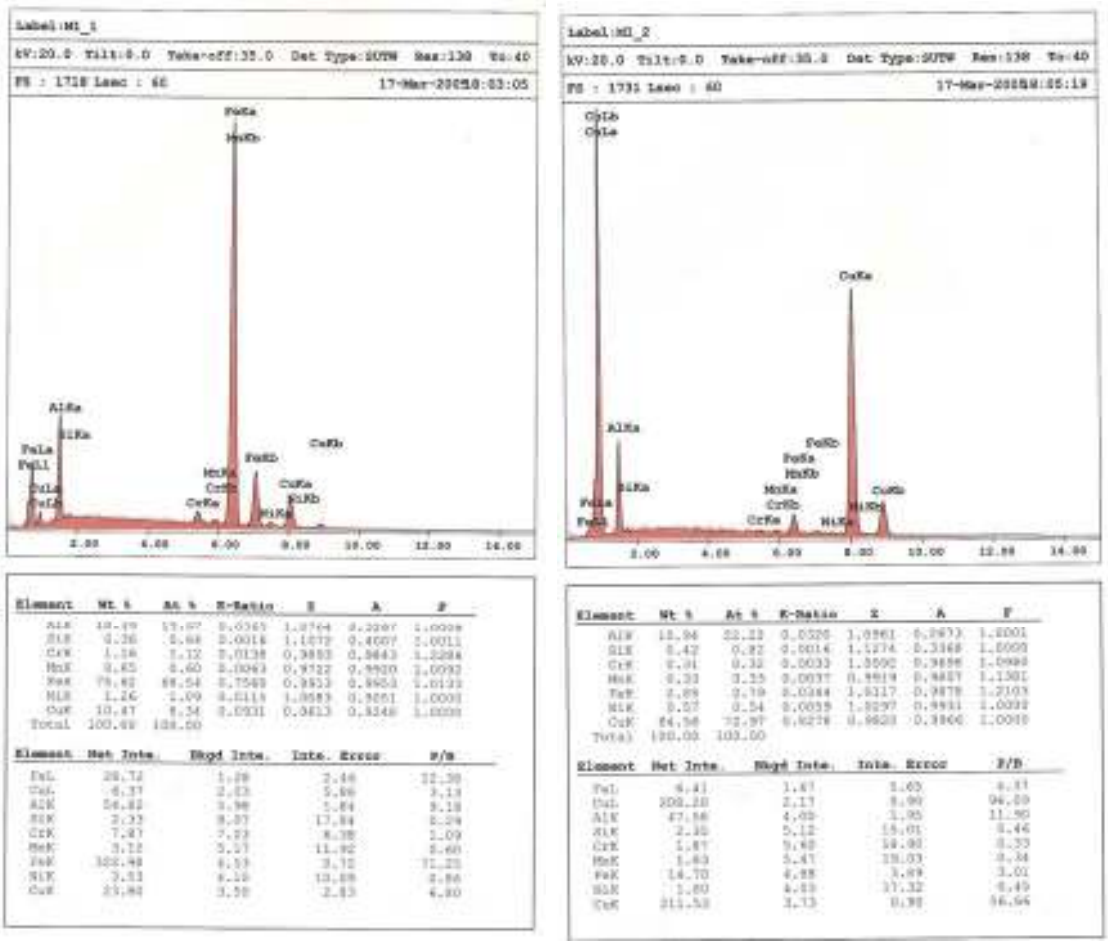

c.

Fig. 6. *Microstructures of bimetal, x 400, 20 kV, BSE (back scattering electrons): a. transition area between bronze and steel; b. bronze in proximity of transition zone; c. EDAX analysis of points 1 and 2 into diffusion zone (according to fig. 6a) [20].*

There are several differences in composition or structure that affect resistance to corrosion: in the cladding made of several layers (deposited successively by multipass welding); between filler and parent metal; in the heat-affected zone adjacent to the weld. In the multipass welds, the relatively high temperature can induce tensions in the welded material, while in the heat affected zones of the basic material cracks may occur due to the combined effect of corrosion and stress.

These can be avoided by thermal treatment applied after welding [4, 5].

The immersion test of the bimetallic materials was carried out to investigate their corrosion resistance in saline water.

Experimental materials were cut into cylindrical specimens with diameters of 50mm [26].

For such systems the corrosion behaviour of the bimetal at the transition zone is important (Figure 7).

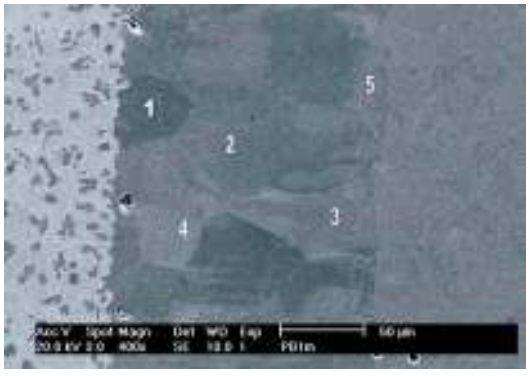

Fig. 7. *Transition area between bronze and steel 20 kV [26].*

The welding develops in this area the diffusion of the elements. The elements content vary on the depth of this zone (Table 4) and as a result selective corrosion phases were observed.

Table 4. *Variation of elements on the depth of transition zone [%wt] (points into depth of diffusion zone according to Fig. 4) [26].*

Elements	Points located into depth of diffusion zone				
	1	4	2	3	5
Al	6.73	6.31	5.90	4.16	1.02
Mn	1.27	1.43	1.20	0.96	1.21
Fe	82.41	83.51	85.84	87.48	93.59
Ni	4.40	4.20	3.47	2.92	3.11
Cu	5.18	4.54	3.58	4.48	1.07

The analysis of the transition zone after exposure to corrosion media put into evidence three subzones that have approximately equal thickness (Figure 8).

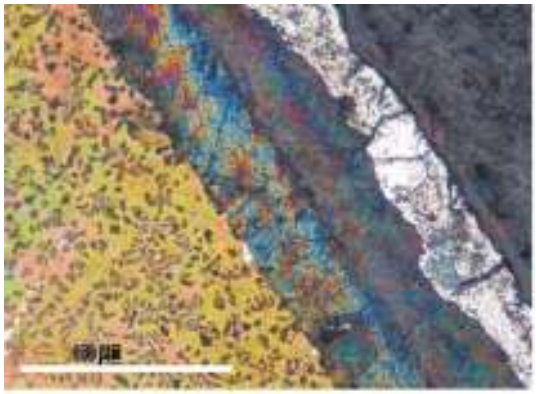

Fig. 8. *Microstructure of bronze-steel bimetal after 48 hours of exposure to sea water [26].*

In the first subzone (to bronze), as a result of copper diffusion and its limited solubility in solid solution, coarse separations of copper occurred. These are arranged to grain boundary and inside solid solution grains. In the next subzone (into central transition zone), the separation of copper was dispersed into solid solution grains as very fine and globular precipitates. In the third subzone (to steel) these copper precipitations do not show; probably copper is in a low concentration, not in excess, and it is fully dissolved in solid solution.

Therefore, the intensity of the corrosion process for these subzones is different.

The subzone adjacent to steel has a good resistance to corrosion, and stability at 3 week exposure to sea water (Figure 9).

Fig. 9. *Microstructure of bronze-steel bimetal after 3 week exposure to sea water [26].*

The entire surface of this subzone is less corroded and uniform. An accelerated and deep corrosion is developed in the central subzone. In brief, the presence of heterogeneous structures (observed in the subzone close the bronze and the central subzone) enhances electrochemical corrosion.

The phases dispersed in the matrix of the solid solution are in contact and have such as behaviour of dissimilar metals available in contact under the corrosive environment (Figure 8). At the same time, close to the transition zone, heat-affected areas developed.

The uncontrolled thermal treatment is produced in both alloys, into certain depths of the bronze and steel, and was manifested by recrystallization of the phases and finishing of the grains (Figure 10).

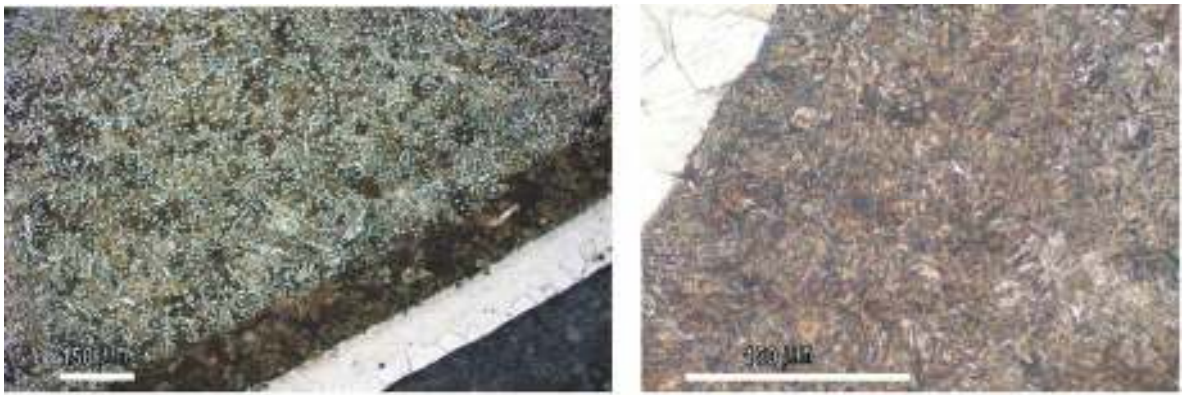

Fig. 10. *Microstructure of the bronze and steel after exposure to metallographic attack (without exposure to sea water) [26].*

Selective phase corrosion occurs in response to different electrochemical potentials between adjacent phases. Nickel-aluminium alloy develops a complex microstructure as indicated by the equilibrium phase diagram.

As a result, small variations in composition and heat treatment had a marked effect on the microstructure and hence the corrosion resistance. In accordance with the working conditions the dissimilar materials must be chosen to minimize the corrosion process.

Conclusions

The variety of combinations in terms of chemical composition and properties of the aluminium copper alloys alloyed with some important elements makes them extremely versatile, useful as wear resisting material in a large number of applications.

The aluminium bronze alloy with determined contents of nickel, manganese and iron is an excellent choice for applications involving heavy loads, adhesive wear, friction, abrasive wear and corrosion. In some applications the bearings as monoblock castings were recommended. For the antifrictions properties the chemical composition of bronzes was correlated with the microstructure. This ensures a soft phase hardened with compound uniformly distributed. In the cases analysed the selected aluminium content leads to obtaining a solid solution α as soft base.

The choice contents of nickel, iron and manganese develop those complex intermetallic κ phases that hardened the material.

Weld cladding was used to obtain a bimetal with good behaviour in working conditions specific to complex applications.

This technical solution involves the welding of an alloy layer on the other base alloy.

The processes taking place when the steel is plated with a non-ferrous alloy using the welding process are similar with the processes specific for a metallic bath formed through a metal melting in the welding zone with the contribution of both involved materials.

The solidification mechanism of added material which caused the formation of a transition structure characterized by variable composition and properties can be different. If the welding process is well done, the transition zone of the melted added material and the superheating based material is formed. The selection of the welding parameters and the heat treatments of bimetals minimize the risks associated of the transition bronze-steel zone.

A most important attention must be given to the additional corrosion process induced by dissimilar metal contacts immersed in an electrically conducting corrosive liquid.

The controlled association of bronze with steel provides systems which satisfy the requirements of mechanical properties associated with strong resistance to corrosion in marine environments.

References

[1]. H. J Meigh - *Cast and Wrought - Aluminum Bronzes - Properties*, Processes and Structure', Institute of Materials, London, 2000

[2]. *Equilibrium Diagrams Selected copper alloy diagrams illustrating the major types of phase transformation*, CDA Publication No 94, 1992

[3]. Aluminium Bronze Alloys Technical Data. CDA Publication 82, 1981

[4]. M. Kaplan and A.K. Yildiz - *Mater Lett* 57 (2003) 4402

[5]. Datong ZHANG, Ruiping CHEN, Weiwen ZHANG, Zongqiang LU, Oand Yuanyuan LI - *Effect of microstructure on the mechanical and corrosion behaviors of a hot-extruded nickel aluminum bronze*, Acta Metall. Sin.(Engl. Lett.) Vol.23 No.2 pp113-120 April 2010

[6]. Fuller, Michael D. - MS Thesis - *"Friction Stir Processing and Fusion Welding in Nickel Aluminum Propeller Bronze"* Naval Postgraduate School, Monterey, CA, Mar 2006

[7]. *Aluminum Bronzes*- Copper Development Association, http://www.copper.org/resources/properties/microstructure/al_bronzes.html

[8]. K. Oh-ishi, A.M. Cuevas, D.L. Swisher and T.R. McNelley - *"The influence of Friction Stir Processing on Microstructure and Properties of a Cast Nickel Aluminium Bronze Material"*, Metallurgical and Materials Transactions A., vol.35A, sept.2004

[9]. D. R. Lenard, C. J. Bayley and B. A. **Noren** - *Detection of selective phase corrosion of nickel aluminum bronze in seawater by electrochemical frequency modulation*, DoD Corrosion Conference, 2009

[10]. Know How Welding Repair for New Propeller, Nakashima Propeller Co. Ltd

[11]. H J Meigh - Resistance to Wear of Aluminium Bronzes, http://www.cda.org.uk/Megab2/corr_rs/allybrwe/default.htm

[12]. S. Sontea, M.Vladoi, N. Zaharia - Metale si aliaje neferoase de turnatorie, Ed. Scrisul românesc, 1981

[13]. Copper.org: Standards & Properties: Metallurgy of Copper Base *Alloys*, www.copper.org/resources/properties/703_5/703_5.html

[14]. Making and casting of economical alloys for bearings used on mill steel that working at high temperature, Project 26/1983

[15]. A.Ciocan - New tips of alloys for SEA drilling installations, Revista Metalurgia 1998

[16]. Project 11/1984, Establishment of chemical composition and the mechanical characteristic of the antifriction alloy as substitute for tin bronzes used at manufacturing of the bearings for the tires vulcanization presses

[17]. Project 22/1983 Obtaining of bimetal used as antifriction parts for ferrites presses

[18]. Welding of Aluminium Bronzes, Publication No 85, 1988, Copper Development Association, www.cda.org.uk

[19]. Project 12/1884, Researches about the cast bars obtaining used for welded the bearings of drilling pipes used into petroleum exploitation industry

[20]. A.Ciocan, F. Bratu - *Chemical and structural changes for bimetallic materials obtained by the welding process*, The Annals of "Dunarea de jos" University of Galati Fascicle IX Metallurgy and Materials Science

[21]. *Bimetallic corrosion, Guides to good practice in corrosion control*, www.npl.co.uk

[22]. H. Campbell - *Aluminum bronzes alloys. Corrosion resistance guide*, Publication 80, Copper Development Association, U.K., pp.1-27, July 1981, www.cda.org.uk

[23]. H. T. Michels and R. M. Kain - *Effect of Composition and Microstructure on the Seawater Corrosion Resistance of Nickel-Aluminum Bronze*, Corrosion/2003, Paper No. 03262 (Houston TX: NACE International, 2003).

[**24]. J. A. Wharton, R. C. Barik, G. Kear, R. J. K. Wood, K. R. Stokes and F. C. Walsh – "**The Corrosion of Nickel-Aluminium Bronze in Seawater", Corrosion Science, Vol. 47 (2005), pp. 3336-3367.

[25]. J R C Strang - *Cast Valve Materials for Seawater Service: Nickel-aluminium Bronze and its Rivals*, Materials for seawater service Strang, 2006

[26]. A. Ciocan, F. Potecasu, E. Drugescu, S. Constantinescu - *Characterization of the diffusion zone developed in a bimetallic steel-bronze at interface*, Advanced Materials Forum V, ISSN 0255 – 5476, Trans Tech Publications LTD Switzerland, UK, USA III, Vols. 636-637, pp 556-563

THE ANNALS OF "DUNAREA DE JOS" UNIVERSITY OF GALATI.
FASCICLE IX. METALLURGY AND MATERIALS SCIENCE
N^0. 2 – 2011, ISSN 1453 – 083X

TWO STEPS FOR AN ENVIRONMENTAL FRIENDLY PROPULSION ENGINE

Edward RAKOSI[1], Gheorghe MANOLACHE[1], Sorinel TALIF[1], Florin POPA[2]
[1]"Gheorghe Asachi" Technical University of Iasi
[2]"Auto Axel" Ltd. Iasi
email: edwardrakosi@yahoo.com

ABSTRACT

A logical way to preserve the natural resources and lowering the pollution level is the improving of the thermal engine efficiency in order to reduce the fuel consumption. Considering the weight factor of the spark ignition engine in automotive market, the authors propose a combined solution to improve the performances of this thermal engine.

First, in order to improving the combustion efficiency, we are trying to obtain a closer approach to the ideal constant volume combustion cycle, specific to the spark ignition engine, by developing a variable sequential ratio engine.

Secondarily, by modifying the architecture of the compression ring, the theoretical model developed allows the determination of a new transversal profile of the compression ring in order to obtain better lubrication conditions, to lower friction ware and increase the mechanical efficiency.

This theoretical and experimental study regards the both modification of these parameters in various situations, aiming at the optimization of this environmental friendly propulsion engine.

KEYWORDS: combustion and mechanical efficiencies, environmental friendly propulsion engine

1. Introduction

The spark ignition engines for automotive propulsion still represent about 65%-70% of the world market, and about 85%-90% of the American market. On the other side, although the alternative (also called hybrid) propulsion solutions are becoming more and more popular, they are not widely spread. The American market, one of the largest fuel consumers in the world, is dominated by medium-large sized spark ignition engines with high fuel consumption. These types of engine have been improved step by step.

The fueling systems have been optimized; improved solutions for gases distribution have been used, the compression ratio has been modified, etc. This is an old area of interest and specialists proposed several solutions. Currently, the most popular solution [1], introduced in small production numbers, is the one developed by SAAB.

On the other hand, in the purpose of improving the spark ignition engines efficiency, the actual researches taken into account the amelioration of constructive and technological solutions.

2. Proposed Engine Solutions

2.1. Improving the operating cycle basis efficiency

The study developed by the authors has the goal of improving the efficiency of the spark ignition engine, in the first step, by improving the basis efficiency of its operating cycle. Moreover, one of the ways consists in obtaining a higher relative efficiency, i.e. a closer match to the ideal thermodynamic cycle (constant volume combustion). This goal can be achieved by assuring an almost constant volume during the combustion process.

An engine functioning in this manner will lead to a higher compression ratio close to the TDC, during the burning process (when the lowest heat quantity is developed). The compression ratio varies only in certain moments of the cycle, remaining unchanged for the rest of the cycle.

The solution proposed by the authors achieves the variation of the compression ratio by moving a small piston in the opposite direction to the main

piston, during a 90 degree angular interval after the TDC, thus achieving an almost constant volume for the main part of the burning process. In the Fig. 1 this solution are shown for a position near the TDC.

Fig.1. *Position near the TDC.*

2.2. Increase of the mechanical efficiency

The second step of the researches consist in the increase of the mechanical efficiency by improving the lubrication condition for the compression ring; this is the consequences of increased values for the minimum film thickness and reduced friction forces inside the cylinder liner-piston ring couple.

The modified compression rings developed by the authors are based upon the rectangular ring (ISO 6621-1); the rings are modified as their peripheral surface has a bi-conical shape.

3. Analysis and Modeling

Aiming to obtain results that would allow a comparison between real conditions and the proposed solution (in terms of differences between efficiencies), we developed a detailed analysis of this engine solution. For improving the basis efficiency of operating cycle, two separate cases were taken into account: the first one presumes a constant bore of the small piston, while displacing it between 1 and 10 mm. The second case preserves the stroke of the same small piston, while its bore varies between 44 and 97 mm. An analysis of the obtained efficiencies led us to the optimization of the mechanical parameters.

3.1 The basis efficiency of operating cycle analysis

First case modeling

The momentary stroke of the main piston is:

$$s(\alpha)=r\cdot\left[1-\cos(\alpha)+\frac{1}{\lambda}\left[1-\left(1-\lambda^2\sin(\alpha)^2\right)^{\frac{1}{2}}\right]\right] \quad (1)$$

and the momentary volume generated by the main piston is:

$$Vp(\alpha)=\frac{Vs}{S}\cdot s(\alpha) \quad (2)$$

The momentary volume of the cylinder is:

$$Vp(\alpha)=Vc+Vp(\alpha) \quad (3)$$

The momentary volume occupied by the small piston is:

$$Vm(\alpha m,Sm)=\frac{Vsm(Sm)}{Sm}\cdot s(\alpha m,Sm) \quad (4)$$

The momentary volume of the cylinder, as affected by the movement of the small piston during the angular interval of its stroke, becomes:

$$V2(\alpha m,Sm)=V(\alpha m)-Vm(\alpha m,Sm) \quad (5)$$

and is shown in Fig. 2, in comparison with the one of standard (unmodified) engine. Further on this engine solution will be named shortly **VSCR** (Variable **S**equential **C**ompression **R**ation).

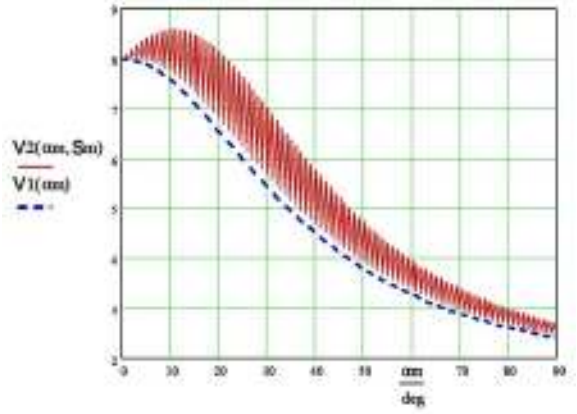

Fig. 2. *Variation of the cylinder volume as affected by the movement of the small piston, for different strokes.*

The momentary compression ration, for the standard engine is given by the expression:

$$\varepsilon 1(\alpha m)=1+\frac{Vs}{V(\alpha m)} \quad (6)$$

while, for the **VSCR** engine, we get:

$$\varepsilon 2(\alpha m,Sm)=1+\frac{Vs}{V2(\alpha m,Sm)} \quad (7)$$

Overlapping the two compression ratios, for the small piston working domain, results in the curves shown in Fig. 3.

Considering an adiabatic coefficient k=1.3 the efficiencies for the two studied cases become:

$$\eta tv1(\alpha m)=\left(1-\frac{1}{\varepsilon 1(\alpha m)^{k-1}}\right)\cdot 100 \quad (8)$$

For the working range of the small piston we get the thermal efficiency gain of the **VSCR** solution as:

$$A\eta tv(\alpha m,Sm)=\left|\eta tv2(\alpha m,Sm)-\eta tv1(\alpha m,Sm)\right|\% \quad (10)$$

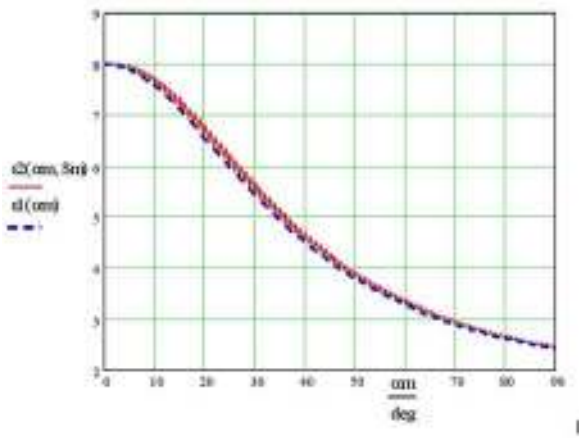

Fig. 3. *Overlapped variation of the compression ratios.*

The efficiency gain variation range for different strokes or diameter of the small piston is shown in Fig. 4 and Fig. 5.

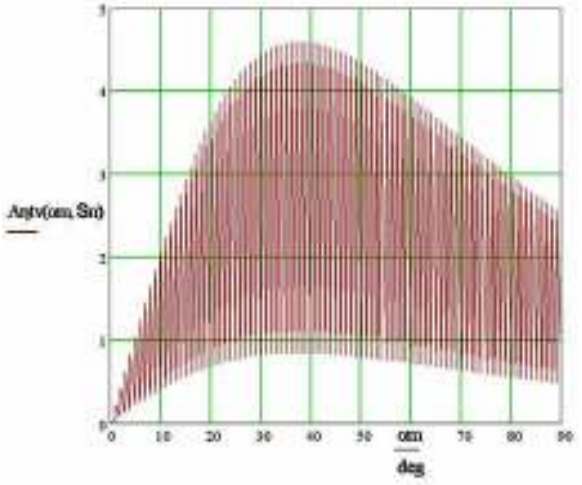

Fig. 4. *Efficiency gain variation for different strokes of the small piston.*

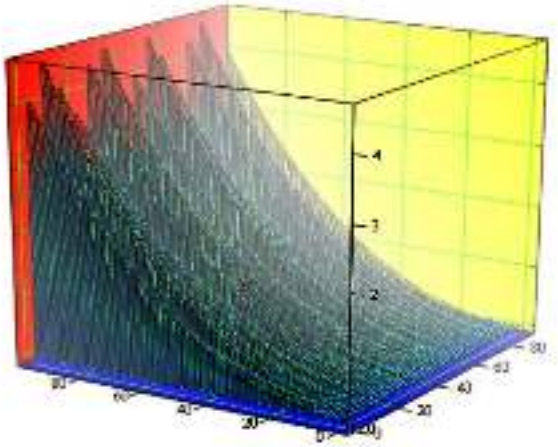

Fig. 5. *Efficiency gain by modifying the diameter of the small piston.*

Second case modeling

In this case the highest value for the small piston stroke (10 mm) is used, which leads to the most significant efficiency increase, while the diameter of the small piston is modified, starting with the lowest value, D_m=44 mm, and ending when the diameter of main piston is reached (D_m=D=97 mm). The previous formulae are modified accordingly, only the intermediate and final results being presented.

For the both cases, stresses and strains of the main piston of the **VSCR** engine were evaluated, using the **F**inite **E**lement **M**ethod (**FEM**); some results are shown in Fig. 6.

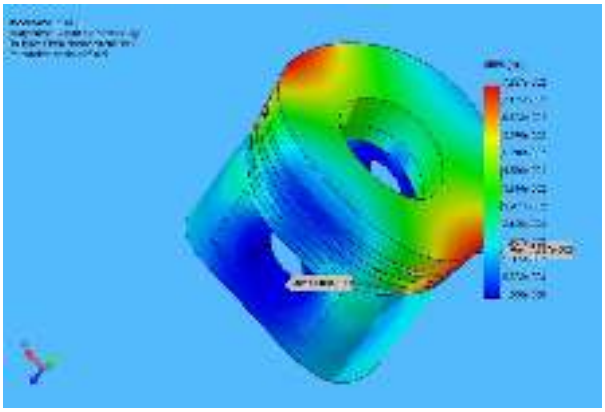

Fig. 6. *Strain for the main piston of the **VSCR** engine obtained using **FEM.***

3.2. Compression rings profile optimization

When the peripheral surface of the piston ring is correctly aligned with the cylinder liner surface, the piston – piston rings-cylinder assembly acts as a labyrinth, insuring an efficient seals [2].

Starting from the p_0 pressure inside the combustion chamber, the pressure decreases to p_{s1} behind the first compression ring, to p_1 after the first ring, to p_{s2} and p_2 behind and after the second ring etc.

Due to the high value of the chamfer angles h_1, only the surface with the length $h_r = h - 2h_1$ [m] is considered as the hydrodynamic active surface of the piston ring-cylinder liner couple.

Thus, for the downward piston stroke, the length of the wedge shaped interstice, marked $h_{efr(d)}$, is:

$$h_{efr(d)} = (1 - X)(h - 2h_1) \text{ [m]} \qquad (11)$$

and accordingly for the upward stroke we have hefs(u)

$$h_{efr(u)} = X(h - 2h_1) \text{ [m]} \qquad (12)$$

The specific relations for the hydrodynamic lubrication regime, correlated with the combustion chamber pressure, are used in order to establish the

conditions for the oil intake and exhaust inside the piston ring-cylinder liner couple, thus leading to the best values for the angles of the conical surfaces that insure a preponderant hydrodynamic lubrication regime.

The oil flow through the cylinder liner-piston ring is calculated using the flow equation for the hydrodynamic reciprocating couples [3].

The equations are:
- for the downward stroke:

$$Q_{L(d)} = \pi \cdot D \cdot \left[\frac{h_1 h_2}{h_1 + h_2} v_p + \frac{1}{6} \frac{(h_1 h_2)^2 (p_1 - p_0)}{\eta (h_2^2 - h_1^2)} \right] [\mathrm{m^3/s}] \quad (13)$$

- for the upward stroke:

$$Q_{L(u)} = \pi \cdot D \cdot \left[\frac{h_1 h_2}{h_1 + h_2} v_p + \frac{1}{6} \frac{(h_1 h_2)^2 (p_0 - p_1)}{\eta (h_2^2 - h_1^2)} \right] [\mathrm{m^3/s}] \quad (14)$$

In order to evaluate the overall oil flow during one engine cycle we define the overall oil circulation Q_{Lt} [m^3/s], calculated by graphical integration of the oil flow according to Fig. 7.

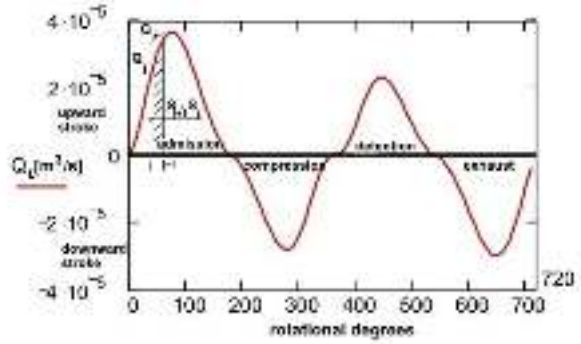

Fig. 7. *The oil flow through the cylinder liner-piston ring and the overall oil circulation QLt calculated by graphical integration.*

The relation for the overall oil circulation is:

$$Q_{Lt} = \sum_{j=0}^{71} \frac{Q_{Li+1} + Q_{Li}}{2S} \left| S_{i+1} - S_i \right| [\mathrm{m^3/s}] \quad (15)$$

A positive value of the overall oil circulation means that the oil flow is directed towards the combustion chamber.

Starting from the shear forces in the reciprocating couple [4], for the hydrodynamic lubrication regime, we evaluate the friction forces inside the cylinder liner-piston ring couple using the equations:
- for the downward stroke:

$$F_{f(d)} = \frac{2 \cdot \pi \cdot D \cdot \eta \cdot v_p}{k_d} \cdot \left[3 \cdot \frac{h_2 - h_1}{h_1 + h_2} - 2 \cdot \ln \frac{h_2}{h_1} \right] + \ldots$$

$$\ldots + \pi \cdot D \cdot k_d \cdot \frac{h_1 \cdot h_2}{h_1 + h_2} \cdot (p_1 - p_0) [\mathrm{N}] \quad (16)$$

- for the upward stroke:

$$F_{f(u)} = \frac{2 \cdot \pi \cdot D \cdot \eta \cdot v_p}{k_u} \cdot \left[3 \cdot \frac{h_2 - h_1}{h_1 + h_2} - 2 \cdot \ln \frac{h_2}{h_1} \right] + \ldots$$

$$\ldots + \pi \cdot D \cdot k_u \cdot \frac{h_1 \cdot h_2}{h_1 + h_2} \cdot (p_0 - p_1) [\mathrm{N}] \quad (17)$$

Defining the piston ring mechanical work of the friction forces L_{fr}[J] we may evaluate the mechanical losses, using a graphical integration method for the variation shown in Fig. 8.

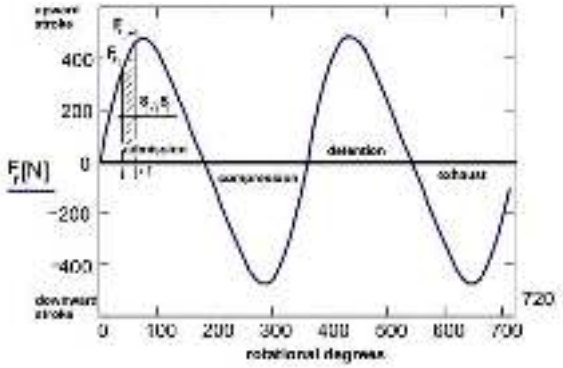

Fig. 8. *The friction forces inside the cylinder liner-piston ring couple and piston ring mechanical work of the friction forces L_{fr}[J] calculated by graphical integration.*

Using the general expression of the mechanical work, we get the relation:

$$L_{fr} = \sum_{j=0}^{71} \frac{\left| F_{ri+1} + F_{ri} \right|}{2} \left| S_{i+1} - S_i \right| [\mathrm{J}]. \quad (18)$$

A high value of this mechanical work means high friction forces inside the couple and diminishes the engine's mechanical efficiency.

Computational procedure

The theoretical model we have developed allows the determination of the transversal profile of the first and the second compression ring in order to obtain a different profile but similar lubrication conditions, to reduce oil consumption, to obtain a lower friction forces and to increase the mechanical efficiency of the piston ring – cylinder line coupling.

So, the slope repartition will be optimized in order to reduce oil flow towards the combustion chamber.

Using the relation (13), (14) and (15) and giving values comprised between 0 and 1 for the slope repartition X, the calculus are made in order to obtain a zero value for the overall oil circulation Q_{Lt}. In that case, the oil flow towards the combustion chamber

and the oil consumption is reduced to the minimum values. The upper and bottom slope angle of the peripheral surface of the rings will be optimized in order to insure a preponderant hydrodynamic lubrication regime and diminish the friction forces and piston rings and cylinder liner wear.
Calculus, using the relation (16), (17) and (18), are made starting at 0 value for the upper and bottom slope angle and is considered ended when we obtain a maximum percentage from entire engine cycle with the hydrodynamic lubrication regime for the piston ring and the minimum value for the piston ring mechanical work of the friction forces L_{fr} [J].

In Fig. 9 will expose the oil flow through the cylinder liner-piston ring and, in Fig. 10, the friction forces inside the cylinder liner-piston ring couple variation for the entire engine cycle for the both compression piston ring.

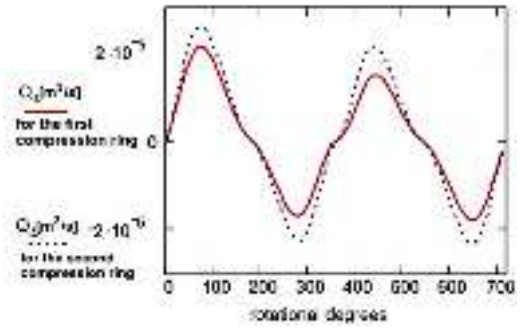

Fig. 9. *The oil flow through the cylinder liner-piston ring for the first and the second modified compression ring of a four-stroke S.I. engine.*

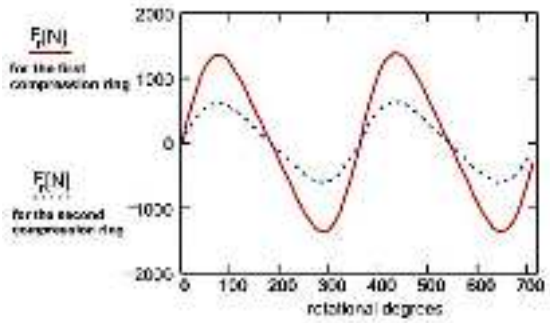

Fig. 10. *The friction forces inside the cylinder liner-piston ring couple for the first and the second modified compression ring of a four-stroke S.I. engine.*

4. Conclusions

- For all the studied cases, the models have revealed a smoother drop in the thermal efficiency of the **VSCR** engine, during the combustion process.

- In the meantime, higher values of the thermal efficiency were recorded during the main phase of the combustion process and towards its end.

- The maximum thermal efficiency increase (up to 4%) was obtained when the small piston's stroke is 10 mm and when its diameter equals the one of the engine's main piston (the "fake piston head" case).

- A study of the efficiency increase shows that, in the first case, its maximum value is obtained at 35 degrees CA after the TDC, while for the second case, the maximum value is attained at 37-38 degrees CA after the TDC, thus showing the advantage of this method in terms of a fuel consumption decrease.

- The lubrication conditions for the second compression ring are better to the first piston ring.

- Several new notions were defined (*overall oil circulation* and *mechanical work of the piston ring friction forces*), in order to improve the profile of the compression rings of an internal combustion engine, to reduce oil consumption, insure a preponderant hydrodynamic lubrication regime and diminish piston rings and cylinder liner wear.

- The tests carried out with modified rings showed a decrease in gas pressure escaped in the crankcase, the situation exposed in Fig. 11, and lower consumption of lubrication oil.

- In conclusion, the modification of those parameters leads to an optimized engine solution for lowering the fuel consumption and the pollution level, an environmental friendly propulsion engine.

References

[1]. Gray Jr. - *Piston in Piston Variable Compression Ratio Engine,* U S Patent, No. 6,752,105 B2, 2004

[2]. Heisler H: *Advanced Engine Technology*, SAE International, 1995

[3]. Taylor C.M. - *Engine Tribology*, Tribology Series, 26, Elsevier Science Publisher B.V., Amsterdam, 1993

[4]. Zhu D., Cheng H.S. - *An Analysis and Computational Procedure for EHL Film Thickness, Friction and Flash Temperature in Line and Point Contacts*, STLE Tribology Transactions, v32, n3, p364-370, Park Ridge, IL, USA, 1989

THE ANNALS OF "DUNAREA DE JOS" UNIVERSITY OF GALATI.
FASCICLE IX. METALLURGY AND MATERIALS SCIENCE
N^0. 2 – 2011, ISSN 1453 – 083X

NEW MATERIALS TO SUPPORT THE PRESERVATION OF OLD WOOD USED FOR ART OBJECTS

Lăcrămioara Gabriela GHERMAN, Ion SANDU, Viorica VASILACHE
Al. I. Cuza University of Iaşi
email: sandu_i03@yahoo.com

ABSTRACT

This paper presents new materials that replaced the main list of substances with a high toxicity level (banned in the European Community), and the interventions in the preservation of old wood used for art objects. Although in the process of stopping the four evolutionary effects of deterioration and degradation of the wood, highly effective methods of preservation were developed, it was found that the toxic atmosphere maintains a high risk for curators. These methods involved the use of derivatives of naphthalene and polymers containing chlorine, bromine-based derivatives, namely a series of highly dangerous pesticides. In this context, most research centers in wood preservation have studied new systems supposing minimal toxicity, compatible with different types of timber, in a series of natural or synthetic substances, such as: Pyrethroids, boron compounds, tannins, woodsulfonates, silicates and phosphates.

KEYWORD: wood, preservation, restoration, toxicity, pesticides, environmental pollution

1. Introduction

The wood, as a structural or ornamental element from within the composition of cultural treasures, is an organic material with low resistance over time. It is known that the environmental and climatic factors, such as heat and fuel sources, microorganisms, acid rain and not lastly the man, lead to a series of micro and macro structural destructions and evolutionary alteration, translated by two effects: deterioration of structural-functional elements and degradation of the basic constituents, lignin and cellulose. To that effect, in order of their frequency and aggressiveness, we mention: putrefaction, carbonization, career, embrittlement, discoloration, waiving, cracking/fracture etc.

Treatments to preserve old or new such wood, most of the times, stop synergistically most of the above processes, using a number of substances as such or as organic dispersions (solutions, emulsions, gels soils etc.) which are toxic or produce unwanted effects on the environment and the operators. Because of that, at present, the subject of active products and solvents involved in these treatments and having a minimal impact on the environment is of great interest for many research institutions. Surface water and groundwater with soils in the immediate vicinity of the areas or treatment facilities are mostly affected by these treatments.

Consequently, we face, on the one hand, the problem of soil and air remediation, wastewater treatment, surface water and groundwater treatment to meet drinking water quality criteria, and, on the other, the selection of most environmentally friendly treatment solutions, involving the cheapest processes and technologies [3-6].

Therefore, the research of new treatment systems of highly toxic substances (polymers and naphthalene derivatives containing chlorine, bromine derivatives, and a series of pesticides) banned by the regulations of the European Agency for Registration, Evaluation and Authorization of Chemicals (REACH) will be taken into account [7].

2. Evolution of degradation and deterioration effects on wood

The experts identified four major types of degradation and deterioration effects on wood: physical (cracking, fracturing, waiving, bending, displacement, swelling, shrinkage), physichochemical (change of color and organoleptic characteristics because of enzyme attack, radiation or heat exposure,

desorption, chemical composition changes as a result of microbiological activity, change of normal range of variation of the hydrous equilibrium under the influence of climatic factors), biological (annual rings contraction, cracking, embrittlement, rotting), functional (reduced or loss of functional and artistic role of the artwork, transformation into a source of pollution for the environment) [1].

Table 1 presents in detail the degradation and deterioration effects, with the associated processes.

Tabel 1. *Most important processes responsible for deterioration and degradation effects of old wood used for art objects* [8]

Deterioration and degradation effects	Process
Putrefaction	Biochemical (enzyme or not)
Carbonization	Thermal combustion (burning)
Radiation degradation	Radiolysis and photolysis
Career	Wood decay attack (bio deterioration and biodegradation)
Molding	Fungal attack (bio degradation)
Embrittlement by β-glycosidic hydrolyse or solubilization of the fragments of cellulose and lignin	Fungal attack + biochemical attack + chemical attack (acidic, alkaline or saline and oxidant)
Color change	Fungal attack, chemical or photochemical
Swelling/shrinkage/waiving/twisting	Mechanical
Cracking/fracturing/splinting	Mechanical + chemical + bio chemical
Fossilization/mineralization	Chemical + biochemical + geochemical

To replace old wood treatment recipes containing highly toxic substances, research centers offer insectofungic systems, fireproof systems, hygrophobic systems, stabilized dimensional systems, based on pyrethroids, boron compounds, tannins, lignosulphonated, silicates and phosphates and synergistic systems with multiple effects.

3. Insectofungic systems

Insectofungic systems have the role to protect or to stop, minimize and remove the effects of microbiological attacks by xylophagous insects, molds, fungi, mushrooms, and others. The most used and most freqeuntly mentioned in literature are the insectofungic compounds containing boron [9, 10]. They are considered multipurpose pesticides (insecticides, fungicides, herbicides etc) and provide nearly 100% protection for heritage objects [11]. Among the boron compounds, mention must be made of synthetic boric acid mixed with glycerin, borax, sodium metaborate, which is the most widely used. A selection of synthetic pyrethroids for insectofungic wood treatment should include: permethrin, deltamethrin, bioresmethrin, cypermetrin. The following organophosphorus insecticides may be used: chlorpyrifos, fenthion, dichlorvos, fenitrothion, malathion, diazinon, triclorfon.

One of the insectofungic procedures in treating wood is to obtain a pesticide emulsion or other formula dispersible in water, with an average particle size of 200 nm. The treatment is particularly effective in protecting wood and timber against common insects (Anobium punctatum, Xestobium rufovillorum), Longhorn pets (Hylotrupes bajulus), dry rot (Serpula / Merulius lacrimans) and wet rot (Coniophora puteena) [12].

Another wood treatment material was used with a synergistic insecticidal action that includes compounds of boron and synthetic pyrethroids. This combination has proved to be particularly effective in conferring resistance to insect attack, with the most cost-effective report in terms of Formosan termites [11].

Another type of insecticide has the form of a dissolved pyrethroide up to saturation into a fluid such as carbon dioxide. The composition may include a co-solvent such as methanol. The treatment method consists in impregnating the wood with this composition and reducing the temperature and pressure under the critical level of the insecticide timber precipitation [13].

Among synthetic pyrethroids, in mixtures with boron derivatives, the following are also used:

- permethrin, an environmentally friendly product, with effective action to halt microbial attack, but also dimensional stability and does not affect or polychrome layer preparation;
- deltamethrin, with median lethal toxicity (LD50 = 135-5000 mg/kg live weight);
- bioresmethrin, decomposes under the action of UV radiation, rapidly hydrolysed in basic medium, median lethal dose (LD50 = 707-800 mg/kg live weight);

- cypermethrin, a non-systemic insecticide with contact and ingestion action (product toxicity - LD50 = 250-4150 mg/kg live weight).

Among organophosphorus insecticides in mixtures with synthetic pyrethroids and/or boron derivatives we would like to mention:

- chlorpyrifos, with a moderate toxicity to vertebrates (LD50 = 135 mg/kg live weight); it is a non-systemic insecticide with contact and ingestion action, that can also act as vapors;
- fenthion, contact and ingestion insecticide with big shock action and good persistence; it is an effective larvicide, with a medium toxicity to mammals (LD50 = 215-316 mg/kg live weight);
- dichlorvos, an insecticide with contact and ingestion action, has an action of shock; its remanence is reduced owing to the great volatility; recommended for Disinfection DDVP indoors. It is a powerful inhibitor of cholinesterase and has a high toxicity to mammals (median lethal dose LD50 = 62 mg/kg live weight);
- fenitrothion, stable to hydrolysis in acidic medium, neutral and basic;
- malathion, an insecticide contact and ingestion, breathing with low action. It has a broad spectrum of activity and a low toxicity to mammals (LD50 = 1300-2800 mg/kg live weight);
- diazinon, an insecticide good contact, ingestion and respiration, has a large share of shock, is also a good acaricide. It has a relatively high toxicity to mammals (LD50 = 108 mg/kg live weight).

4. Fireproof systems

Fireproof systems strengthen the wood fibers to withstand the larger and more frequent variations in temperature than the normal range. The recipes we used are based on inorganic compounds, metal oxides or insoluble salts (fine powders of ZnO, CaO, TiO_2, Sb_2O_3 [14, 15, 16], talcum or micronized asbestos, thermal ash, chalk powder, plaster, colloidal barite, silicon dioxide, zeolite or colloidal volcanic tuffs [17], dry metal sludge, etc.), in mixtures or dispersions that can be diluted with water, usable only inside buildings, as water paints, not to protect exterior surfaces exposed to weather factors.

For fireproof wood protection we also use water soluble products based on boron, ammonium, sulfate, phosphate, silicate etc. salts, and products that form films or coatings on the surface (thermofoaming paints and other products generating inert gas or inert steam or hot melt products, making the fireproof process) [18-20].

Thus, the most widely used system for protecting wood and wood construction materials is the aqueous dispersion based on ammonium phosphate and ammonium sulfate or boric acid and sodium fluoride. These products have a good fireproof action but a small antiseptic action, while having a pronounced corrosive action on metals, causing degradation of joint elements and of metallic reinforcement after application.

Protection products soluble in water and based on soluble salts of copper, chromium, fluoride, boron, arsenic, ammonium, phosphate, silicate etc. have the disadvantage that they produce the rewetting of elements.

5. Hygrophobic and dimensional stability systems

Hygrophobic systems ensure a significant reduction of the hydrophobic character of the wood, so typical of this material. The coated systems the wood fiber retains a constant size in the presence of water.

This feature is very important to achieve the other effects of preservation, because any wood treatment system is based on a liquid.

A very important treatment for the elements located in humid climates or for those exposed to the weather, includes higher hydrocarbons (paraffin), waxes, natural and synthetic resins [21].

Wood treatment with calcium silicate significantly increases its resistance to humidity, deformation, and ensures environmental protection, having a very low cost of implementation [22].

To treat wood with a very low degree of permeability to a preservation agent, we mention the injection method under pressure (from 0.08 mA to 1.2 mA) of an aqueous solution of an antibacterial agent containing quaternary ammonium salt and polyalkyleneglycol, with 8 as pH minimum value [23].

6. Materials and methods of preservation with multiple action

A number of processes and technologies for wood treatment are known to use for insectofungic and fireproof action different tar and petroleum products as such, or as macerated containing extracts from various plants such as oak tannin, chestnut glucosides, conifer terpenes etc. [13, 24, 25].

Old traditional technologies based on oil, mainly used to treat wood for construction, furniture, carpentry, floors, paneling etc., are intensely discussed today although they gave good results. Their weaknesses are due to the staining of wood and to creating artificial skates to polychromy.

Red oil has some great features, such as very low density and viscosity, flammability and high evaporation rate, a very small concentration in solid paraffin (colorless or white), an enough high

concentration of aromatics and other products, and a good ability to extract active ingredients from plants or other natural products by maceration at room temperature.

Of all organic systems containing red oil in various active ingredients the following are very effective in treating wood: pentachlorophenol, sodium pentaclorfenolat (PCP-Na), copper pentaclorfenolat (PCF-Cu), silver pentaclorfenolat (PCF-Ag), lindane.

Propolis is presented as a heterogeneous mass of resin with a solid consistency, sometimes compact and waxy due to malleable and adhering particles, sometimes granular or friable, taking the appearance of powdery debris. This composition, which shows some strength at ambient temperature, becomes friable at low temperatures, below 15°C, even for waxy ways. It is insoluble in water and soluble in alcohol, acetone, ether, chloroform, propylene, benzene, dimethylsulfoxide, ethylenediamine. Depending on the temperature, the dissolution rate varies and so does the passing or not in solution of some fractions to, for example, wax that dissolves in hot alcohol, but is hardly soluble in cold alcohol.

Mainly resins, waxes, volatile oils, pollen, carbohydrates, amino acids, vitamins, enzymes, mineral salts and impurities have been reported in the chemical composition of raw propolis.

Tannins are polyphenols substances (derivatives of 3-hydroxy-flavan or polyesters of gallic acid) soluble in water, gusto astringent, which are reactions characteristic of phenols and alkaloids and precipitated with protein, forming waterproof and rot-proof combinations. As types of relationship between polyphenols and phenolic acids we can consider: hydrolyzable tannins and condensed tannins or unhydrolyzed.

Among synergistic systems with insecticide and firepoof action, impregnations with protective agents are widely used. In the past, copper arsenite water based and pentachlorophenol and creoset oil based were used with protection effect against biological deterioration. As inflamed agents were used phosphates, ammonium salts, bromides, ammonium oxide were used as inflammable agents. Colloidal aqueous solutions with silicon dioxide were used against pest appearance and development [26].

A method of treating wood with multiple protection action against aging, mildew and degradation by ultraviolet light contains zinc oxide in combination with salt dimetilalchilamină monocarboxylic acid [27].

A treatment with fireproof and antiseptic role contains a fireproof substance based on an aqueous solution of diammonium phosphate, ammonium sulphate and a humidifier, and an insecticide in the form of an aqueous solution of poly-hexamethyleneguanidinephosphate chloride [28].

The wood treatment laboratories can also provoke soil pollution by products of Cu, As, Cr; soil electrodialysis in distilled water or in an aqueous solution of HNO_3 effects pollutant cleaning simultaneously [6].

Another method for wood residue preservation uses polycyclic aromatic hydrocarbons (PAHs) and As, high molecular weight products; its extraction from soil by aerobic biodegradation was carried out [6] and its concentration is evaluated with sequential extraction. Under the action of a nonionic surfactant, the degradation of PAHs with both low and high molecular weight was obtained. The negative effect of this method is its increased toxicity as a result of microbial activity. For the near future, the use of standardized tests using the bacterium Vibrio eco Fischer (Microtox ®) is anticipated.

Conclusions

There is a constant concern for finding more multiple action treatments able to ensure the conservation of wood. Synergistic wood treatment should be less polluting for the environment and for the human factor working to turn the wood used for art objects more resistent to degradation as a complex of environmental factors.

References

[1]. I. Sandu - *Deterioration and degradation of goods of cultural heritage*, vol. I and II, University „Al. I. Cuza" Publishing House, Iaşi, 2008.

[2]. V. Vasilache, I. Sandu, C. Luca, I.C.A. Sandu - *News concerning Scientific Conservation of the Old Polychrome Wood***,** "Al.I.Cuza" University Publishing House, 2009.

[3]. M. Gavrilescu, M. Nicu - *Reducing pollution at source and waste minimalization,* Ecozone Publishing House, Iaşi, 2004.

[4]. M. Macoveanu, *Environmental politicies and strategies,* Ecozone Publishing House Iaşi, 2006.

[5]. B. Robu, M. Macoveanu - *Environmenal assessment for sustainable,* Ecozone Publishing House, Iaşi, 2010.

[6]. M. L. Ottosen - *Electrodialytic Remediation of Soil Slurry-Removal of Cu, Cr, and As*, în Separation Science and Technology vol. 44, Ed. Taylor&Francis Group, 2009, pp. 2245–2268.

[7]. Regulation (CE) nr. 1907/2006 of the European Parliament and of the council, 18 december 2006, www.minind.ro/domenii_sectoare/leg_ar.

[8]. O. Petreuş et all - *Modern methods of conservation of old wood made into opera. Polymer matrix and active principles* in Products and technologies for conservation of cultural heritage and historic patrimony, Second edition, Publishing House, Iaşi, 26- 27 mai 2006.

[9]. N. Luţă et all - *Boron compounds and pesticides polyvalent (insecticides, fungicides, etc.) used worldwide for wood in Products and technologies for conservation of cultural heritage and historic patrimony*, Performantica Publishing House, Iaşi, 2006.

[10]. N. Luţă - "*Organophosphorus Pesticides are certainly ecological anti-pests ecological"*, Scientific papers at the symposium "Chemistry Performance in the Third Millennium"organized by CHIMINFORMDATA, 2003.

[11]. R. Bener et all - *Synergistic combination of insecticides to protect wood and wood- based products from insect damage*, Patent US 6.582.732 B1, jun. 24, 2003.

[12]. B. D. Howard, E. Derby - *Treatment of wood and timber with pesticidal formulation,* Patent 5.407.920, 19 aprilie 1995.
[13]. A. Quaeder et all - *Wood preservation,* Patent US 6,638,574, 23 oct. 2003.
[14]. Patent WO2005025824/2005-03-24.
[15]. Patent CA2429286/2004-03-10.
[16]. Brevet RO120975/30.10.2006.
[17]. Patent DE10063127/2002-06-20.
[18]. Patent UA8963U/2005-08-15.
[19]. Patent CN1587591/2005-03-02.
[20]. Patent CN1663394/2005-09-07.
[21]. Brevet RO112463B1/2004-07-30.
[22]. CN 1587591 / 2005- 03- 02.
[23]. JP 11156812/1999-06-15.
[24]. Brevet RO111667/1997.
[25]. Brevet RO1083326/1994-03-31.
[26]. DE10063127/2002-06-20.
[27]. CA2429286/2004-03-10.
[28]. UA8963U/2005-08-15.
[29]. K. Elgh-Dalgren, Z. Arwidsson, V. Ribé, S. Waara, T. von Kronhelm, P. A. W. van Hees - *Bioremediation of a Soil Industrially Contaminated by Wood. Preservatives—Degradation of Polycyclic Aromatic. Hydrocarbons and Monitoring of Coupled ArsenicTranslocation* în Water Air Soil Pollut, 2011, vol. 214, pp. 275–285.

THE ANNALS OF "DUNAREA DE JOS" UNIVERSITY OF GALATI.
FASCICLE IX. METALLURGY AND MATERIALS SCIENCE
N^0. 2 – 2011, ISSN 1453 – 083X

UP TO DATE METHODS AND TECHNICS INVOLVED IN MONITORING THE AEROSOLS FROM NATURAL AND ARTIFICIAL HALOCHAMBERS

Maria CANACHE[1], Ion SANDU[2], Tudor LUPAŞCU[3], Constantin PASCU[4]

[1] Bolotău School, Zemeş, County of Bacău Romania;
[2] "Al.I.Cuza" University of Iaşi Romania;
[3] Chemistry Institute of the Moldavia Science Academy, Chisinau, R.Moldova
[4] S.C. Tehnobionic SRL, Buzău, Romania

ABSTRACT

This paper presents the main modern methods and techniques used in monitoring the aerosols in natural and artificial halochambers, with implications for research of the therapeutic environments optimization conditions. There are focused the "in situ" methods to determine in real time the morphological and functional characteristics of NaCl based aerosols, highlighting the solions with multiple effect.

KEYWORD: chemical analysis, environment factors, halochamber, particles counter, solions

1. Introduction

Environmental pollution has grown and diversified over time with serious consequences on human, animals and plants health, becoming today one of the important concerns of specialists in various fields of science and technology, focused on the following areas: reducing to minimmum the pollution effects, development of green technologies and efficient technologies for treating industrial and domestic waste water, the treatment of surface and ground water for drinking purposes, the detoxofocation of the soil and air, and in the prevention and treatment of diseases and occupational illnesses [1, 2].

To limit the harmful effects of pollution on health, in all EU countries there are programs compiled for anticipating and preventing illness, to increase body resistance, especially for children and the elderly. A relatively clean atmosphere at a given time, may be pollutted by contaminated air masses transported from great distances, thus influencing the climatic elements regime: intensity of solar radiation, visibility, cloudiness, precipitation and through them, all the physical chemical and biological processes occurring in the environment. To prevent and reduce harmful effects on the living environment (water, air, soil, vegetation) and implicitly on man, measurements on environmental parameters are performed. The control of the environmental pollution includes detection and measurement of pollutants problems, the organization of monitoring and surveillance system on the ground and adopting rules on the maximum permissible exposure of people to action of those pollutants (these measures are extended to all the flora and fauna and environmental resources) [1, 3, 4].

There might be a positive influence on the functioning of the body in case of a program of sporting activities tailored to age and individual peculiarities, in a therapeutic environment, with saline aerosols from halochambers (natural or artificial). Among the benefits of movement in an indoor environment with saline aerosols, are included: increase of the respiratory power of ventilation, enhancing of the functional capacity of the circulatory system by increasing blood levels and hormonal activity, speeding up metabolism, boost of the growth processes, mulsculare mass development, increase resistance to stress and the increase of overall comfort (movement improves will, creativity, concentration power, memory, emotional stability etc.) [3].

Achieving optimal aerosol salt concentrations required for such activities occur in a special room with 150 m^3 capacity, ionized windows, UV filters, equipped with a dry air electricity generation, which consists of fan, heat exchanger and a diaphragm, made of 50 blocks of rock salt and/or other salts, such

as KCl, $MgCl_2$, $CaCl_2$ and KI, each cake obtained by pressing or melting salt containing a single kind of salt, while on the active surface has a dense network of small channels. The device continuously recirculats air in the room, which is conditioned to 60...65% RH and 20...22ºC, using a ventilator, which allows circulation of 0.25...0.35 m³/s, after which the air stream passes through a heat exchanger oil-based, allowing to raise the temperature at 90...120ºC to the diaphragm level, which passes through the holes in salt blocks and by the thermal effects of erosion takes negative salt-loaded nanoparticles [5-10].

Healthy or apparently healthy people may be exposed to the saline atmosphere about 30 min/day for prevention and mineralisation of the body, for 12 to 18 days a cure, which may be repeated cyclically at approx. 1 month or more as needed. In the cold light treatment - a complementary treatment is between 30 and 60 min/day for at least 12 days [5, 6].

This paper presents the main methods and technics used in monitoring environmental pollution and atmospheric characterization of halochambers used in the prevention and treatment of respiratory diseases, as well as improving cardio-respiratory and psycho-neuro-motor parameters of the human subject. Also, taking into account the effects of pollutants concentration in closed working or living spaces, it is studied the impact of internal microclimate factors on human body.

2. Methods and Techniques for monitoring the environmental pollution

Detection and measurement of environmental pollution it is performed in the following ways: organoleptic, based on the biological indicators and by using physico-chemical methods [11, 12].

The organoleptic determination is limited by the physical properties of the pollutants and by the sensitivity of the human body to pollutants (for a pollutant to be detected by the senses, the arousal is required to have as low as possible concentrations to give a sufficient margin of safety for personnel exposed to it).

Organoleptic examination involves the following senses:

- *sight*, which helps to detect smoke, smog, air and water turbidity and coloration, finding oil slicks and other pollutants on the ground, and to observe side effects of pollution, particularly those that lead to damage of the vegetation;

- *smell* is the most effective sense for detecting air pollutants, and because of the sensitivity of the respiratory system can take into account in the study of air pollution and its first symptoms of irritation;

- *taste* may be involved in assessing water quality. As regards food, he gives us an indication of their flavor and freshness, the contents of the DDT or other pesticide with specific odor and flavor;

- *hearing* is a fine indicator for noise, it can replace any other means of detection in daily practice (no effectiveness in the field of ultrasound and infrasound, which can be as dangerous as the audible sound).

Biological indicators are also very useful and effective in characterizing the degree of environmental pollution, by using biological reactions of individuals, populations and biocenoses under different conditions of environmental pollution.

Specialized instrumental methods for determining real-time air pollution are the most used and can be classified as follows:

- global methods, which give the result of a group of pollutants, such as atmospheric turbidity, without specifying the nature of impurifying particles or beta global radioactivity, without specifying individual radionuclides;

- analytical methods in detail, separating the components of air pollution;

- physical methods involving instruments determining specific parameters physico-mechanical, optical and acoustic radiative (temperature, light, radiation, vibration etc.).

- chemical methods involving chemical and radio-chemical processing (implicitly radio-activation analysis) and physical processing machines or devices such as electronic, photonic, thermal, X-rays or γ etc., by electrochemical, biochemical, photochemical, radiochemical and other processes;

- biological methods, involving bacterial impurities and other microbiological contaminants, with specific markers for identifying pollutant agents.

Of great practical importance is the division of instrumental methods for determining air pollution: methods "in situ" and laboratory methods (which in turn can be physical and chemical).

Methods "in situ", by place of observation may be: terrestrial or spatial.

The **terrestrial analysis** can determine:

- thermal pollution with the help of ordinary meteorologic thermometers, thermographic devies or thermometers with relay signal to central station;

- acoustic noise with special equipment for recording mechanical radiation intensity with different frequencies;

- ionizing radiation dose rate in air, which can be operatively measured using radiometers. If the device is equipped with scintillation probes and an electronic scheme analyzing the gamma radiation energy, valuable results can be achieved even for the individual components of pollution;

- atmospheric turbidity, by optoelectronic devices, whose data are necessary as an indication of

visibility and as an indication of power of the pollutant sources.

Spatial analysis are possible by means of satellites, which measure terrestrial atmospheric pollution levels in some areas (function on longitude, latitude and altitude) and on different moments or periods of time. These include:

- the radiation level, that can be determined using radiometers placed on satellites, but only in the area crossed by them;
- atmospheric turbidity is determined by optical methods. This concerns not only the hint of smoke and other microparticles, but also nebulosity (cloud coverage) which is very important in terms of weather (specialized satellites are launched into orbit for such remarks, which oversee development of nebulosity allover the globe).

Analysis of atmospheric composition in detail may be made by conventional spectrographic methods or by new methods involving lasers.

Among laboratory methods, must be mentioned the specific analytical chemistry ones and the physical methods by instrumental disciplinary or transdisciplinary techniques, in co-assisted system or in conjunction, whether or not involving sampling and/or processing of samples for analysis, that can influence the determinations results. The presence of some chemical compounds in the atmosphere is not an indication of pollution, since many of the major polluting agents are normally presnt in very small quantities also in what we consider clean air. Therefore, it is not sufficient to study only qualitative the presence of these substances in the air, but it is necessary to determine their quantity too, in order to define the passage "threshold" or "level" of pollution. The technical details of collecting samples for analysis depend on the condition of the pollutant agent (gas, aerosols, dust etc.).

In oder to collect samples for analysis, they are used:

- filtering and impact agents, for particle-from substances which are particles with diameters exceeding 5 micrometers;
- absorbents, (PbO_2 cylinders for sulfur, paper impregnated with calcium carbonate, for fluorides, lead acetate impregnated plates for sulphide, rubber for ozone etc.).
- catchments of gases in balloons, by absobing on liquids or solids, in triethanolamine or $KHCO_3$;

Taking of air samples must be representative, to contain in a fair manner the same qualities and characteristics of the volume of air from which is collected. Sampling should be done in areas not blazed (corners) or the right of the evacuation areas/entry (vehicular), with strong currents, which masks the true state of pollution. Sampling device should be placed in the breathing zone of the human, where it absorbs air can be inspired from places not located too high or too low.

Sampling must meet the actual composition of pollutants, both physically (particle size) and chemical (chemical composition). Sampling is done separately using fiters for diferrent particle size and function on chemical nature, when there are used porous materials with ad- or absorbent capacity, which separates the components of pollutants after their chemical reactivity. The speed of airflow that enters the sampling probe or reaching the collector has to be equal to the overall speed of the airflow in the sampling (isokinetic sampling). This ensures the maintaining the composition of the dispersed by size. From this point of view, particle collectors can be integral, ie the kind that captures all the particles in the air unlike those which separate the particles after their granulometry [13].

3. Methods and techniques for determining the characteristics of the atmosphere in halochambers

Natural or artificial halochambers are saline aerosol enclosures, which allow acquiring solion concentration levels and varying the chemical nature of active cations or anions in their structure, conditions required for different prophylactic purposes and in the treatment of respiratory diseases, as well as in improving cardio-respiratory parameters and psycho-neuromotor of the human subjects involved in strenous phisical activities [14-19].

Our team have developed several halochamber systems, static and dynamic, for different diseases, but also to improve sports and intellectual performance of pupils and students, who have been subject to inventions files patented by AGEPI Chisinau and pending for patent at OSIM Bucharest [20-22].

For measuring and monitoring atmospheric composition of a halochamber there are used methods to determine the microclimatic parameters of an enclosure, such as: work rooms or halls, gyms, swimming pools etc. and also a number of specific methods, such as: the solions concentration conductometric determination, of the quantity of particles with laser beam particle counting, airions dosage and other [5].

Below we present specific methods for determining the solions characteristics in halochambers, much used by our research team, one of which having an absolute degree of novelty, being recently patented [23, 24].

Characteristics of aerosols particles and generally of the aerosol are determined by the source and also by the microclimate and environmental factors.

Therefore, functional characteristics that describe the source of saline aerosol are discussed (size and density of aerosol, particle formation rate, flow of the source, respectively the enrichment factor of the environmental gaseous particle, the lifetime of particles), in order to select the optimal model generator and of the nano-structural and micro-physical properties of aerosols (aerosol concentration and its variation over time, particle size distribution, dynamic behavior of aerosol, the diffusion, mobility and drift velocity of particles, and also the limits of environmental humidity which allow the formation of condensation nuclei), for a better understanding of their involvement in microclimates [5, 15, 16, 19].

In order to determine the concentration, granulometry, volume and lifespan of the negative saline aerions (solions) inside the halochamaber have been corroborated two instrumental methods: laser optical particle counter and differential conductometry.

Laser particle counter method

Solions concentration represent the number of particles per unit volume. Usually, numerical concentration of all aerosol particles is equivalent to the number of Aitken particles per unit volume, as the number of medium and large particles is insignificant in comparison with Aitken particles [5, 15, 16]. Measuring the concentration of particles can be made using laser optical device, known as SIBATA GT 321 particle counter (Fig. 1).

Fig. 1. *SIBATA GT 321 – the particle counter.*

The particle meter SIBATA GT 321 allows the following determinations grids: number of solions between 0 and 10^8 particles/m^3; size range (particle diameter): 0.3; 0.5; 1.0; 2.0 and 5.0 μm; operating temperature range for the halochamber: 0 – 50ºC; aerosol gas flow processed: 2.83 L/min.

The particle counting method, the only available "in situ" method of analysis, which allows verification of conductometric method, has a number of disadvantages, on one hand due to calculus errors, and secondly because of the presence in the halochamber of other particle types [15, 16].

Method using the differential conductometry

The disadvantages mentioned can be eliminated by using, to determine NaCl discreet concentrations in gaseous environments, the differential conductivity technique, using a set of glass devices (Fig. 2) for aerosol bubbling through suction, with flows controlled by rotameters, each having an adjustment/filling of the bubbling volume with de-oxygenized and tridistilled water and a set of electrodes transducers (conductive and temperature compensating) encapsulated within a standard cell amde of rigid plastic, integrated to a differential analysis installation (Fig. 3), and coupled to a digital conductometer, also endowed with a computer interface [23]. In the analysis equipment chart, a C833 Conductometer has been used, made by CONSORT Belgium company, and it has the following functional characteristics: pH range: -2 ... +16; potential range: ±2000 V; conductivity: 0 ... 2000 mS/cm; resistivity: 0 ... 200 MΩcm; salinity: 0 ... 100 g/L; temperature: 0 ... 100ºC [5, 15, 16].

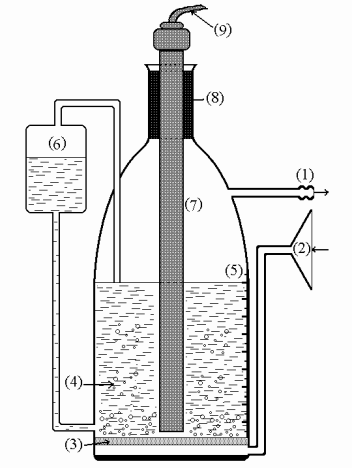

Fig. 2. *Glass bubbler aerosol generator, with enclosed transducers:*
1 – extension to the vacuum pump; 2 – aerosol intake funnel; 3 – bubbling dissipator;
4 – solution under analysis; 5 – indicator for solution volume; 6 – system to adjust /complete the volume of the bubbler with tri-distilled and de-oxygenized water;
7 – electrodes transducers encapsulated in a rigid plastic sheath, type standard cell;
8 – rubber stopper for encapsulated electrodes and sealing device;
9 – connection conductor to the digital conductometer.

Fig. 3. *General view of the laboratory analysis Equipment by differential conductometry.*

Differential analysis equipment is based on the chart in Fig. 4.

Branches I and II of the equipment allow parallel measurements while branch III permits to determine basic conductometric variations of the air lacking NaCl and being retained by the washing recipients (5) and (6). The flow in all three branches has been equally adjusted by taps (2a, 2b and 2c) and flow controllers (3a, 3b and 3c) VEB MLW Prufgerate – Werk Medingen Sitz Freital, type LD, while the air containing solions has been further bubbled by sucking it in a volume of 10 cm^3 of three-distilled and de-oxygenized water (through washing it with a purified argon stream). During the bubbling process, any aerosol emission from the capsule into the tank (halochamber) is closed. After the bubbling process, the NaCl saline charge of the aerosol is retained by the tri-distilled and de-oxygenized water inside the glass device. After a bubbling time pre-set between 10 and 60 minutes, the conductivity variation of the solution inside the three glass devices (4a, 4b and 4c) is measured [5].

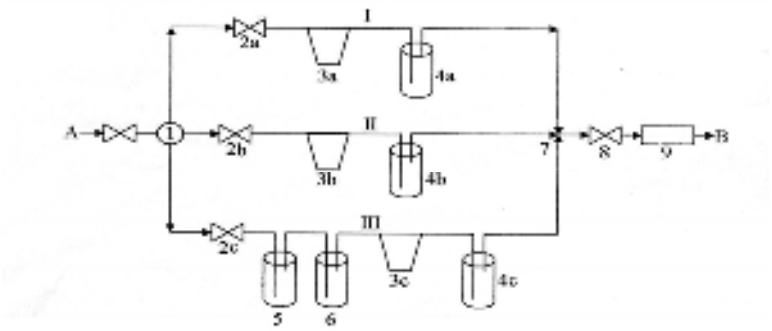

Fig. 4. *Operating chart of the analysis equipment: I, II and III – branches or routes; A – gas intake point; B – gas discharge; 1 – distributor; 2 (a, b and c) – flow taps; 3(a, b and c) – rotation meters or manometers; 4 (a, b and c) – glass devices for bubbling aerosol generator; 5 and 6 – additional recipients for restraining NaCl solions; 7 – differential collector; 8 – final tap; 9 –vacuum pump.*

4. The impact of internal microclimate on human body

Internal microclimate factors (temperature, atmospheric humidity and pressure, natural/artificial light, air currents, turbidity etc.) can affect both reliability and conservability of goods from the respective enclosure, as well as humans who work or are cured inside. Temperature, the most important climate factor, by its fluctuations, can influence environment humidity, especially in the cold season. High temperatures lead to lower relative humidity, while temperature with short fluctuations can cause in time to the phenomenon of exudate and dew on the cold walls, leading to efflorescence activation and mold, the atmosphere becoming thus unfit for some activities, particularly inside halochamber [3, 13, 19].

The atmospheric humidity in the enclosed spaces of halochambers and sport systems must be always maintained at values of 50-65%, while temperature should be between 18 and 22°C (fluctuations must be ± 3ºC, to seek an adjustment of the microclimate factors).

Between the effects of environment temperature increase there are also some aspects of human health (especially people with heart or lung diseases) resulting in increased mortality due to heat and boosting carriers of infectious diseases (high temperatures allow the development and spread of certain diseases and viruses), and increased seasonal production of pollen or other allergen nanodispersions.

The quench of the body by air bath, sun, aerosols etc. may increase the body's resistance, not only to bad weather, but also to gas agresivity, dust and infectious diseases. Among the diseases that negatively affect the human body as a result of the decrease of its resistance to natural environmental factors, there are the ENT (rhinitis, sinusitis, laryngitis, tonsillitis etc.), pulmonology/respiratory

(asthma, bronchopneumonia, silicosis etc.) and cardiac. Decreasing of the body's resistance, following a insufficient quench tells his word especially in young ages, in children and the elderly, clean air movement or in negative aerosls being beneficial for the proper functioning of the heart and lungs. Increased morbidity of people suffering from an inflammatory lung disease such as asthma or bronchitis, is associated with increased pollution [10].

Pursuit of sporting activities in saline aerosol environments helps to quench the body.

Starting from the undeniable benefits of speleotherapy, it has sought creating microclimates to "simulate" the conditions in the mine. Artificial saline (halochambers) became a convenient and considerably cheaper alternative to natural ones. Both the natural and the artificial saline aerosols used in therapy lead to improved quality of life. Halotherapy/salinotherapy is a very simple process of treatment, by no means not involving the administration of medicines or food supplements, diet or bed rest. Yet, how simple is the process, the more complex the mechanism of salt in the body. Halotherapy involves on the one hand, respiratory inhalation of saline aerosols, and on the other hand, their absorption through the skin. Negative ion charge neutralizes the positive charges caused by tobacco smoke, or electrosmog, thus restoring balance in the body. Salt is an essential element in the functioning of the body, and has multiple local effects. Salt therapy, as a natural therapy, has many advantages, including fast action and high salt concentration, which has no contraindications [4, 10, 25-29].

In order to use a solion environment there are needed information on solion lifetime, solion size distribution and concentration, processes for obtaining artificial solions, solion characteristics and their therapeutic applications. Stringent control of concentration and dimensional distributions of solions in the halotherapy environment is very important for the medical effect of various respiratory diseases treatment and for creating an environment of "clean air" [4, 15, 16]. Depending on the solions concentration, saline areas can have both therapeutic effect (in case of high concentrations of NaCl solions of 1-6 mg/m³ in the stationary during 1-4 hours) and a prophylactic one (concentration of NaCl is 1 mg/m³, but with a longer presence, 8-16 hours per day).

To determine the role of therapeutic or prophylactic of saline areas is necessary the knowledge and application of methods and techniques for determining structural-functional solion characteristics from saline environments.

In the exploitation of natural halochambers - salt mines, there are used measuring devices for determining and verifying micocroclimate parameters, but also those used in solions characterizing. Measurement of underground caverns resulted from salt mining is done using sonic cavernmeter. This device helps to determine the level/depth, shape and size of enclosures and galleries, by measuring the time required for directional beams of sound pulse from a transmitter into the probe to the mining room wall and back to the sender. It is necessary to know the shape and size of the chamber for driving the aeration process, activation of solions and reaching the optimal concentration etc.[12, 24].

In order to determine the chemical composition of air in salt mines, samples are taken resembling to the artificial halochambers, to include fresh air circuit from entrance to exit.

Time-keeping device for prelevation is 30 minutes in each sampling point, average results of minimum five measurements and analysis being recorded. Following measurements and qualitative analysis of air samples saline air characteristics are determined, namely the NaCl concentration.

Solions and general aerosols characteristics are determined by the source, but also by environmental factors. Among the functional characteristics that describe a solion source are mentioned: size and aerosol density, particle formation rate, the flow source, gaseous environment enrichment factor, the lifetime of aerosols particles.

Both the size and density of aerosol and particle speed formation and flow source, are depending on obtaining processes or technologies, on the compositional characteristics of saline solutions, namely on the nature and pressure of the gas dispersed. Lifetime and concentration of aerosol particles in the environment are determined by reliability of sources and the dynamics of aerosol particles. The most important characteristic for therapeutic applications and air conditioning is the flow source, which is expressed by Aitken and medium particle concentration produced per unit time (seconds).

For Aitken particles, their lifetime vary between 12 and 72 hours, depending on environmental factors, and for medium and large particles lifetime can vary up to several weeks. Depending on the lifetime and on the source flow, there can be achieved certain levels or thresholds of chemical load, characterized by an optimal enrichment factor (the two gives a measure of stability and uniformity to the microeterogenous dispersed system) [9, 10, 14-16, 18].

NaCl solions composition can change due to interaction with atmospheric humidity and other particles or gases in the atmosphere, coagulation processes taking place, peptizing, condensation or sedimentation.

Also illuminating radiation can influence the composition and physical microstructure of particles for co-assisting systems with other salts, such as

potassium, calcium or magnesium chloride and sodium or potassium iodide [9, 10, 14, 18].

For the characterization solions, together with the three variables: number, volume and total surface of particles, there are involved other parameters, such as: solions concentration and its variation in time under the influence of coagulation, peptization, condensation or settling processes etc.; solions dimensional distribution, the degree of electrostatic charge of the surface (measured through the distance between solions in liquid dispersed systems); degree of hydration, the dynamic behavior of solions, diffusion, mobility and speed drift of them; environmental humidity limit at which begins the condensation nuclei formation [9, 10, 14, 18].

Usually, numerical concentration of all aerosol particles is equivalent to the Aitken particles number per unit volume, as the number of medium and large particles is insignificant in comparison with Aitken, that can be easily measured with meter or particle laser beam counter.

In case of air-conditioning systems, for therapeutic and environmental purposes, an important parameter of variation is the size distribution of solions. The study by Whitby [30] on dimensional distributions obtained by several methods (optical meter, electric mobility and relaxation room) led to the fact that the dimensional distribution is composed of three log-normal Gauss curves (areas with characteristic behavior for a given global distribution and generally corresponding to different chemical compositions, whether due to different sources of generation, or to the influence of disruptive exogenous factors).

Solions dynamic behavior characteristics were the subject of a study conducted by Hidy and Brock [29] who concluded the following: particle sedimentation rate varies over time, the ratio of inertial forces and viscous forces is small (inertial effects of the movement of particles can be neglected) there is a significant Brownian motion of particles, particle surface is large compared to their volume.

These features have microphysical and nano-structural specific meanings, because they are based on both diffusion and sedimentation processes and coagulation, condensation and deflocculation physico-chemical processes.

Another feature of the solion is environment humidity limity in the formation of condensation nuclei. Condensation and deflocculation processes of the microparticles of salt depend on the nature of salt, on its total mass, the degree of solubility and the environmental conditions (nuclei formed on aerosol particles consume large amounts of water vapor in the environment, causing a decrease in the supersaturation and relative humidity values).

Saline environment, therapeutic by its constant climate in terms of thermo-hygro-baric is free from air currents and polluting products, with a minimum concentration of microorganisms and antibacterial properties.

The speleotherapeutic cure has a mucolytic effect, antiinflammatory, hypo-sensitizing, activation of the hemostatic effects mechanisms that assure resistance to microorganisms, to different allergens, and an immunomodulating effect. It is known that it is much easier to help avoid disease than to treat it. But nowadays it's hard to breathe clean air in cities, given the pollution that surrounds us.

In order to be able to do this, a trip to the mountains or the sea is necessary (which is not always available because of cost or lack of free time) or purchase a device that brings freshness and purity of mountain air, neutralizing the positive ions emitted by electronical devices (computers, televisions, radios etc.) [3, 17].

5. Conclusions

Monitoring environmental pollution is an activity that falls within the requirements of both the business companies and labels in the category of point polluters, and the institutions empowered to determine and prevention of pollution risk and those concerned with hygiene and public health, and also the safety and security at work.

From this point of view we distinguish two ways of involvement of the monitoring methods and techniques, namely: determining the degree of environmental pollution and the sources affecting air, water and soil and atmosphere that characterize the work premises, for habitat and halotherapy, establishing on one hand the concentrations of generating noxes cumulated "in situ" and on the other hand the levels of aerosols involved in prevention and treatments.

To determine the role of preventive or prophylactic aerosol spaces is necessary to apply specific methods and techniques, for determining structural-functional characteristics of halochambers and solions.

The therapy of respiratory diseases, the improving cardio-respiratory parameters and psycho-neuromotor system of human subjects requires a strict control of concentration and particle size distribution of aerosols halochamber.

Determining of concentration, granulometry, volume and lifetime of solions in halochamber can be achieved by corroborating two instrumental methods: the particle counter based on a laser optical system and differential conductivity.

References

[1]. Barnea, E. - *Effects of air pollution on the respiratory in children*, Medical Publishing House, Bucharest, 1978.
[2]. Ciplea, L.I., Ciplea, Al. - *Environmental Pollution,* Technical Publishing, Bucharest, 1978.
[3]. Sandu I., Chirazi M. - *Sports Systems Ecology,* Ed Performantica, Iasi, 2010.
[4]. Sandu I., Atyim P., Sandu I. C. A. - *Complements of descriptive chemistry*, Ed Dacia, .
[5]. Sandu I., Chirazi M., Canache M., Sandu G.I., Alexeianu M.T., Sandu V.A., Vasilache V. - *Research on NaCl saline aerosols II. New artificial halochamber characteristics*, Environmental Engineering and Management Journal, vol. 9, nr 8, (2010), pp. 1105-1113.
[6]. Sandu, I., Canache, M., Vasilache, V. - *The Role of Salt Solins on Human Subjects*, Present Environment & Sustainable Development, 5, (2011), p.57-64.
[7]. Sandu I., Poruciuc A., Alexianu, M., Curcă R-G., Weller O. - *Salt and Human Health: Science, Archaeology, Ancient Texts and Traditional Practices of Eastern Romania*, Mankind Quarterly, 50, 3-4, (2010), pp. 225-256.
[8]. Sandu I., Alexianu M., Curcă R-G., Weller O., Pascu C. - *Halotherapy: From Ethnoscience to Scientific Explanations*, Environmental Engineering and Management Journal, vol. 8, 6, (2009), pp.1331-1338, Cluj-Napoca, 2002.
[9]. Chernova, O., Matiushina, S, Volianik, M. - *The dinamics of the persistence characteristics of a speleotherapy mine*, Zh. Mikrobiol Immunobiol, 3, (1996), pp 78-80.
[10]. Chervinskaya, A.V., Zilber, N.A. - *Halotherapy for treatment of respiratory diseases*, Journal of aerosol medicine: deposition, clearance, and effects in the lung, 8, 3, (1995), pp. 221-232.
[11]. Căluianu, S. - Measurement and control of air pollution, Matrix Rom Publishing House, Bucharest, 1999.
[12]. **Deák, E., Deák, G., Aurelian, F., Găman, M.** - Techniques to control and prevent environmental pollution to the mines in Romania, Universitas Publishing House, Petrosani, 2007.
[13]. Sommer, K., Wünsch, K.H., Zettler, M. - Compediu chemistry, ALL Publishing House, Bucharest, 2000.
[14]. Sandu I., Pascu C., Sandu I.G., Ciobanu G., Vasile V. - Ciobanu O., *The obtaining and characterization of NaCl nanocrystalline dispersions for saline – type therapeutical media. I. Theoretical aspects*, Revista de Chimie, 54, 10, (2003), pp. 807-812.
[15]. Sandu I., Pascu C., Sandu I.G., Ciobanu G., Sandu A.V., Ciobanu O. - *The obtaining and characterization of NaCl nanocrystalline dispersions for saline – type therapeutical climate. III. The evaluation of the SALIN device reliability*, Revista de Chimie, 55, 11, (2004), pp.971-978.
[16]. Sandu I., Pascu C., Sandu I.G., Ciobanu G., Sandu A.V., Ciobanu O. - *The obtaining and characterization of NaCl nanocrystalline dispersions for saline – type therapeutical environments. II. The in situ analysis of saline room aerosols,* Revista de Chimie, 55, 10, (2004), pp.791-797.
[17]. Sandu I., Pascu C., Vasile V. - *Obtaining of dry mixt aerosols for therapeutical environments*, Haloteherapy, Adjuvant Therapy in the Treatment of Respiratory Disorders, http://saltmed.blogspot.com/, 13, (2006), 4, pp.15–19.
[18]. Sandu I., Chirazi M., Canache M., Sandu G.I., Alexeianu M.T., Sandu V.A., Vasilache V. - *Research on NaCl saline aerosols I. Natural and artificial sources and their implications*, Environmental Engineering and Management Journal, vol. 9, nr 6, (2010), pp. 881-888.
[19]. Ştefan, S. - *Atmospheric aerosol physics,* ALL Publishing House, Bucharest, 1998.
[20]. Sandu I., Canache M., Lupascu T., Sandu I. G., Sandu A.V. - *Surface Artificial Halochamber,* Patent MD4040(B1)/2010. 05.31.
[21]. Sandu I., Stirbu C., Chirazi M., Stirbu C., Sandu A. V. - *Surface Artificial Microsalt Mine,* Patent MD4039(B1)/2010.05.31.
[22]. Sandu I., Stirbu C., Lupascu T., Chirazi M., Stirbu C., Sandu A. V. - *Artificial Surface Halochamber",* Patent MD4089(B1)/2011.01.31.
[22]. Pascu, C., Sandu, I., Ciobanu, G., Sandu I.G., Vasile, V., Ciobanu, O., Sandu, A. V., Pascu, A. - *Method and Device for Determining Saline Aerosols "in situ"*, Patent RO122232/27.03.2009,
[23]. Mulholland, G.W., Hartman, A.W., Hembree, G.C., Marx, E. and Lettieri, T. R. - *Development of a One-Micrometer Diameter Particle Size Standard Reference Material*, Journal of research of the National Bureau of Standards, 90, (1985), pp. 3-26.
[24]. Pascu C. - *Procedure and Devices for the Controlled Obtaining of Dry Saline Aerosols with Therapeutic Effect and Air Purification*, Patents WO03024568(A2)/2003.
[25]. Pascu C. - *Procedure and devices for the controlled obtaining of dry saline aerosols with therapeutic effect and air purification*, Patents RO120787(B1)/2006.
[26]. Pascu C. - *Procedure and devices for the controlled obtaining of dry saline aerosols with therapeutic effect and air purification*, Patents RO121371(B1)/2007.
[27]. Pascu C. - *Procedure and Devices for the Controlled Obtaining of Dry Saline Aerosols with Therapeutic Effect*, Patent WO2008060173 (A2)/2008.
[28]. Pascu C. - *Process and Device for Intensive Generation of Dry Aerosols with Therapeutical Effect*, Patent RO122128 (B1)/2009.
[29]. Hidy, G.M, Brock, J. R. - *Topics in Current Aerosol Research*, International Reviews in Aerosol Physics and Chemistry, vol. I, Pergamon Press, London, 1972.
[30]. Whitby, K. T. - *The physical characteristics of sulphur aerosols*, Atmospheric Environment, 12, (1978), pp. 135-159.

THE ANNALS OF "DUNAREA DE JOS" UNIVERSITY OF GALATI.
FASCICLE IX. METALLURGY AND MATERIALS SCIENCE
N^0. 2 – 2011, ISSN 1453 – 083X

Cu-Ag-REAR METALS FOR WIRES: PROCESSING AND CHARACTERISATION

C. IORDACHE[1], M. STOICA[2], S. MOHSEN[2], M.VLAD[1]
[1] Dunarea de Jos University of Galati, Romania
[2] IFW Dresden, Germany
email: Cristina.Iordache@ugal.ro

ABSTRACT

Cu based alloy microalloyed with rear metals (RM) (in our case, sample with Nb) for wires were prepared by two different techniques arc-melting and mechanical alloying. Microstructure characterisation was carried out by SEM including EDX and X-ray measurements. Mechanical measurements at room temperature were performed and the results of materials obtained by different techniques are analised.

Nanocristaline microstructure it was observed and this is associated with fine graine refinament of CuAgRM material after both technologies.

KEYWORDS: Cu based alloy; arc-melting; mechanical alloying; microstructure; microhardness

1. Introduction

Cu based alloy microalloyed with Nb was produced using preparation conditions typically applied for manufacturing of bulk metallic glasses (BMGs) which is prepared by arc melting (AM) with cold drawing [1] and similar composed alloy prepared by powder metallurgical (PM) technique in order to study the microstructure and the mechanical properties

In the first technique called „in-situ" thermodynamical aspects and kinetic limitations on the specific solidification process of phase formation and it is strongly dominated by controlled diffusion mechanism [2]. A distribution of Ag dendrites in the Cu matrix can be achieved by casting. During cold drawing the Ag dendrites are deformed to fine filaments.

The second techinque, PM is a new one which combine powder metallurgy, heat treatments and deformation mechanism. Some advantages of this technique are known: the microstructural features to be developed are independent from the size of sample. In this case, almost any geometry of the sample can be obtaine depending only on the equipment that is used.

In the last period some studies shown remarkable advances have been made in the development and comprehensive understanding of Cu-Nb alloys, used for wires. Such wires can be produced by casting with a logarithmic strain η=15 and leads to a finally obtained cross section of wire with 0.2 mm depending on their forming ability [3].

To outstanding the mechanism and the mechanical properties of Cu-Ag-RM alloys, one short description about the material obtained by arc melting and similar material obtained by PM, it will be presented in this work.

However, there are no detailed informations about the manufacturing of the materials because there are a substantial difference between sample preparation under clean laboratory conditions using high purity elements and in small quantities for wires preparation.

Consequently, the aim of this paper was to prepare and to investigate a common Cu-Ag-RM composition under optimum conditions concerning the cooling rate for special phase formation and the purity of the elements in different techniques to avoid unpredictable effects and to compare the microstructure and the mechanical properties of this before preparring wires from them [4, 5].

The conditions that we used here are typically used for obtaining wires with very good properties.

2. Experimental procedure

2.1. Arc-melting technique

A 50 g ingot of this alloys with nominal composition Cu−7Ag-0.05RM (at.%), with RM = Nb,

and purity > 99.9 wt.% for all elements, were prepared by arc melting in argon atmosphere. The ingots were remelted several times in order to achieve a homogeneous master alloy. From these ingots, cylindrical bulk samples with 2.5 mm diameter and 70mm length were prepared by centrifugal casting device in copper mould casting.

The structure of the samples was studied by X-ray diffraction (XRD) using a Philips PW 1050 diffractometer (CoK-radiation) and optical microscopy. Scanning electron microscop equipped with an X-ray spectrometer were employed for detailed microstructural analysis.

The microstructure was imaged using conventional SEM. The test conditions to figur out the mechanical properties should be the same like those typically used for cristaline material [6]. Measurements of mechanical properties were performed at room-temperature and quasistatic conditions. According to the ASTM standard for micro hardness testing, cylinders with a length/diameter ratio of 2.5mm diameter were prepared from the cast samples. The specimens were tested with an SHIMADZU maschine. The conditions of microhardnes measurements according to Vickers HV 0.01 were: compressive force 10 N, time of load 10 s. Data obtained from microhardness testing machine were evaluated by software LECO.

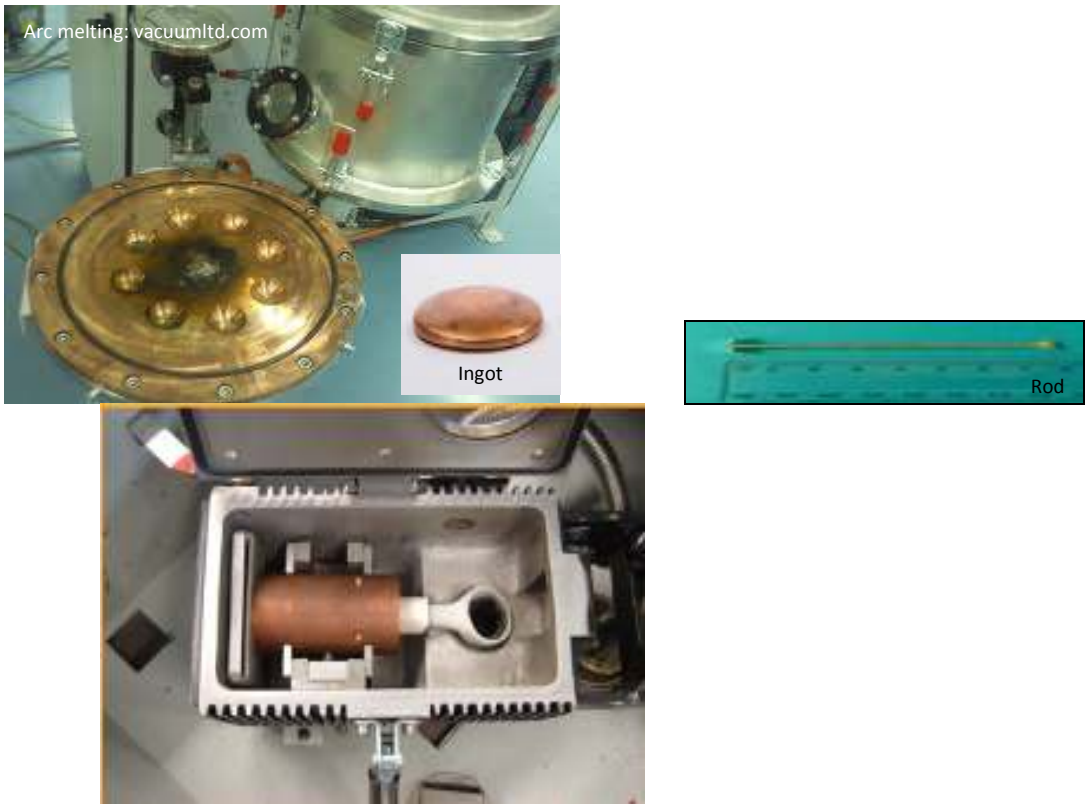

Fig.2. *Arc melting for preparring ingot and centrifugal casting for preparring rod of Cu7Ag 0.05Nb.*

2.2. PM technique

Milling experiments starting from pure elemental powder mixtures (purity >99.9 wt. %) with nominal compositions Cu−7Ag-0.05RM (at.%), with RM = Nb and Cu, Ag were performed using a Retsch PM400 planetary ball mill and hardened steel balls and vials. No process control agent was used.

The powders were milled for 30 h with a ball-to-powder mass ratio (BPR) of 13:1 and a milling intensity of 200 rpm cooling by liquid N_2 at liquid nitogen temperature (77K) [7]. To avoid or minimize possible atmosphere contamination during milling, vial charging and any subsequent sample handling was carried out in a glove box under purified argon atmosphere (less than 1 ppm O_2 and H_2O). The phases and the microstructure were characterized by X-ray diffraction (XRD) using a Philips PW 1050 diffractometer (CoK-radiation). The alloying was performed until complet solid solution of Ag and Nb within the Cu matrix has been achieved.

The microstructure of the alloys was investigated by electron microscopy using a high-resolution scanning electron microscope (REM LEO 1530) with energy dispersive X-ray analisis (EDX) after diferent time of milling. From the SEM micrographs the size of the alloying particles as well as the aspect ratio of the Nb filaments after

deformation were determined. The latice structure and the lattice constants (at room temperature) as well as the phase purity of the sample were investigated with an X-ray difractometer (Philips, PW 1830) in Bragg Bretano geometry using Co radiation. Based on the X-ray data the average grain size of Cu matrix was determined using Sherrer eqution and Williamson-Hall plot. Microhardnes by Vickers was performed by SHIMADZU maschine at room-temperature and quasistatic conditions.

Fig. 3. *Retsch maschine and steel vials for preparring mixted powder of* ***Cu7Ag 0.05Nb*** *for compressed rods.*

3. Results and discussions

By arc-melting, CuAg forms a simple eutectic phase diagram with limited solubility. At binary Cu-7Ag alloy are detected two phases, namely a saturated Cu(Ag) solid solution and regions which show a reduced amount of Cu in comparison to the matrix. This situation changes for the Cu-7Ag-0.05Nb alloy.

The addition of Nb leads to a slower decomposition reaction which in this case is found to be only continuous.

The grain boundary it was modify by the addition of a insoluble element like Nb.

This suppresses the diffusion along the grain boundary and hence enhances the formation of continuous precipitates [8]. Because of the specific solidification conditions in the arc-melter (relatively high cooling rate) and the particular composition with high carbon content a phase formation it can be obtained. The reasons for the astonishing ductility of the arc-melted Cu-Ag alloy are likely manifold, which together give the capability for plastic deformation.

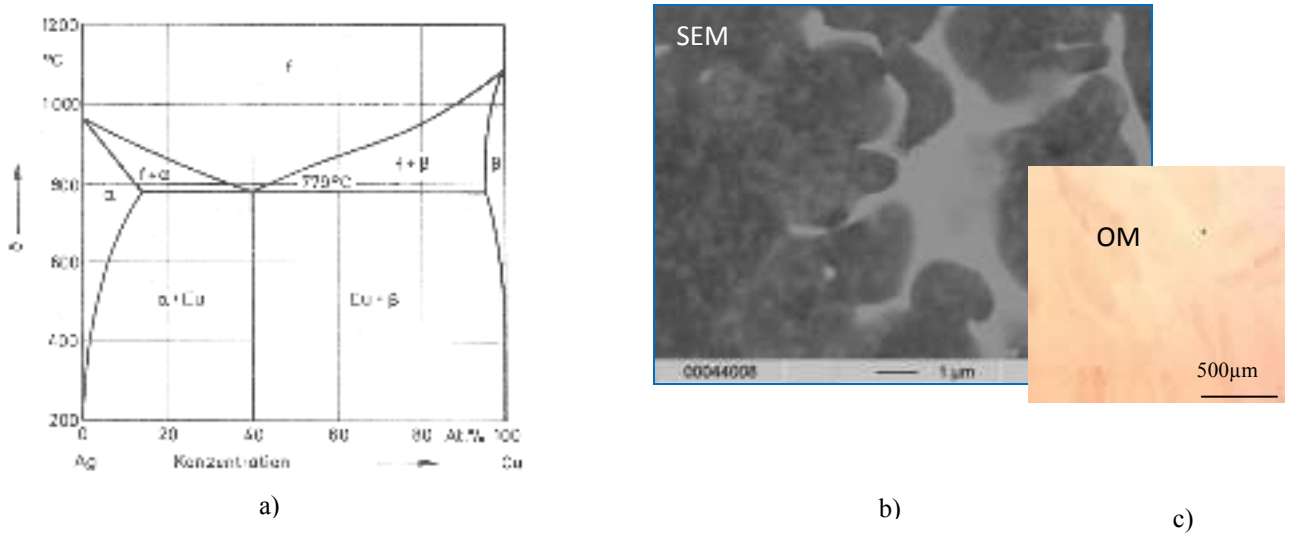

a) b) c)

Fig.3. *Phase diagram (a) of CuAg and precipitation modes as well as structure (c) and microstructures (b) of Cu7Ag 0.05Nb by arc melting with discontinous precipitates (80-100HV).*

Composition profiles measured by EDX (Fig. 3-b) show that the chemical composition frequently changes within a short distance (about once per 1μm), indicate the formation of different very finely dispersed phases, which give the material its high strength and large ductility. Copper based materials leads to distinctively values of microhardnes in surface.

At the second technique it was observed an intense mechanical alloying among all three phases (Cu, Ag, Nb) because of the high energy of ball milling. During milling time Nb shows a negligibly solubility in the solid state and it was observed niobium partly dissolves in the copper lattice during milling (fig. 4) [6].

The present investigation demonstrates that this solubility can be improved to a strongly supersaturated Cu solid solution provided the appropriate mechanical alloying method is applied, by cryomilling. Scanning electron microscopy reveal a homogeneous single-phase microstructure after more then 10 hours of milling.

Elemental Nb could no more be detected, indicating the formation of a metastable supersaturated Cu-Nb solid solution.

Cryomilling time influences the the graine size of elements and their miscibility. After cryomilling the structure of powder mixed is uniform. Microhardness increase with number of hours milling. (Fig. 5).

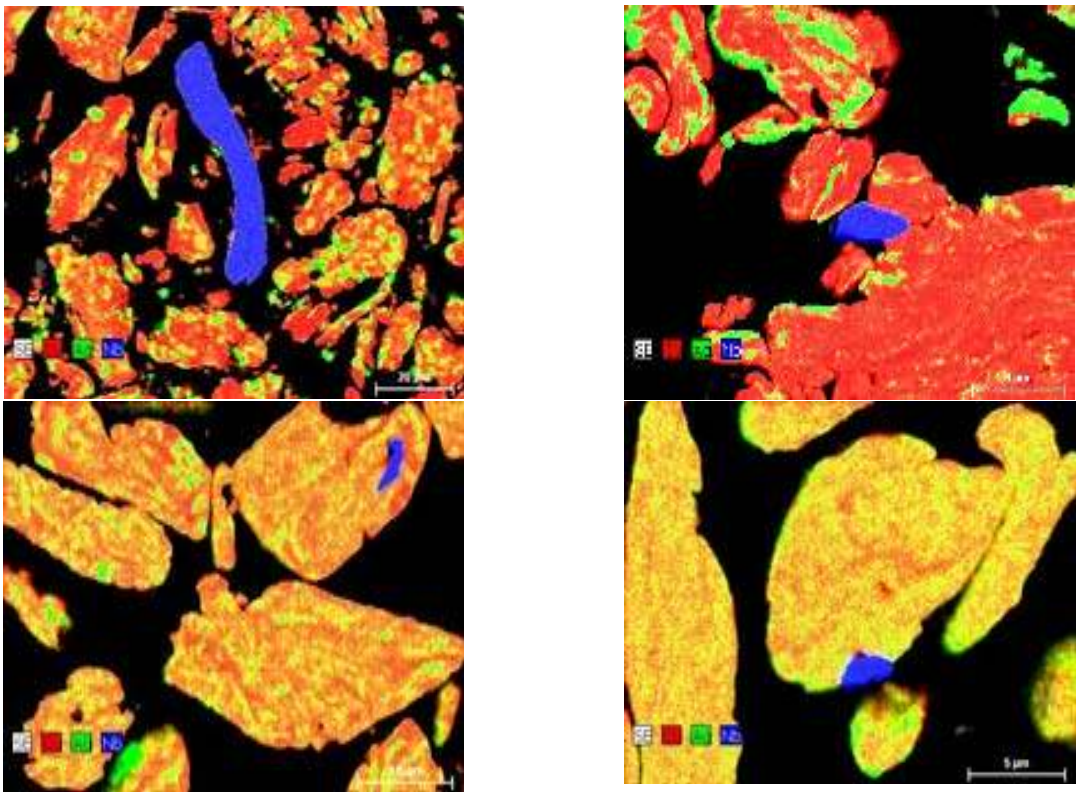

Fig. 4. *SEM study of microstructure of Cu-7%Ag-0.05%Nb powder with mechanical alloying after 1h (a), 3h (b), 5h(c) and 10h(d) milling time.*

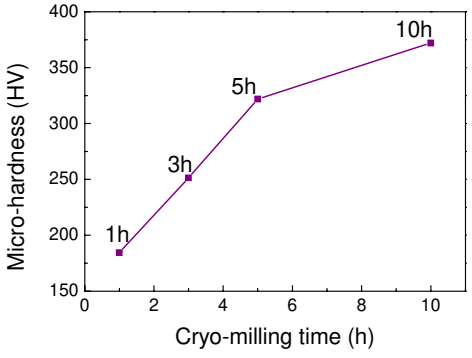

Fig. 5. *Room-temperature microhardness curves for CuAgNb mecahnical alloying samples. The inset shows how increas cryomilling time with microhardness curves of the alloy.*

4. Conclusions

Conventional cast metallurgy cannot be applied on a large scale. Manufacturing of alloys from immiscible metal system can be carried out by using the following two techniques: rapid solidification (RS) and mechanical alloying (MA). By RS a fine distribution of two phases can be produced, but the formation of solid solution with a high content of the alloyed element is not possible. In contrast, by mechanical alloying, alloys with better homogeneity and a higher content of the alloyed element in solid solution can be manufactured. Due the high energy impact during milling, the region of solid state solution extends and alloys with very high homogeneity in the microstructure can be achieved by the use of under the appropriate conditions. In conclusion, applying preparation conditions typically used for the fabrication of bulk metallic glasses to the manufacturing of the Cu based alloy, superior mechanical properties have been achieved, due to the formation of a cristaline structure, with a ductile phase and finestructured Nb filamentary phase.

Also the work hardening behaviour of the crystalline alloy made by PM is excellent. Therefore, the most important benefit of this material is its distinct of uniform distribution of fine Nb particles in Cu-Ag matrix with very good plasticity, which is, as is known, a strong requisite for engineering applications.

Comparing the microhardness properties of crystalline metallic alloys obtained after two different techiniques, arc-melting and PM, also the latter ones offer very interesting perspectives for novel applications as functional and structural materials for a variety of engineering applications when processed under appropriate conditions. This opens new opportunities for the "processing for properties" of advanced materials with superior properties.

Acknowledgements

My work is supported by EU Project SOP HRD – EFICIENT 61445/2009.

This work was possible because o cooperation between IKM-Dresden/Germany and University Dunarea de Jos, Galati/Romania.

References

[1]. V.I. Pantsyrnyi, A.K. Shikov, A.D. Nikulin, A.E. Vorobova, E.A. Dergunova, A.G. Silaev, N.A. Bel'akov, I.I. Potapenko, IEEE Trans. Magn. 32 (4) (1996) 2866

[2]. A. Inoue, T. Zhang, A. Takeuchi: Appl. Phys. Lett. 71 (1997) 464

[3]. E. Botcharova, J. Freudenberger, A. Gaganov, Materials Science and Engineering A 416 (2006) 261–268

[4]. X.H. Lin, W.L. Johnson, W.K. Rhim: Mater. Trans. JIM 38 (1997) 5

[5]. A. Gebert, J. Eckert, L. Schultz: Acta Mater. 46 (1998) 5

[6]. K. Werniewicz, U.Kuhn, N. Mattern, B. Bartusch, J. Eckert, J. Das, L. Schultz, T. Kulik: Acta. Mater. 55 3513 (2007)

[7]. S. Ichikawa, K. Miyazawa, H. Ichinose, K. Ito, Nanostruct. Mater. 11(1999) 1301

[8]. E.Bocharova, Ph.D. Thesis, TU Dresden, Germany, www.ifw-dresden.de/imw/theses/Dr Bocharova.pdf.

THE ANNALS OF "DUNAREA DE JOS" UNIVERSITY OF GALATI.
FASCICLE IX. METALLURGY AND MATERIALS SCIENCE
N^0. 2 – 2011, ISSN 1453 – 083X

EXPERIMENTAL STUDIES AND RESEARCH DURING HEAT TREATMENT ON THE BEHAVIOUR/AGING OF Al-Zn ALLOY SYSTEM WITH DIFFERENT Zn CONTENTS

Marian NEACSU, Elena DRUGESCU, Elisabeta VASILESCU
„Dunarea de Jos" University of Galati
email: uscaeni@yahoo.com

ABSTRACT

The paper presents the results of a research on the behavior at artificial aging heat treatment carried out on three different chemical compositions of the alloys belonging to Al-Zn system.

We studied the behavior of the three alloys after applying more thermal regimes during artificial aging. Following the experiments conducted, we can notice an increase in strength properties with increasing zinc content of the alloys investigated.

KEYWORDS: aluminum alloy, heat treatment, Zn content, microstructures

1. Introduction

The alloys studied in the Al-Zn system are aluminum alloys in the 7000 series, which, due to their special characteristics are used mainly in the aviation industry and machine building [7]. The alloys are deformable and hardenable by applying heat treatment and/or thermo-mechanical treatment. Some of them have mechanical properties comparable to copper-based alloys or to some brands of steels and even metallic titanium, but have the advantage that they have a much lower density.

For Aeronautical industry where alloys are subject to multidirectional service requests, they must provide an optimal combination of mechanical strength, plasticity, toughness, fatigue resistance and good resistance to stress corrosion.

To achieve this optimum level, it is necessary to replace the coarse grain structure obtained in the process of casting alloys and to amend fiber structure of semi-finished rolled products; they are decisive factors in order to achieve optimal properties.

Therefore the aim of the experimental research in this work was to obtain semi-finished products with a structure able to give the desired properties to the material.

Basic requirements for an aluminum alloy to be heat treated by quenching and artificial aging implementing solution are that they should allow in the equilibrium diagram phase transformations in solid state. Such a type of alloy is the one able to support an order-disorder reaction; the hardening which accompanies this process (similar to the precipitation hardening) is determined by the order-hardening reaction.

However, for this form of hardening conditions are quite strict so that the most important methods often used for alloys are based on precipitation from supersaturated solid solution and by eutectic decomposition. Precipitation reaction occurs following a decrease in solubility with temperature of solid solutions when there is a line of variation of solubility in the equilibrium phase diagram of the system [6], [7].

The breaking strength of Al-Zn-Mg alloy-Cu is even greater as the precipitates formed, which represent the hardening stage in the process of natural or artificial aging, are more numerous, finer and more dispersed in the basic solution mass (solid solution).

2. Experimental conditions

Experimental researches were conducted on samples of Al-Zn alloy, three chemical compositions shown in Table 1 and physical-mechanical characteristics in Table 2. Samples were processed in accordance with the technological scheme shown in Figure 1, showing the sequence of technological operations in the experimental variants adopted.

Table 1. *Chemical composition of researched alloys*

Element / Alloy	Zn	Mg	Cu	Si	Fe	Pb	Cr	Mn	Al
1 AlZn2.6Mg2	2.67	2.06	1.22	0.31	0.29	0.0025	0.06	0.47	rest
2 AlZn4.5Mg1	4.5	1.4	0.2	0.35	0.4	-	0.35	0.5	rest
3 AlZn5.7MgCu	5.76	2.61	1.55	0.15	0.19	0.021	0.19	0.10	rest

Table 2. *Physico-mechanical properties imposed by European norm EN 485-2-2007*

Element / Aliajul	Rm. [MPa]	$Rp_{0.2}$ [MPa]	A_5 [%]	HB
1 AlZn2.6Mg2	160	130	16	45
2 AlZn4.5Mg1	350	280	11	104
3 AlZn5.7MgCu	470	395	7	135

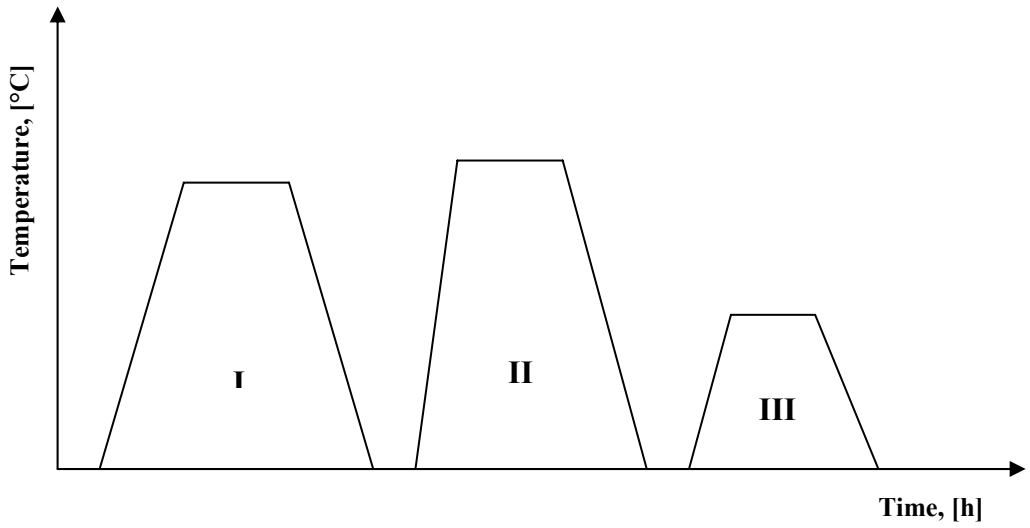

Fig. 1. *Technological scheme of realization of experiments*
I- homogenization; II- Solution quenching; III – artificial aging.

After the homogenization of ingots, corresponding to the three chemical compositions at a temperature of 480 °C and slow cooling in the oven, samples were cut from them which were heated to 500 C, maintained at this temperature for 120 minutes followed by cooling in water solution for implementing quenching in solution. As a result of structural changes, homogenization, improves alloys plasticity and unifies their final properties, leads to reduction of internal tensions and to changes in microstructure. In the first phase of homogenization some part of the $MgZn_2$ becomes Al_2CuMg while the other, unchanged, is dissolved in the mass of solid solution. The phase containing AlFeSi is partially transformed into Al_7Cu_2Fe. Mg_2Si compound undergoes small changes and slow cooling from homogenization temperature to room temperature leads to precipitation of $MgZn_2$

Solution quenching is intended to get the solid solution with maximum amount of alloying elements dissolved and to maintain this structure of homogeneous solution to the ordinary temperature. Aging of hardened alloys leads to decomposition of oversaturated solid solution with the appearance of secondary phases in a controlled dispersion and solid solution near the equilibrium. Type, size, distribution

and amount of precipitates particles in an alloy depend on temperature, aging time and the initial state of microstructure. [6], [7]

Artificial aging was performed at the following temperatures:120 C, 140°C, 160°C,180 C and 200 C and duration of maintenance: 4 hours, 8 hours, 12 hours, 16 hours and 20 hours for each temperature of aging.

3. Experimental results

The variation of some mechanical properties achieved after thermal /thermo-mechanical processing, according to the diagram in Figure 1 is illustrated in figures 2, 3, and 4 for alloy composition 1 (Table 1).

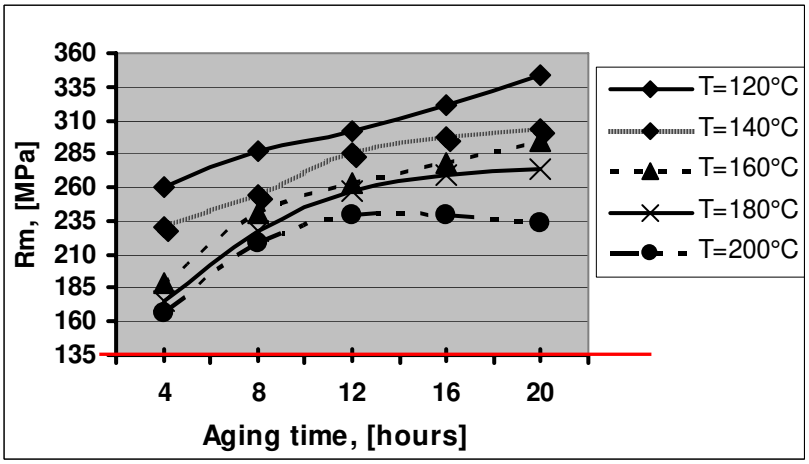

Fig.2. *Variation of mechanical resistance for an alloy based on the time of artificial aging.*

From Figures 2 and 3 we can see that for all times and all artificial aging temperatures studied, the values required by the Euronorm (160 MPa for Rm and 45HB) are met.

Mechanical resistance values as well as those of Brinell hardness increase as artificial aging temperature decreases and the maintaining time at these temperatures increases. For the temperature of 200 C it can be seen that the value of properties (Rm, HB) reaches a maximum for a maintaining time of 12 hours, after which both mechanical strength and hardness begin to decline.

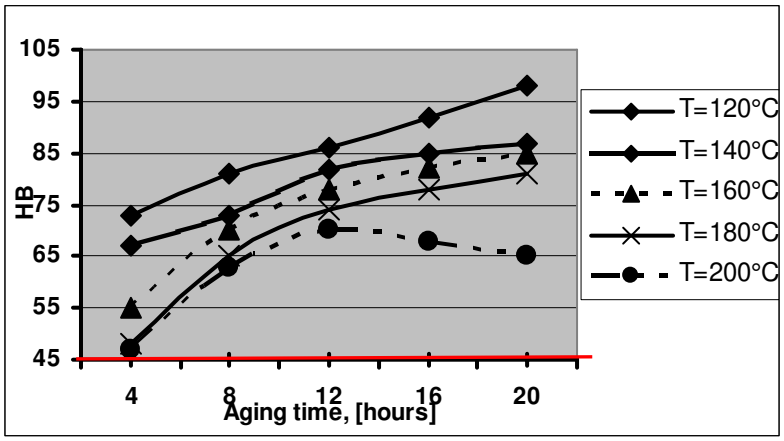

Fig.3. *HB hardness variation for alloy 1 according to artificial aging time.*

As Figure 3 shows, breaking elongation records values greater than or equal to the value required only for some artificial aging temperatures and times. For maintenance during 4 hours, only 160 °C, 180 C and 200 C lead to elongation values which satisfy the requirements. For maintenance times of 8, 12 and 20 hours, only the temperature of 200°C provides the samples with an elongation greater than 16% (fig. 4). For the retention time of 16 hours none of aging temperatures leads to an elongation of at least 16%.

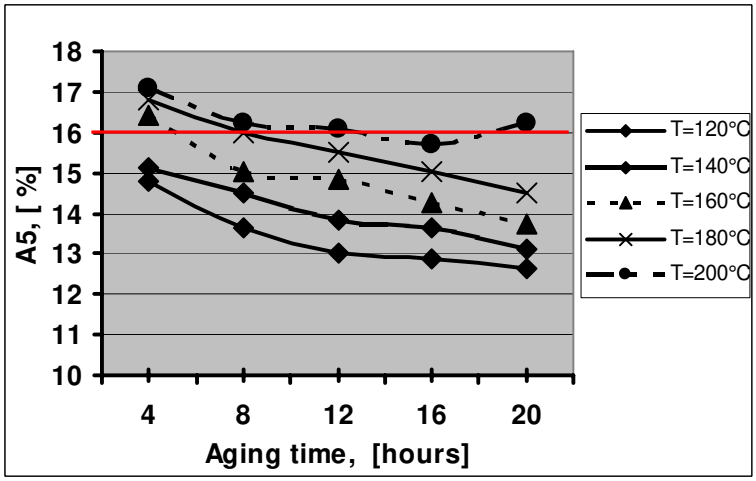

Fig.4 *Change in elongation at break for alloy 1 according to artificial aging time.*

For alloy 2, as shown in Figure 5, the strength as imposed minimum value is obtained for aging temperatures of 120°C and 140°C with maintenance times higher than 8 hours and at a temperature of 16°C with maintaining times higher than 16 hours. The minimum value required for strength is not achieved for temperatures of treatment of 180 and 200°C regardless of the maintenance time considered in these experiments. Figure 6 illustrates the results obtained for Brinell hardness in the case of alloy 2. For the temperature of 120 C at maintaining times of more than 8 hours, it is obtained the value imposed for the alloy to be used.

For the temperature of 140 C at maintenance times higher than 16 hours, it is ensured an HB value greater than the one imposed. This value, in case of artificial aging at a temperature of 160 C, is performed only during a maintenance time of 20 hours while for the other treatment temperatures studied we can see that it is not done.

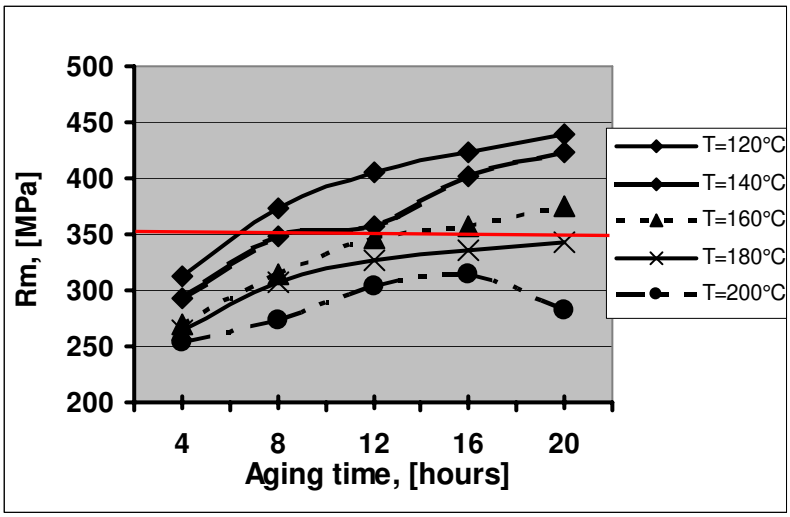

Fig.5. *Variation of mechanical resistance for alloy 2 depending on the time of artificial aging.*

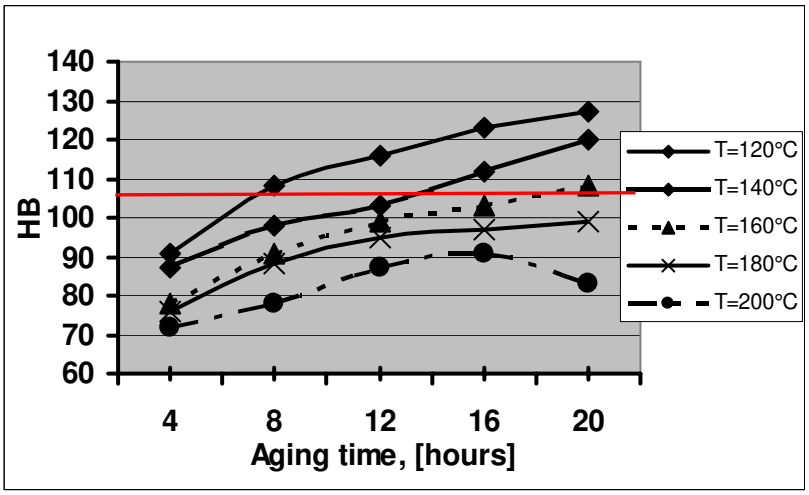

Fig.6. *HB for two alloy hardness variation depending on the time of artificial aging.*

From Figure 7, we can see that for elongation at break the value imposed by Euronorm is not made only for the temperature of 120°C during the maintenance of 16 to 20 hours. For alloy 3 experimental research results are shown in Figure 9 for strength, in figure 10HB hardness and in Figure 11 for elongation at break. Tensile strength has values over the rules imposed after artificial aging at a temperature of 120°C for all treatment times. For a temperature of 140°C, the limit value is exceeded for maintenance times higher than 8 hours, and for the temperature of 160°C this minimum value imposed is achieved only for maintaining times exceeding 16 hours. For other aging temperatures, regardless of the maintaining time, the value required by Euronorm is not obtained.

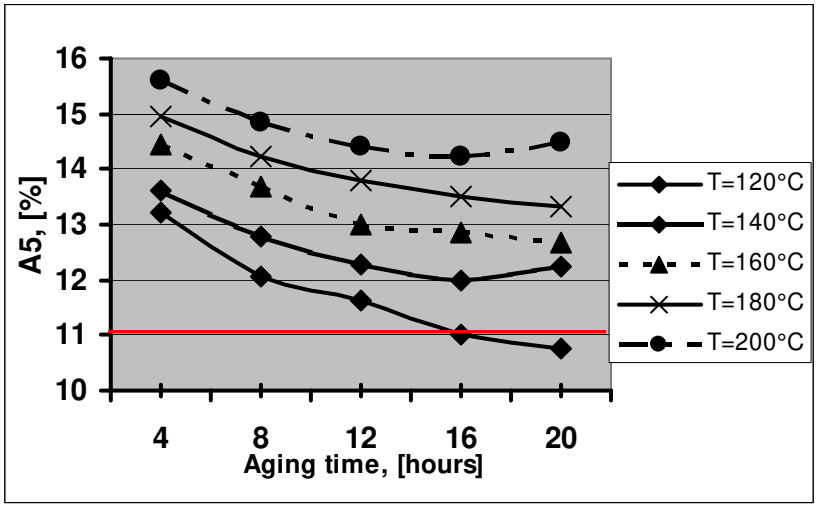

Fig. 7. *Change in elongation at break for alloy 2 depending on artificial aging time.*

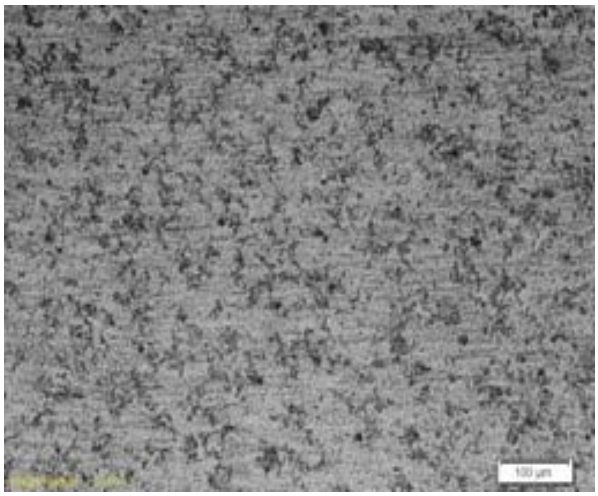

Fig.8. *Microstructure of alloy 2 aged artificially at a temperature of 120°C with a retention time of 12 hours (X100).*

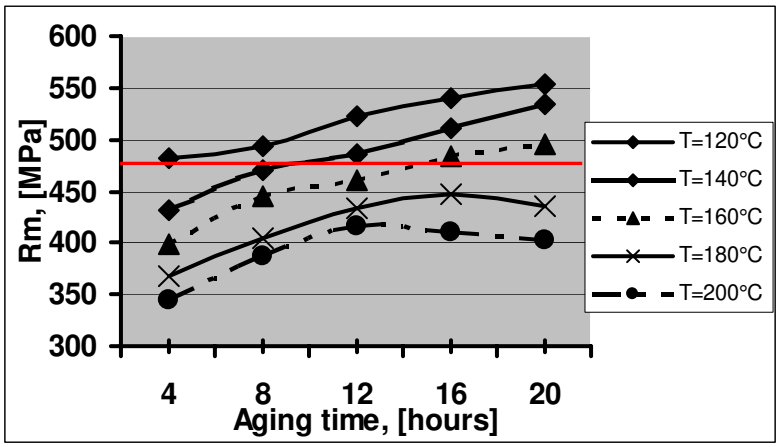

Fig.9. *Variation of mechanical resistance for alloy 3 according to the time of artificial aging.*

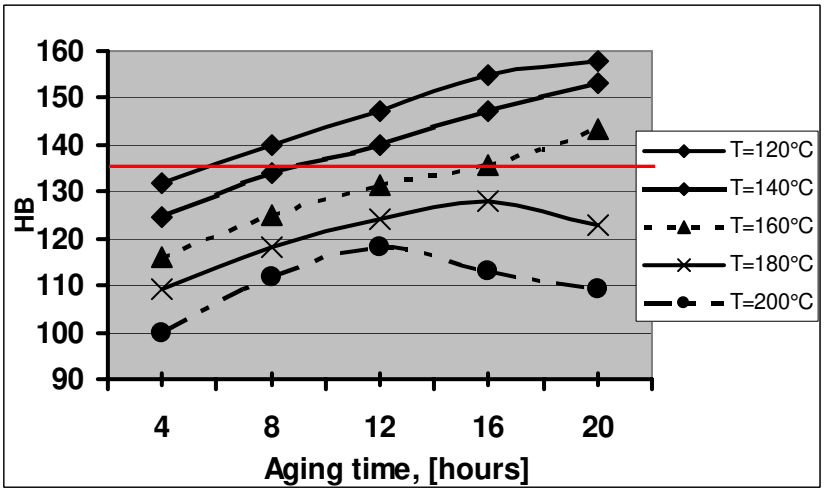

Fig.10. *Change in hardness for alloy HB 3 depending on the time of artificial aging.*

By analyzing the variation of HB in Figure 10, it can be seen that hardness varies similarly to tensile strength. The required value for hardness is not achieved at the artificial aging temperatures of 180 C and 200 C regardless of the maintaining time at these temperatures. The highest values were obtained for a temperature of 120°C for 20 hours. Elongation at break for alloy 3 obtained after artificial aging heat treatment (fig.11) was higher than the value imposed for any of the variants investigated.

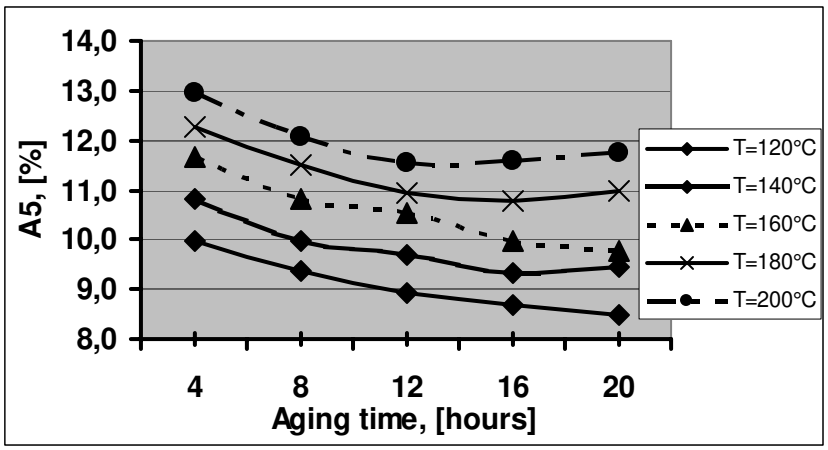

***Fig.11**. Change in elongation at break for alloy 3 according to the time of artificial aging.*

4. Conclusions

Mechanical properties of alloys vary continuously with temperature and aging time. Mechanical strength and hardness increase as the artificial aging temperature drops and artificial aging time increases, except for the temperature of 200^{0}C that records a maximum for 12 hours after which the values of Rm and HB decrease for retention times higher than 12 hours. Elongation at break increases as heat treatment temperature increases and decreases with increasing treatment time.

The highest values of properties were registered for alloy 3 which has the highest content of Zn and the lowest for alloy 1 where the Zn content is the lowest.

Therefore it can be concluded from the research that for the studied alloys of Al-Zn system, mechanical strength properties after artificial aging heat treatment, increase as the Zn content increases. As far as elongation is concerned, it decreases with increasing Zn content. Increasing the aging temperature or extending duration decrease resistance properties, but this gives a good dimensional and properties stability (overaging with precipitate coagulation).

References

[1]. N. Geru – *Teoria structurală a proprietăţilor metalelor*- Editura Didactică şi Pedagogică –Bucureşti 1980
[2]. *** *Aluminium Association - Aluminium Standards and Data* – 2004
[3]. L. F. Moldolfo –*Aluminium Alloys Structure and Properties*- Butterworth 1996
[4]. *** *Aluminium Asociation- SR-EN 485/2/2004 – Aluminium and aluminium Alloys- Sheet strip and plate-* Mechanical Properties.
[5] SECIM – *Laminoirs pour bandes d"aluminium,* 1989
[6]. IMNR - *Studiu de documentare privind capacităţile de producţie şi de prelucrare a metalelor neferoase*, 1994
[7]. Ioan Fara –*Aluminiul de la materia primă la produse finite*- Editura tehnică-2000
[8]. Fielding - *Situaţia actuală şi perspectivele aliajelor de aluminiu utilizate in industria aerospaţială*,1987
[9]. *** European norm EN 485-2-2007 Aluminiu şi aliaje de aluminiu – Produse deformabile-Simbolizarea starilor.
[10]. Sinclair S. - *Modelling microstructural formation in two phase aluminium alloys after hot deformation.* In rev. Materials science and technology, vol. 12, nr. 2, 1996.
[11]. Vermeşan, G. - *Tratamente termice*. Editura Dacia, Cluj-Napoca,1987.
[12]. *** *EN 573-3 - Aluminium and Aluminium Alloys Chemical composition and form of wrought products - Part 3 Chemical composition.*
[13]. *** *Metallic Materials Properties Development and Standardization* (MMPDS)\MMPDS - 03 Volume 2a (Chapter 3, Part 1) – 2006.

can be encountered during mechanical processing of materials.

The general form of constitutive equation is:

$$\overline{\sigma} = f(\varepsilon, \dot{\varepsilon}, T, \sigma^*) \quad (1)$$

where: σ, true stress; ε, true plastic strain; $\dot{\varepsilon}$, strain rate; T, temperature; σ^*, parameter dependent of the history of deformation.

Considerable efforts have been carried out over decades to develop quantitative constitutive relations which describe the flow strength of materials as a function of process variables, i.e., strain, strain rate and temperature, for the correct modeling of processes.

Empirical and semi-empirical relations obtained from experimental data are widely used in deformation models because they are easier to develop.

Idealized stress–strain curves that are frequently used in applications are illustrated in Fig. 1.

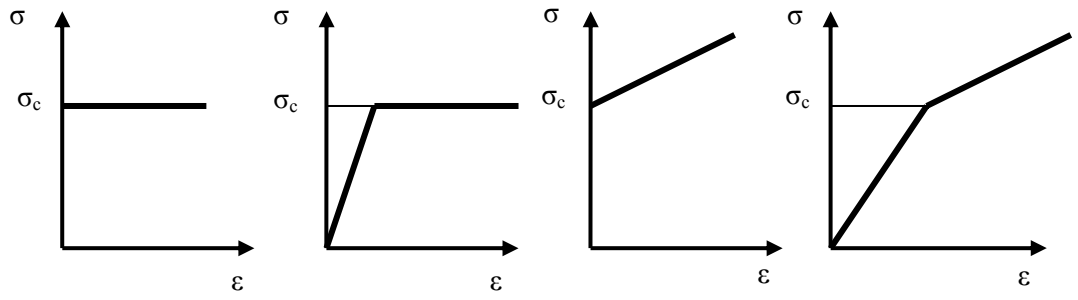

a. rigid - perfectly plastic | b. elastic-perfectly plastic | c. rigid-work hardening | d. elastic-work hardening

Fig. 1.

Most non-uniform distributions of stress and plastic deformation have been analyzed by an approximate two- or three-dimensional combined stress generalization of one of these idealized uniaxial curves. An approach to achieve a satisfying formulation for time dependent behavior is to generalize plasticity to cases within the strain-rate-sensitive range. One such generalization has been provided by the theory of visco-plasticity.

The most widely used constitutive equations for the analysis, the simulation and the design processes of metal forming at ambient temperature and at relatively low rates of deformation, are [3]:

Hollomon equation:

$$\sigma = C\varepsilon^n \quad (2)$$

Ludwik equation:

$$\sigma = \sigma_0 + C\varepsilon^n \quad (3)$$

Swift equation:

$$\sigma = C(\varepsilon + \varepsilon_0)^n \quad (4)$$

Voce equation:

$$\sigma = \sigma_s - (\sigma_s - \sigma_0)\exp(-n\varepsilon) \quad (5)$$

None of the above equations is entirely satisfactory for all materials and deformation conditions. These simple equations can be used for a satisfactory description of the stress-strain behaviour of particular materials such as steels, copper and aluminium alloys.

There is also a group of equations that also take into account the strain rate, apart from the strain. Some of them are: Backofen equation:

$$\sigma = C\varepsilon^n \dot{\varepsilon}^m \quad (6)$$

Hart equation:

$$\sigma = \sigma^* \exp[-(\frac{\dot{\varepsilon}^*}{\dot{\varepsilon}})^{\lambda}] + \sigma_0 (\dot{\varepsilon})^{1/M} \quad (7)$$

Wagoner equation:

$$\sigma = C(\varepsilon + \varepsilon_0)^n (\frac{\dot{\varepsilon}}{\dot{\varepsilon}_0})^m \quad (8)$$

Equations that take into account the strain, the strain rate but also the temperature have the following forms:

$$\sigma = C\varepsilon^n \exp(n_1\varepsilon)\dot{\varepsilon}^m \exp(a_1 T) \quad (9)$$

$$\sigma = C\varepsilon^n \exp(n_1\varepsilon)\dot{\varepsilon}^{(m+bT)} \exp(a_1 T) \quad (10)$$

In the case of hot working processes for large strain, the effect of strain on flow stress can be neglected. There is a particular relationship among flow stress, strain rate, and deformation temperature. The combined effects of temperature and strain rate on the deformation behaviors can be expressed by the Zener–Hollomon parameter [5, 8,9,14,15].

$$\sigma = f(\dot{\varepsilon}\exp\frac{Q}{RT}) = f(Z) \qquad (11)$$

$$Z = \dot{\varepsilon}\exp\frac{Q}{RT}$$

In the above relations the parameters have the following signification: σ_0, the yield point; σ, the flow stress; σ_s, n, n_1, the coefficients of strain hardening; m, strain rate sensitivity; ε_0, pre-strain; C, M, λ, a, a1, b, b1, experimentally determined parameters or functions; Q, activation energy for deformation (kJ/mol), R is the universal gas constant (8.314 J/(mol K)); Z, Zener-Hollomon parameter.

2. Example of simulation of advanced forming processes

The main objective of the forging process designer is to produce a workpiece of a given shape and dimensions without any defect. In general complex shapes of the workpiece require several forging phases to be manufactured. The selection of the number and configuration of the intermediate stages, dies geometries and forging conditions for every phase are the basic tasks involved in the process design. Other aspects, playing a major role at the moment of designing a suitable forging sequence, are the forces required to form the piece, the material flow during deformation, the die wear, etc. Regarding these aspects, the designer can obtain useful information from a FEM simulation. The visualization of the deformation process at each stage help to design or improve the required performances in order to ensure that the dies are totally filled with forged material as well as that no flow defects appear. Also the geometrical parameters of the performances can be optimized on the basis of improving the flow pattern or reducing the amount of die wearing.

The numerical models can advance the critical areas where the material flow or the strain and stress are likely to produce a damaged piece or an unacceptable tool wearing. Figure 2 presents the type of information which can be extracted from numerical simulation [1, 2, 4].

When professional softwares such as ABACUS, MARC, DEFORM, AUTOFORGE, FORGE, as well as a new-generation of large-capacity computers, were developed, it became possible to analyse various manufacturing processes with descriptions of the real behaviour of materials.

Forge (a commercial software developed at CEMEF, Ecole des Mines de Paris) was developed for the analysis of plastic deformation processes.

The program is based on the finite element method for cold and hot metal forming. It enables the thermo-mechanical simulation of the plastic deformation processes of metals in an axisymmetric, homogeneous and isotropic state of deformation and obeys the von Mises criterion. In this work was used the version 2009 of Forge software.

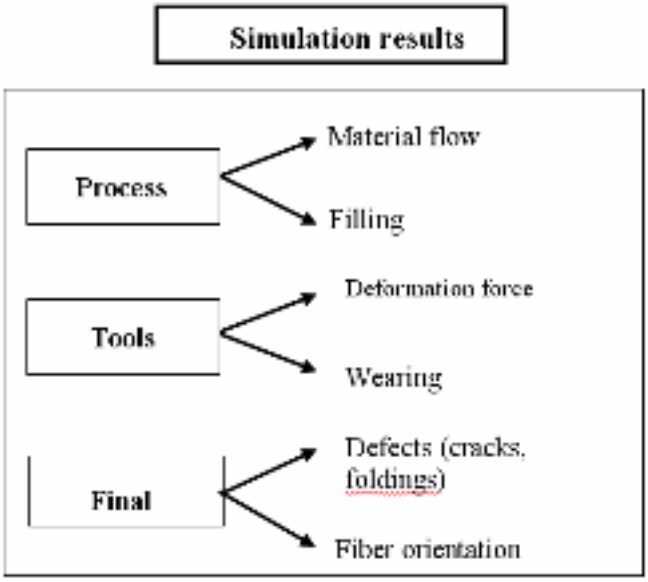

Fig. 2.

The calculations of the metal flow, stress field, strain, strain rate and temperature are conducted on the assumption of the viscoplastic model of the deformed body.

The tensorial form of the Norton-Hoff law used in **FORGE2009®** is written as:

$$s = 2A(T,\bar{\varepsilon},...)(\sqrt{3}*\dot{\bar{\varepsilon}})^{m-1}\dot{\varepsilon} \quad (12)$$

$$A(T,\bar{\varepsilon}) = A_0*(\bar{\varepsilon}+\bar{\varepsilon}_0)^n*e^{\frac{\beta}{T}} \quad (13)$$

Where ***s*** is the deviatoric stress tensor, A is the consistency of material, $\bar{\varepsilon}$ the equivalent strain, m the strain rate sensitivity, $\dot{\varepsilon}$ the equivalent strain rate, β material constant, n the strain hardening index and $\bar{\varepsilon}_0$ is a small constant.

The flow formulation introduced by Hensel and Spittel is written as:

$$\sigma = A*e^{m_1T}*T^{m9}*\varepsilon^{m2}*e^{m4/\varepsilon}*(1+\varepsilon)^{m5T}*e^{m7\varepsilon}*\dot{\varepsilon}^{m3}*\dot{\varepsilon}^{m8T} \quad (14)$$

Where $m_{1...9}$ are sensitivity parameters.

In the following an application of **Forge** in order to simulate an advanced plastic deformation process is presented [5]. Dieless drawing is an incremental process of plastic deformation, which permits the deformation of usual industrial materials (wires, tubes, bars) by controlling the heat temperature/local cooling without dies. The concept of dieless drawing is: to cause necking, the semiproduct is locally heated, and to stop further deformation, the necked part is cooled. The principle of dieless drawing is presented in Figure 3.

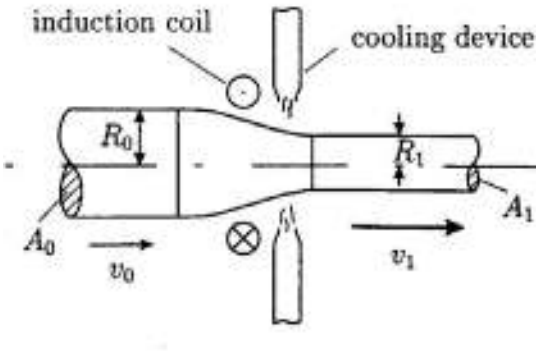

Fig. 3. *Principle of dieless drawing.*

Finite element simulation with thermo-mechanical analysis was carried out using the **FORGE2009®** software. Figure 4 shows the axisymmetric model used and Figure 5 shows the part discretisation. A 3D axisymmetrical model of the wire was constructed and meshed with tetraedrical elements. The model was both thermally and mechanically loaded to simulate dieless drawing conditions. A mesh of the wire was generated using three-node axisymmetric element.

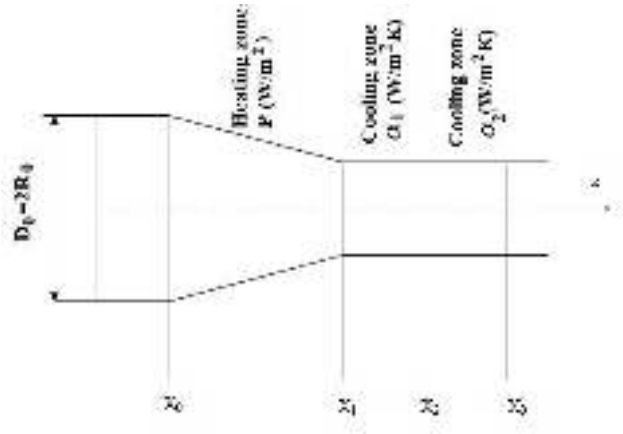

Fig. 4. *Simulation model.*

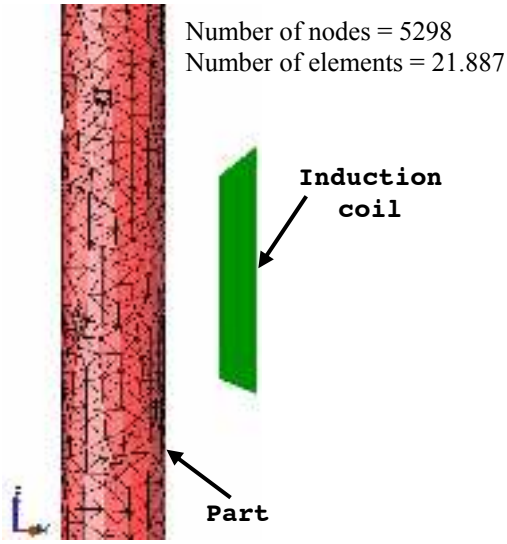

Fig. 5. *Part discretisation*

Table 1

Wire diameter, D_0, mm	4
Length of wire, L,mm	400
Heating width, H, mm	40
Cooling width 1, C_1, mm	5
Cooling width 2, C_2, mm	20
Drawing velocity, V_0, mm/s	1,76
Drawing velocity, V_1, mm/s	2,8
Heat transfer coefficient, α_1, W/m^{2}K	10000
Heat transfer coefficient, α_2, W/m^{2}K	30

Table 2

Thermal conductivity, W/mK	46
Specific heat, J/kg K	500
Mass density, kg/m^3	7850

Dimensional and process parameters used in finite element simulation are presented in Table 1. The material used for dieless drawing simulation is steel C45, with the thermal coefficients presented in Table 2.

The following pictures represent the distribution of the main deformation parameters: temperature, equivalent strain, strain rate and von Mises stress.

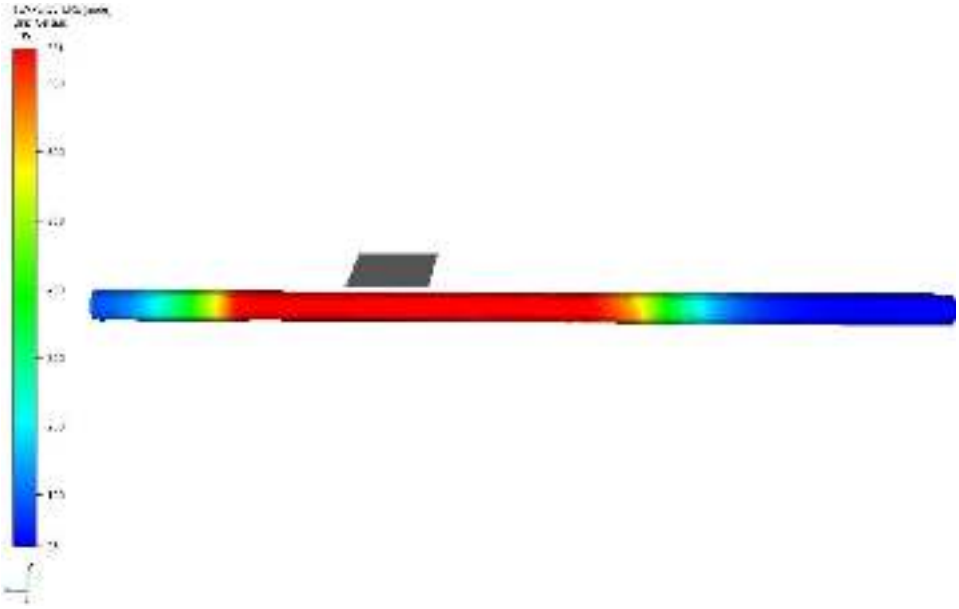

Temperature distribution

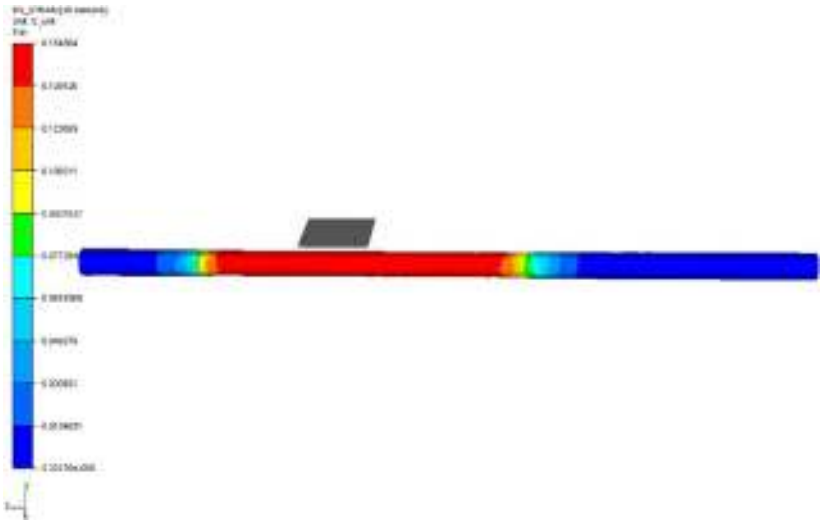

Equivalent strain distribution

Strain rate distribution

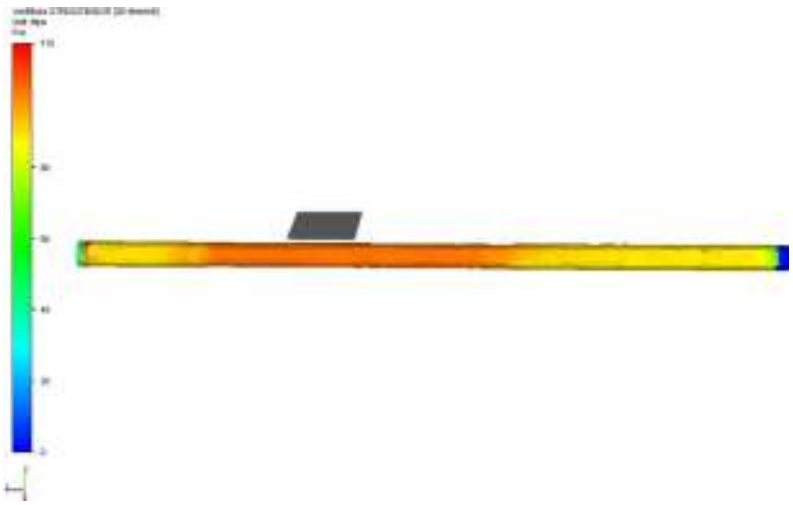

Von Mises stress distribution

Fig. 6. *Dieless drawing parameters distribution.*

The mathematical model presented can be used to describe the occurrence of deformation during the process. For modeling purposes, velocities V_0 and V_1 were assigned to the incoming and outgoing material nodes, respectively. The simulation calculation consisted principally of a thermomechanical analysis of the plastic deformation of the wire. The temperature distribution of a wire in the dieless drawing process is determined by the heat quantity supplied by the heating coil, the thermal conductivity of the tubes, heat transfer induced by cooling coil and radiation to the air. The researchers concluded that successful dieless drawing was achievable if the drawing velocities and temperature profiles permitted the occurrence of transformation plasticity. In this class of plasticity, deformation occurs during a phase change where a threshold stress is necessary to initiate deformation.

From the images presented in figure 6 it can be observed that the evolution of deformation parameters (temperature, strain, strain rate, von Mises stress) in the deformation zone are in accordance to theoretical principles of plastic deformation. The mathematical model presented can be used to describe the occurrence of deformation during the dieless drawing process.

4. Conclusions

After a brief survey of the mathematical basic formulations suitable for material constitutive equations, some theoretical and numerical issues were discussed. To demonstrate the interest of numerical modeling and simulation for design of the forming processes, an example was presented.

The aspects regarding the FEM analysis are concentrated on the **FORGE2009®** software. It appears that the main deformation parameters of the processes can be predicted with existing models or with reasonable updates of these computer codes. The aim of future research is to verify the validity of FEM model by experiment for the dieless drawing process.

References

[1]. J.-L. Chenot, E. Massoni - *Finite element modelling and control of new metal forming processes*, International J. Machine Tools & Manufacture, 46, (2006), pp. 1194–1200.
[2]. F. Espiga, A. Jugo, J.J. Anza - *Industrial applications of numerical simulation to the design and optimization of forging processes*, J. Mater. Process. Technol., 45, (1994), pp. 81-86.
[3]. Z. Gronostajski - *The constitutive equations for FEM analysis*, J. Mater. Process. Technol. 106 (2000) pp. 40-44.
[4]. P. Hartley, I. Pillinger - *Numerical simulation of the forging process*, Comput. Methods Appl. Mech. Engrg. 195 (2006) pp. 6676–6690.
[5]. X.Huanga, H. Zhanga, s.a. - *Hot deformation behavior of 2026 aluminum alloy during compression at elevated temperature,* Materials Science and Engineering A 527 (2010) 485–490.
[6]. Ji Hyun Sung , Ji Hoon Kim , R.H. Wagoner - *A plastic constitutive equation incorporating strain, strain-rate, and temperature,* International Journal of Plasticity 26 (2010) 1746–1771.
[7]. Y. Lee, B.M. Kim, K.J. Park, S.W. Seo, O. Min - *A study for the constitutive equation of carbon steel subjected to large strains, high temperatures and high strain rates,* Journal of Materials Processing Technology 130–131 (2002) 181–188
[8]. Y.C. Lin, Ming-Song Chen, Jue Zhong - *Constitutive modeling for elevated temperature flow behavior of 42CrMo steel,* Computational Materials Science 42 (2008) 470–477.
[9]. H. Mirzadeh, A. Najafizadeh, *Flow stress prediction at hot working conditions,* Materials Science and Engineering A 527 (2010) 1160–1164
[10]. F. Parvizian, T. Kayser, C. Hortig, B. Svendsen - *Thermomechanical modeling and simulation of aluminum alloy behavior during extrusion and cooling*, J. Mater. Process. Technol. 209 (2009) p.876–883.
[11]. M. Pop, A. Neag - *Numerical study on deformation behavior in dieless drawing process*, Metalurgia, 5, (2010), p.13-17.
[12]. M. Poursinaa, H. Ebrahimib, J. Parvizianc - *Flow stress behavior of two stainless steels, An experimental–numerical investigation*, J. Mater. Process. Technol. 199(2008) p. 287–294.
[13]. R.G. Snape, S.E. Clift, A.N. Bramley - *Sensitivity of finite element analysis of forging to input parameters,* Journal of Materials Processing Technology 82 (1998) 21–26.
[14]. Soheil Solhjoo, *Analysis of flow stress up to the peak at hot deformation,* Materials and Design 30 (2009) 3036–3040.
[15]. H. Takuda, H. Fujimoto, N. Hatta - *Modelling on flow stress of Mg–Al–Zn alloys at elevated temperatures,* Journal of Materials Processing Technology 80–81 (1998) 513–516.

THE ANNALS OF "DUNAREA DE JOS" UNIVERSITY OF GALATI.
FASCICLE IX. METALLURGY AND MATERIALS SCIENCE
N^0. 2 – 2011, ISSN 1453 – 083X

ASPECTS REGARDING THE CONSTITUTIVE EQUATIONS FOR FEM ANALYSIS OF ADVANCED METAL FORMING PROCESSES

Mariana POP, Adriana NEAG
Technical University of Cluj-Napoca
e-mail: mariana.pop@ipm.utcluj.ro

ABSTRACT

The main aim of this paper is to review some different models, from simple to very complicated, for computing the changes in flow stress depending on the deformation conditions. Some of the models can be applied to cold forming and some to hot and warm forming. A finite element analysis (FEA) of the dieless drawing process was undertaken. The FEA simulation was carried out using Forge3, a FEA software, specifically produced for metal forming simulation. An axisymmetrical 3D geometric model of the tooling and billet was constructed for the analysis. The data obtained from the FE model included temperature, equivalent von Mises stress, equivalent strain and material deformation velocity.

KEYWORDS: metal forming, constitutive equations, Forge3, dieless drawing

1. Introduction

Cold and hot forging are regarded as two of the most important processes for the manufacturing of products with good mechanical properties and fine metallurgical structures.

An important objective of the deformation processing of metals and alloys is the production of defect-free parts, with the desired microstructure and properties. This goal can be achieved by better design and calculation methods and better control of the parameters of the deformation processes. This should be based on a deeper knowledge of the phenomena that accompany the deformation of materials and of the relationships between the properties of the deformed materials and the conditions of deformation.

The progress in computer hardware and simulation tools has, in recent years, enabled complicated simulations of industrial forming processes. However, the accuracy of such simulations will remain dependant on the reliability of the material data, most important of all the true flow stress. Experimental tests at different strains, strain rates and temperatures reached during metal forming application are performed to reveal this constitutive relationship, which relates the deformation behavior to stress.

The most important aspect of mechanical design in metal forming processes is the determination of forces and forming energy, which requires the knowledge of the flow stress of alloys. Experiments to find the flow stress of alloys at different loading conditions, i.e. various strain rates and temperatures, are necessary but very expensive and time consuming. Therefore, developing mathematical models to predict the stress–strain curves under different forming conditions is of great importance. Many researchers tried to model the stress–strain curves for different alloys. The main difference between these models is the level of physical theories which is used to obtain them.

One of the most important elements of a computer simulation of plastic deformation processes is the model of deformed materials, usually describing the flow stress as a function of the deformation conditions. The accuracy of such a material model depends on both the mathematical structure of the model and the proper experimental determination of the material parameters used in the model. The mathematical structure should take into account the physical phenomena occurring in the material and depending on its kind, the conditions of forming, the history of deformation. Considering the different structural phenomena, cold, warm, and hot forming processes should be distinguished. Recently, the progress in computer hardware and simulation tools led to a wide application of FEM simulations to study the forging process [1, 4, 6, 7, 12,13].

Constitutive equations are used to describe the changes in strength observed to occur in materials being deformed. These formulations are empirical and relate changes in strength produced by variation in strain, temperature or strain rate. Such equations are used to predict forces, distortions, stresses, etc. that

THE ANNALS OF "DUNAREA DE JOS" UNIVERSITY OF GALATI.
FASCICLE IX. METALLURGY AND MATERIALS SCIENCE
N^0. 2 – 2011, ISSN 1453 – 083X

THE USE OF MAGNETIC NANOMATERIALS FOR THE RETAINING OF Cu(II) IONS OUT OF RESIDUAL WATER

[1]Claudia Maria SIMONESCU,[2]Florea GHEORGHE,[3]Elena PARASCHIV,
[3]Victor PĂUNESCU,[4]Teodora CUCU

[1]Politehnica University of Bucharest
[2]Dunărea de Jos University of Galati,
[3]Dacia High School, Bucharest,
[4]General Eremia Grigorescu School, Bucharest

ABSTRACT

In the developed countries the removal of hard materials from residual waters using advanced technologies such as ionic change, precipitation, ultrafiltration or electrochemical deposits seems inconvenient from the economic point of view for the industry because its high costs. Therefore, it is necessary to introduce new technologies that imply low costs.

By linking chitosan and magnetite particles (Fe_3O_4), a new magnetic adsorbent with 100-200 nm particles and of great efficiency to move off the metalic ions is obtained. That is why this study aims to obtain a new magnetic material with great efficiency to retain copper out of synthetic solutions, and then to compare it, from the retaining point of view, with simple synthesized magnetide (Fe_3O_4).

KEYWORDS: nanomaterial, composite, chitosan, water

1. Introduction

Water is an important factor in the ecological balance and its pollution is a contemporany issue with more or less serious consequences on the population. The effects of the pollution of water resources are complex and various depending on the nature and concentration of impurification substances.

The presence of heavy metals in the enviroment is a problem of great significance because of the great volume of residual water with metalic ions, of their ionic nature and of the negative effects that they have on natural waters. For the human health, one of the most dangerous materials in industrial residual waters (metals industry, cellulose and paper industry, fertilizers industry, electronic industry, photographic industry, copperfield) is copper.

Copper is a necessary microelement for the human body; the daily dose is 2-3 mg of copper for adults and 0.05 mg/kilogram for children. When it is swallowed in great amounts, it becomes toxic thus leading to such manifestations as icterus, anaemia or to an exaggerated consumption of water, etc.

One of the less expensive methods to remove copper from residual waters is absorbtion. An absorbent for copper could be chitosan, a natural polysaccharide with various properties such as hydrophilicity, biocompatibility, biodegradability, antihaeterian properties and a remarcable affinity towards various biomacromolecules. The chitosan and its derivates have various potential applications in such domains as: biotechnology, biomedicine, food ingredients and cosmetics. Furthermore, the chitosan is capable to retain a great number of metalic ions because it contains nano groups used as chelatic points.

This biosorbent has also disadvantages such as: the tendency to heap up, a low capacity of getting soaked, the capacity of making gels into watery solutions thus making unavailable the linking reactive centers.

These are the reasons that have prevented this potential absorbent from being used at an industrial scale except in laboratory experiments. In order to overcome these restrictions and other difficulties during the sorption process, a compound, called magnetite-chitosan, has been obtained as a new potential sorbent to retain the Cu(II) from watery solutions efficiently.

Therefore the purpose of this study was to obtain a new magnetic material with great efficiency in retaining cooper out of synthetic solutions and comparing it with simple synthesized magnetide, from the retaining capacity point of view.

Consequently:

- two materials have been obtained: magnetite and chitosan, joined by the coprecipitation method, which have been characterized by using well-known methods;

- a study has been carried out to identify the characteristics of the obtained composite material (magnetite/chitosan);

- the composite has been used to retain copper ions out of synthetic solutions in static situations;

- the influence of some parameters has been established: the initial concentration of the Cu(II) synthetic solution, the contact time on the absorbtion of Cu(II) using the composite material with magnetic properties – magnetite – chitosan.

Besides fixing the humidity, the materials have also been analized by FTIR (Fig. 2), spectrography difraction analysis, transmission electron microscopy (TEM).

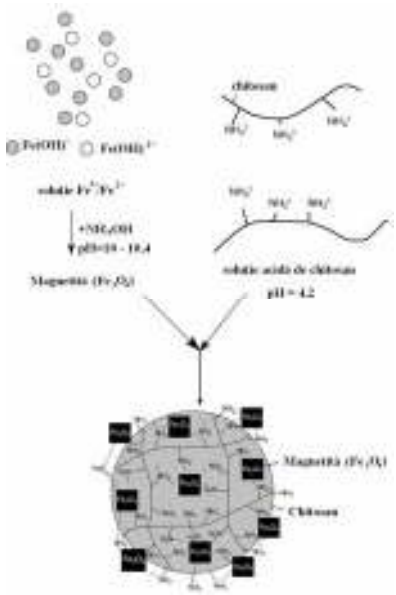

Fig. 1. *Sketchy plotting of the process of making magnetite/chitosan composite.*

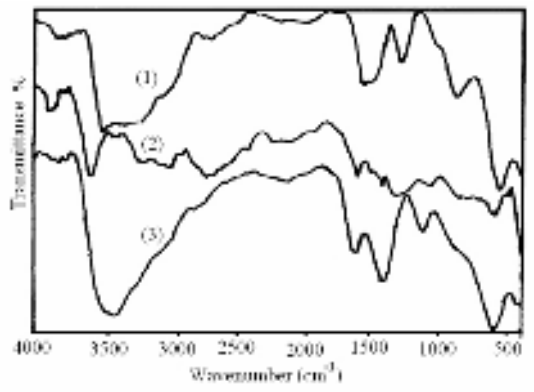

Fig. 2. *FTIR spectroscopy magnetite (1) chitosan (2) and magnetite–chitosan (3).*

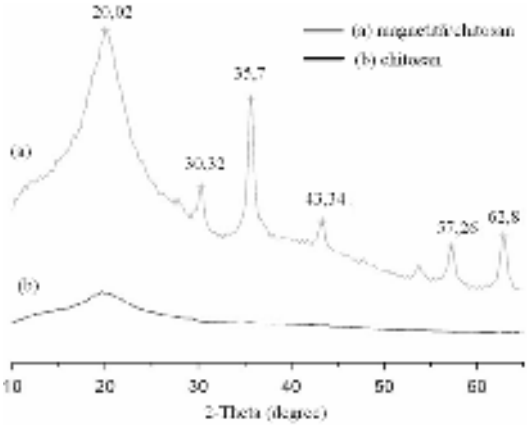

Fig. 3*. Diffraction analysis.*

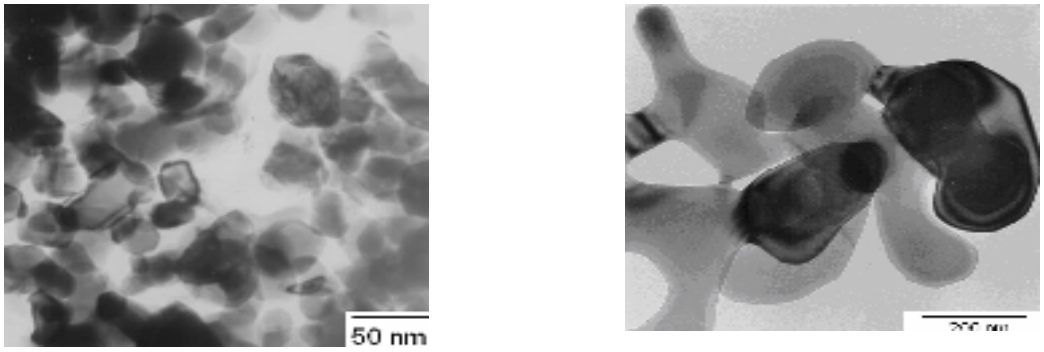

a *b*

Fig. 4*. TEM images for magnetite (a) and magnetite - chitosan (b).*

IR spectroscopies have been recorded in the 400 - 4000 cm^{-1} domain, using a FT-IR 620 spectometer (Jasco, Japan).

Figure 2 presents FTIR spectroscopy of the magnetite, chitosan and the composite made up in the reaction between the magnetite and the chitosan.

In spectroscopy (1), characteristic to the magnetite, the presence of bands in the area 3250-3600 cm^{-1} and 1550-1700 cm^{-1} is associated to the water molecules net. This indicates the presence of crystallization of water in the magnetite test. The 610 cm^{-1} band is caracteristic to the streching vibration of the M-O joint which confirms the presence of Fe-O joints in the magnetite.

The presence of a characteristic band at the 3594 cm^{-1} wavelength in the chitosan spectroscopy shows the existence of the HO hidroxil groups in the chitosan molecule, while the bands appearing at the 1650 cm^{-1} and 1449 cm^{-1} wavelengths corespond to the frequency of streching vibrations characteristic to the amid group in the chitosan molecule.

Spectroscopy (3) in Figure 2 shows all the characteristic bands of magnetite and chitosan, and more than that the bands characteristic to water molecules are much more intense, which proves the existence of the magnetite – chitosan composite.

The diffraction analysis of unmodified chitosan in Figure 3b shows only one band of diffraction of 20º. This band is due to reflections (2 0 2) according to the literature data.

The sharp diffraction bands appearing at angles 2θ = 30.32; 35.7; 43.34; 57.26 and 62.8 in the diffraction analysis of magnetite chitosan composite corespond to the magnetite. Consequently the iron oxide in the obtained composite is the magnetite. The difference of the band intensity from angle 2θ = 20.02 indicates that the degree of crystallinity of the chitosan rises because of the orientation of the chitosan chains. The oriented magnetite particles lead to the formation of an ordered structure regarding the chitosan composite. These are according to the scientific literature.

The transmission electron microscopy (TEM) was used to fix the morphology of the reaction product obtained through a method specific to the study of crystallin dust. The obtained dust was spread into alchool and then deposited on a TEM grid with carbon support. The TEM study was realised by the help of an electronic miroscope, Jeol 200CX. One can notice in Figure 4 that the magnetic particle have an average diameter of 30-70 nm.

Figure 4b shows that the magnetite particles are in the chitosan particles because of two simultaneous processes. The first process refers to the formation of magnetite and the second process to the precipitation of chitosan in an alkaline solution.

In Figure 4a it is to be noticed that both stages (magnetite and chitosan) are visible. The agglomeration of magnetite – chitosan composite is probably due to the lack of a stabilizing agent in the reaction system and also to the tendency of the chitosan to agglomerate.

2. The use of the magnetite – chitosan composite for the retaining of Cu(II) ions from residual waters

In order to realise the absorbtion of copper on magnetite/chitosan composite experiments, synthetic solutions prepared in the laboratory have been used. The stored solution of concentrated Cu(II) n0,1M was dilluted and solutions of Cu(II) with concentrations of 800 mg/L, 400 mg/L, 200 mg/L, 100 mg/L were obtained.

The spectrophotometric determination of copper (a method based on the reaction of copper with ammonia) showed a blue complex that has gone to spectrotemetry to the λ = 620 nm wavelength.

The absorbed copper quantity on the magnetite/chitosan composite was calculated according to the contact time between the two stages; the data obtained can be seen in Figures 5 and 6.

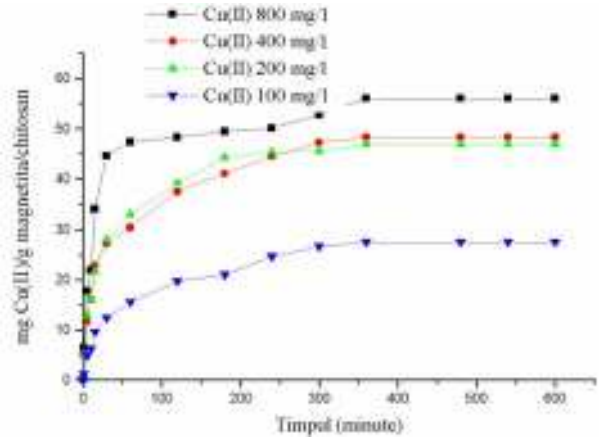

Fig.5. *Cu(II) quantity retained on the magnetite/chitosan composite according to contact time.*

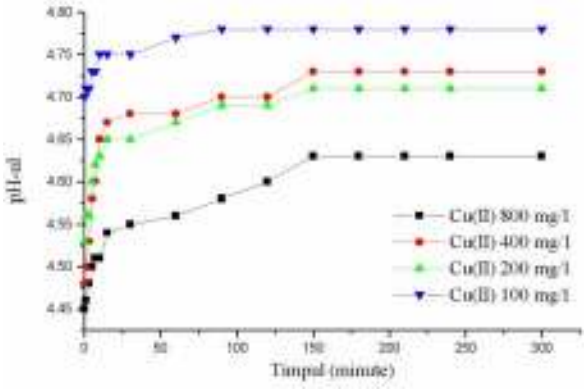

***Fig.6**. Variation of the pH of Cu(II) of 800 mg/L, 400 mg/L, 200 mg/L, 100 mg/L at contact with 0.1 g magnetite/chitosan composite according to time.*

Studying Figure 5, the first conclusion is that the Cu(II) quantity retained on each gram of magnetite/chitosan composite grows with the contact time between the two stages. The process of moving copper off watery solutions by using magnetite/chitosan composite is a slow process, the equilibrium reaching 5 hours. This is a very important result, because the time necessary to reach the equilibrium is a very important parameter in creating an economic water treatment system. Figure 6 shows that there is a very small variation of the pH solution according to the contact time between the two stages. This variation is about 0.08-0.25 units, which leads to the conclusion that the process of retaining copper out of synthetic solutions by the magnetite/ chitosan composite is not a process that implies a chemical reaction but physical sorption.

The Kinetics of the copper ion sorption process by the magnetite/ chitosan composite

In order to identify the checking mechanisms of adsorption processes as a transfer of mass and chemical reaction, the equations of order I, order II and intraparticle diffusion have been used to test the experimental data.

The first order kinetic model is given as:

$$\log(Q_e - Q_t) = \log Q_e - \frac{k_1}{2{,}303} \cdot t \qquad (1)$$

where Q_e and Q_t are the amounts of Cu(II) adsorbed on adsorbent (mg/g) at equilibrium and at time t; k_1 is the rate constant of first-order adsorption (min^{-1});

The second-order equation may be expressed as:

$$\frac{t}{Q_t} = \frac{1}{k_2 Q_e^2} + \frac{t}{Q_e} \qquad (2)$$

where: k_2 – is the rate constant of second-order adsorption (g/mg·min); Q_e and Q_t are the amounts of Cu(II) adsorbed by the magnetite/chitosan composite (mg/g) et equilibrium and at time t.

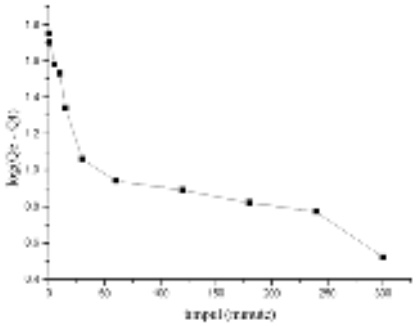

***Fig.7.** Kinetics of first–order adsorption of the Cu(II) on the magnetite/chitosan composite (0,1 g) at an initial concentration of 800 mg/L*

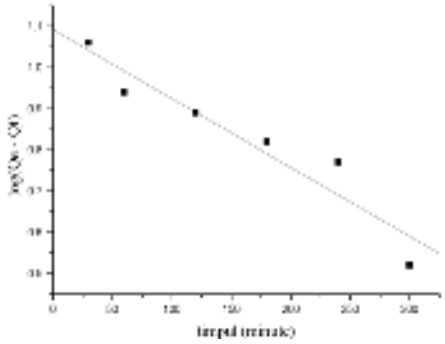

***Fig. 8.** Kinetics of pseudo first-order adsorption of the Cu(II) on the magnetite/chitosan composite (0,1 g) at an initial concentration of 800 mg/L at an interval of 30-300 minutes*

The diagram of the proportion t/Q_t according to time t shows the following parameters: the speed constant k_2 and the correlation coefficient R^2 for the adsorption of copper by the magnetite/chitosan composite.

The rate of the intraparticle diffusion is described by the equation:

$$Q_t = k_i t^{0.5}$$

where k_i is the intraparticle diffusion rate ($mg \cdot g^{-1} \cdot min^{-0.5}$).

The k is the slope of straight-line obtained in the diagram of the intraparticle diffusion rate. Q_t according to the time of dividing into halves, $t^{0.5}$. The obtained data are shown in Figures 7-16.

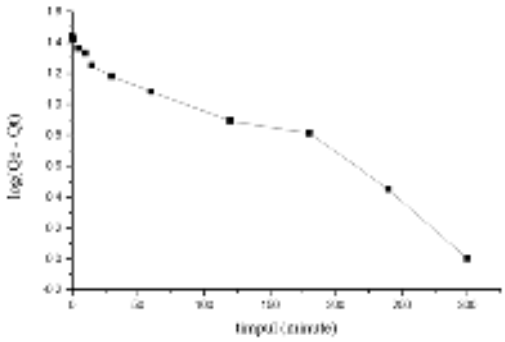

Fig. 9. *Kinetics of first–order adsorption of the Cu(II) on the magnetite/chitosan composite (0.1 g) at an initial concentration of 100 mg/L.*

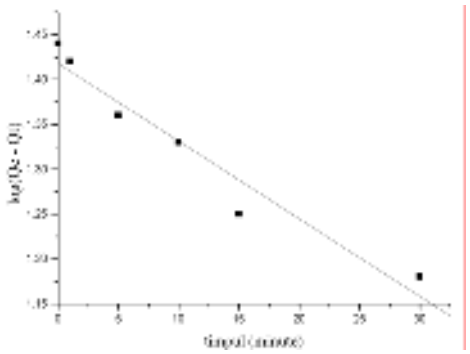

Fig. 10. *Kinetics of pseudo first-order adsorption of the Cu(II) on the magnetite/chitosan composite (0.1 g) at an initial concentration of 100 mg/L at an interval of 0-30 minutes.*

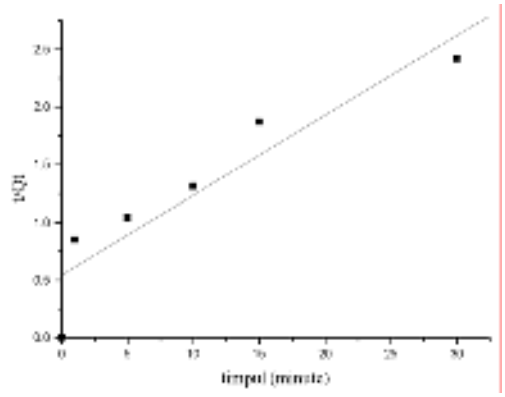

Fig. 11. *Kinetics of pseudo second-order adsorption of the Cu(II) on the magnetite/chitosan composite (0.1 g) at an initial concentration of 100 mg/L at an interval of 0-30 minutes.*

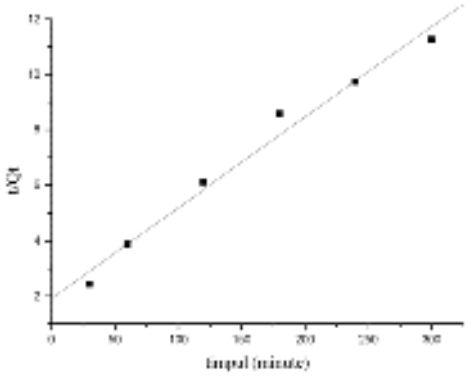

Fig.12*. Kinetics of pseudo first-order adsorption of the Cu(II) on the magnetite/chitosan composite (0.1 g) at an initial concentration of 100 mg/L at an interval of 30-300 minutes.*

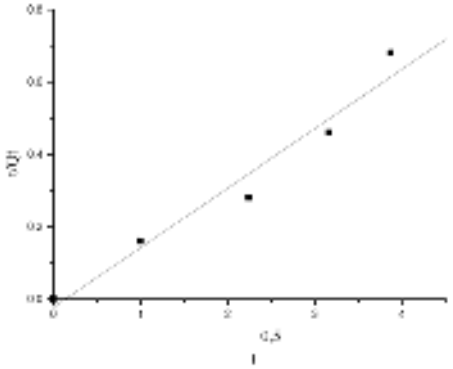

Fig. 13. *Kinetics of sorption of intraparticle diffusion of Cu(II) on the magnetite/chitosan composite (0.1 g) at an initial concentration of 800 mg/L in an interval of 0 -30 minutes.*

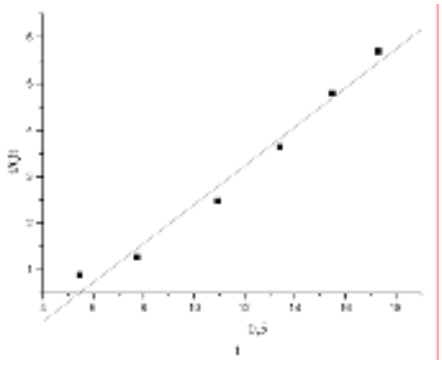

Fig. 14. *Kinetics of sorption of intraparticle diffusion of Cu(II) on the magnetite/chitosan composite (0.1 g) at an initial concentration of 800 mg/L in an interval of 30-300 minutes.*

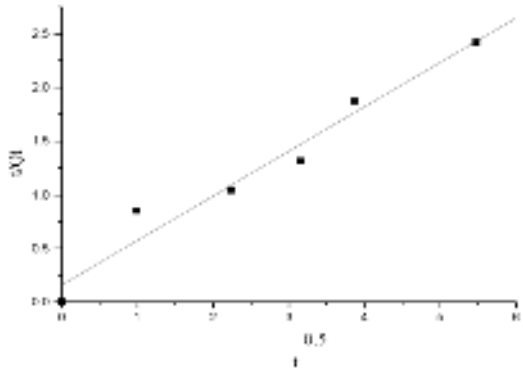

Fig. 15. *Kinetics of sorption of intraparticle diffusion of Cu(II) on the magnetite/chitosan composite (0.1 g) at an initial concentration of 100 mg/L in an interval of 0 -30 minutes.*

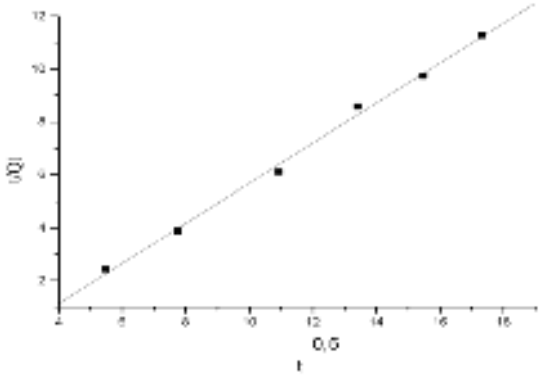

Fig. 16*. Kinetics of sorption of intraparticle diffusion of Cu(II) on the magnetite/chitosan composite (0.1 g) at an initial concentration of 100 mg/L in an interval of 30-300 minutes.*

The constant rate and the correlation coefficient of the models Lagergren (the pseudo first-order), the pseudo second-order and the intraparticle diffusion in the mentioned intervals are shown in Tables 1 and 2.

Table 1. *The constant rate and the correlation coefficients for Cu(II) adsorption on chitosan and an initial concentration of Cu(II) of 800 mg/L, the amount of magnetite/chitosan composite is 0.1 g*

The kinetic model	*0 – 30 min.*		*30 - 300 min.*	
	k_i	R^2	k_i	R^2
Lagergren (pseudo first-order)	$5.2185 \cdot 10^{-2}$ (min^{-1})	*0.9851*	$3.846 \cdot 10^{-3}$ (min^{-1})	*0.9979*
Pseudo second-order	$2.8617 \cdot 10^{-2}$ $(g/mg \cdot min)$	*0.9735*	$1.1903 \cdot 10^{-3}$ $(g/mg \cdot min)$	*0.9104*
Intraparticle diffusion	*0.1646* $(mg \cdot g^{-1} \cdot min^{-0.5})$	*0.9608*	*0.4176* $(mg \cdot g^{-1} \cdot min^{-0.5})$	*0.9795*

Table 2. *The constant rate and the correlation coefficients for Cu(II) adsorption on chitosan and an initial concentration of Cu(II) of 100 mg/L, the amount of magnetite/chitosan composite is 0.1 g*

The kinetic model	*0 – 30 min.*		*30 - 300 min.*	
	k_i	R^2	k_i	R^2
Lagergren (pseudo first-order)	$1.9943 \cdot 10^{-2}$ (min^{-1})	*0.9451*	$9.3732 \cdot 10^{-3}$ (min^{-1})	*0.9361*
Pseudo second-order	$8.7892 \cdot 10^{-3}$ $(g/mg \cdot min)$	*0.8573*	$5.5713 \cdot 10^{-4}$ $(g/mg \cdot min)$	*0.9816*
Intraparticle diffusion	*0.4147* $(mg \cdot g^{-1} \cdot min^{-0.5})$	*0.9601*	*0.7568* $(mg \cdot g^{-1} \cdot min^{-0.5})$	*0.9960*

According to the correlation coefficients, it can be seen that on the entire time interval (0 – 300 minutes) the adsorption of Cu(II) on the magnetite/chitosan composite is best described by the first equation Lagergren (R^2 = 0,9851; 0,9979) for the Cu(II) solution of 800 mg/L concentration, which leads to the conclusion that the important stage of rate is the physic adsorption.

Table 2 shows that for the Cu(II) solution of 100 mg/L the Cu(II) sorption on magnetite/chitosan may be best described by the equation characteristic to the intraparticle diffusion on the entire time interval because the values of the correlation coefficient R^2 are 0.9601 şi 0.9960.

3. Conclusions

The results of this study prove the posibility of using a magnetic material such as the magnetite/chitosan composite to remove Cu(II) from aqueous solutions.

Taking into account the experiments and their results, here are the conclusions:

- based on a simple method, a magnetic material magnetite/chitosan composite has been obtained;
- the material was morphologically and structurally characterized;
- the experimental data show that a magnetite/chitosan composite with magnetic properties and 100-200 nm particles has been obtained;
- the material was used in the process of retaining Cu(II) ions out of synthetic solutions;
- the kinetic studies show that the equilibrium in adsorption of Cu(II) was reached after five hours of contact between the composite and the aqueous solution; consequently, the process of retaining Cu(II) is slow;
- the amount of Cu(II) retained by the composite grows with the Cu(II) concentration in the initial solution;
- according to the correlation coefficients, the sorption of copper on the composite in the 0-300 minutes interval is well described for a high concentration (Cu 800 mg/L) by the first equation (R2 = 0.9851; 0.9979), which leads to the conclusion that on this time interval, for the respective concentration, the important stage of rate is the physic sorption (adsorption);
- for the solution of a small concentration (100 mg/l) it may be seen that on this time interval, the sorption of Cu(II) on the composite is best described by the third equation (RDI2 = 0.9601 şi 0.9960), which means that the important stage of rate is the intraparticle diffusion;
- the results are also established by the studies on variations of pH according to the contact time between the two stages;
- the experiments show that there was not a significant variation of the pH value of the sollution at the contact between the two stages according to the time contact and that is why the sorption process between the Cu(II) ions and the composite is a physic process not a chemical one, this implying a chemical reaction between the Cu(II) ions and the sorbent.

Consequently, the composite magnetic material may be used in the process of retaining Cu(II) ions out of residual waters, its separation being an easy process when a magnetic field is used.

References

[1]. Apak R, Tutem E, Hugul M, Hizal J. - *Heavy metal cation retention by unconventional sorbents (red muds and fly ashes). Water* Res., 32, p. 430–40, 1998.

[2]. **Ben-Shalom, N., Kudabaeva, N., Borisover, M.** - *Chemosphere*, 59, p. 1309 -1312, 2005.

[3]. Chiou, M.S., Li, H.Y. - "*Adsorption behavior of reactive dye in aqueous solution on chemical cross-linked chitosan beads*", Chemosphere, 50(8), p. 1095-1103, 2003.

[4]. Fergusson, E. - The Heavy *Elements Chemistry, Environmental Impact and Health Effect,* Pergamon Press, Inc., New York, p. 400, 1990.

[5]. Ho, Y.S., & McKay, G. - *Pseudo second-order model for sorption processes*. Process Biochemistry, 34, p. 451, 1999.

[6]. Li, B., Jia, D., Zhou, Y., Hu, Q., Cai, W. - *In situ hybridization to chitosan/magnetite nanocomposite induced by the magnetic field*, Journal of Magnetism and Magnetic Materials 306, 223–227, 2006.

[7]. Liu, X., Hu, Q., Fang, Z., Zhang, X., Zhang, B. - *Magnetic chitosan nanocomposites: a useful recyclable tool for heavy metal ion removal.* Langmuir 25, 3–8, 2009.

[8]. Nascimento, M., Soares, P.S.M., de Souza, V.P. - *Adsorption of heavy metal cations using coal fly ash modified by hydrothermal method,* Fuel 88, p. 1714-1719, 2009.

[9]. Starkar, N.S., Hilt, J.S. - *Magnetic hydrogel anocomposites for remote controlled pulsatile drug release.* Journal of Controlled Release 130, 246–251, 2008b.

[10]. Wang, Y., Li, B., Zhou, Y., Jia, D. - *Chitosan-induced synthesis of magnetite nanoparticles via iron ions assembly*. Polymers for Advanced Technologies 19, 1256–1261, 2008.

[11]. **Zhou, L., Wang, Y., Liu, Z., Huang, Q.** - *Characteristics of equilibrium, kinetics studies for adsorption of Hg(II), Cu(II), and Ni(II) ions by thiourea-modified magnetic chitosan microspheres.* Journal of Hazardous Materials 161, 995–1002, 2009a.

[12]. Zhou, Y.T., Nie, H.L., White, C.B., He, Z.Y., Zhu, L.M. -. *Removal of Cu*2+ *from aqueous solution by chitosan-coated magnetic nanoparticles modified with a-ketoglutaric acid. Journal of Colloid and Interface* Science 330, 29–3, 2009b.

THE ANNALS OF "DUNAREA DE JOS" UNIVERSITY OF GALATI.
FASCICLE IX. METALLURGY AND MATERIALS SCIENCE
N^0. 2 – 2011, ISSN 1453 – 083X

RESEARCH ON CORROSION RESISTANCE OF STEEL PLATES FOR SHIPBUILDING

Beatrice TUDOR, Marian BORDEI
Faculty of Metallurgy, Materials Sciences and Environment
"Dunarea de Jos" University of Galati
email: beatrice.tudor@yahoo.com

ABSTRACT

The corrosion of metallic materials is their partial or total destruction through chemical, electrochemical or biochemical reactions, by spontaneous interaction between the surface and the corrosive medium pollution. Generally, corrosion is defined as a medium attack to a material, an attack that leads to a worsening of the properties or destruction. Corrosion is not limited to the destruction of metallic materials; it affects equally plastics, ceramics, concrete and even the environment with which they interact.

KEYWORDS: corrosion resistance, steel plates, shipbuilding

1. Introduction

Most metals in their natural conditions are not thermodynamically stable elementary metallic forms, but a combined state (oxidized or corroded) (Figure 1).

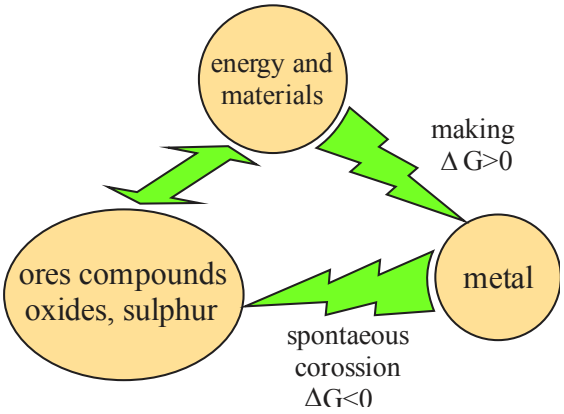

Fig. 1. *Spontaneous thermodynamic tendency to corrode metals*

In the process of corrosion, material (solid) and environment (liquid or gas) must considered as a place where corrosion processes that occur after the general laws heterogeneous reactions of metal-environment interface (Figure 2).

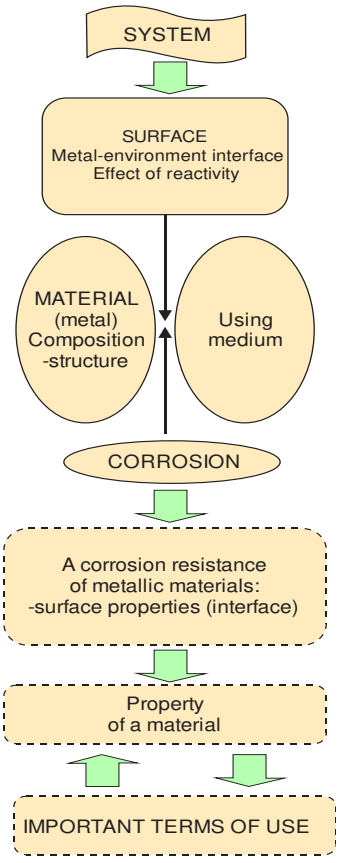

Fig. 2. *Schematic representation of a corrosion system.*

2. Electrochemical corrosion

Electrochemical corrosion is a process involving the presence of an electrolyte, usually water or an aqueous solution, in contact with a metal. At the interface between the two, electron transfer occurs as a result of the simultaneous deployment of two types of reactions:

- ionization anode reaction (oxidation) of metal, representing its destruction/ corrosion:

$M + n\ H_2O \xrightarrow{-ze} M^{z+} * n\ H_2O + ze$

- cathodic reduction reaction of an agent capable of accepting electrons yielded by the metal:

$X + ze \rightarrow X^{z-}$

The influence of electrochemical corrosion depends on material factors and external environmental factors.

2.1. Electrochemical corrosion in natural environments

2.1 Underwater Corrosion

Underwater corrosion is primarily dependent on the nature and concentration of solutions, *i.e.* cathodic depolarization of existing agents in water by oxygen. Its concentration varies widely depending on the nature of the water (sweet, salty), its depth and temperature (Table 1). Oxygen dissolved into water acts as a cathode depolarizer; the extent to which that water contains other substances (dissolved salts, in general) increases its conductivity.

With increasing concentration of salts in the water, the corrosion rate of steel by oxygen depolarization increases to a maximum and then decreases due to decreased O_2 concentration. Both the presence and the absence of O_2 in water (increased CO_2 concentration) lead to an increased corrosion rate.

Table 1. *The concentration of O_2 dissolved in freshwater and seawater at different temperatures*

Temperature, (ºC)	**Weight of dissolved oxygen**, (pp.m.)			
	Freshwater	**Sea water with chlorine**		
		5000 p.p.m. Cl^-	10000 p.p.m.Cl^-	20000 p.p.m. Cl^-
0	14.62	13.79	12.97	11.32
5	12.80	12.09	11.39	10.01
10	11.33	10.73	10.13	8.98
15	10.15	9.65	9.14	8.14
20	9.17	8,73	8.30	7.42
25	8.38	7.96	7.56	6.74
30	7.63	7.25	6.86	6.13

Assessment criteria corrosion of the vehicles are:

- optical examination - naked eye examination, microscopic examination;
- quantitative criteria: gravimetric index, penetration index;
- depending on the amount of corrosion or penetration rate (estimated by the condition of standard), the extract is shown in Table 2.

Table 2. *General assessment of corrosion condition*

	Assessment groups	**Assessment scale**	**Corrosion rate for metals with ρ< 7500 kg ·m^{-3}**	**Penetration**
			[10^{-3}kg/m^2·day]	[mm/year]
I.	Perfect resistant	1	< 0.021	< 0.001
II.	Very resistant	2 3	0.021...0.10 0.10...0.21	0.001...0.005 0.005...0.01
III.	Resistant	4 5	0.21 ...1 1.....2.1	0.01...0.05 0.05...0.1
IV.	Average resistance*	6 7	2.1...10.5 10.5...21	0.1...0.5 0.5...1
V.	Not resistant	8 9	21...105 105...210	1...5 5...10

* The metal can be used on a case by case

3. Research on salt spray corrosion resistance of steel plates for shipbuilding

The chemical composition of steel plates for shipbuilding is given in Table 3.

The NVA steel sheet was degreased with a solvent and, after blasting, the sheet was blown with air in order to obtain a clean surface.

Table 3. *Chemical composition of steel shipping,* (%)

NVA									
Chemical composition	C	Mn	Si	P	S	Al	Ni	Cu	Cr
	0.105	0.76	0.25	0.014	0.012	0.035	0.015	0.018	0.028

Then the NVA steel sheet was coated with anticorrosive primer (EGA intergard-269), a second protective layer (interseld ENA-300) and the final layer of gloss (LAC interfin 979). The physical and chemical properties of protective varnishes are shown in Tables 4, 5, 6.

In the next stage the NVA steel sheet was subjected to the salt spray test.

Table 4. *Physical and chemical properties of INTERGARD RED 269*

State	**Liquid**
Color	Red
Ignition temperature (C º)	26
Auto - ignition temperature (Cº)	340
Viscosity	Unspecified
Density	1.29
Weight of solvent (%)	22.95
Vapor density	Heavier than air
PH	0.0
Lower explosion limit (% v / v de aer)	1.1
Solubility in water	Immiscible
Ventilation (air quantity required to reach the lower explosion limit)	87
Odour	Solvent odour

Table 5. *Physical and chemical properties of INTERSHIELD 300 BRONZE*

State	**Liquid**
Color	Dark
Ignition temperature (C º)	28
Auto - ignition temperature (Cº)	340
Viscosity	Unspecified
Density	1.138
Weight of solvent (%)	21.98
Vapor density	Heavier than air
PH	0.0
Lower explosion limit (% v / v de aer)	1.1
Solubility in water	Immiscible
Ventilation (air quantity required to reach the lower explosion limit)	62
Odour	Solvent odour

Table 6. *Physical and chemical properties of INTERFINE 979*

State	**Liquid**
Color	Dark
Ignition temperature (C º)	27
Auto - ignition temperature (Cº)	425
Viscosity	Unspecified
Density	1.19
Weight of solvent (%)	5.00
Vapor density	Heavier than air
PH	Unspecified
Lower explosion limit (% v / v de aer)	2.0
Solubility in water	Immiscible
Ventilation (air quantity required to reach the lower explosion limit)	12.91
Odour	Solvent odour

Accelerated corrosion test in salt spray

The test was conducted according to ISO 9227 in a corrosion chamber (Figure 3).

Fig. 3. *Salt spray chamber used for testing corrosion resistance.*

To carry out the test, sodium chloride solution was prepared by dissolving (conductivity less than or equal to 20 ± 2 μS/cm^2 at 25 ± 2°C) a quantity of sodium chloride in distilled water to obtain a concentration of 50 ± 5 g / L. The relative density of a solution of this concentration is between 1.00255 and 1.0400. The sodium chloride used contains less than 0.001% copper and 0.001% nickel. Also, the sodium iodide content must not exceed 0.1% and the total content of impurities must not be higher than 0.5%.

The pH of the saline solution was adjusted so that the pH of the spray solution collected in the chamber is between 6.5 and 7.2.

For this we used a pH meter HI-991001, produced by "Hanna Instruments", equipped with a temperature indicator. The saline solution supply device comprises a fresh air supply system, a reservoir containing the solution and an aerosol spray. The sprayer with compressed air supply was achieved through a filter which retains any trace of solid material or oil at a pressure of about 100 kPa. To prevent evaporation of water droplets was sprayed with air being moistened before entry into the sprayer, by passing it through a bowl of water. The spray is made of plastic (textolit), inert to corrosive environment. To prevent the direct impact of the solution sprayed samples, they were placed in the direction of the salt spray flow.

The corrosion test was conducted over 168 hours at 35°C. Initially, the samples were degreased with acetone and then weighed on a 0.01 mg precision analytical balance: on the first day, then, after three days, daily until the seventh day. The weighed samples were not placed in closed corrosion, to avoid errors due to removal of corrosion products.

Table 7. *Corrosion speed control and coated samples*

Samples	**Corrosion rate (g/m^2 day) at:**				
	3 days	4 days	5 days	6 days	7 days
Witness samples	3.85	3.02	2.17	1.86	1.79
Covered samples	0.067	0.060	0.054	0.050	0.042

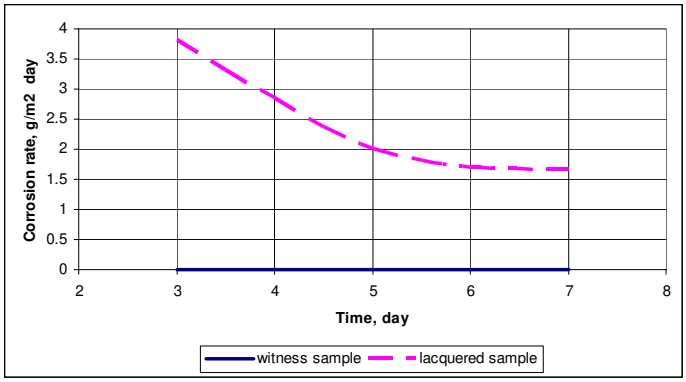

Fig. 4. *Variation of corrosion rate of steel sample.*

At the end of the test, the samples were removed from the room and were allowed to dry for 30 minutes.

To determine mass loss, corrosion products were removed by pickling resulting in 50% hydrochloric acid solution (volumetric concentration); the inhibitor was added to 3.5 g/L hexamethylenetetramine.

After the attack, the samples were well washed, at room temperature, first with water then with acetone until they were dry. Then the samples were weighed again and the mass loss and the corrosion rate were calculated using the relationship:

$$V_C = \frac{\Delta G}{S \cdot t}$$

where: V_C = corrosion rate [g/m^2 day]; ΔG = difference between initial and final sample weight [g]; S = sample area [m^2]; t = time [days].

The results are given in Table 7. The variation of the corrosion rate in time is shown in Figure 4. As shown in the graph, the corrosion resistance of samples coated with varnish is greater than that of the uncoated ones.

The general state of the corrosion rate and of the penetration index values is given in Table 8.

Table 8. *General state of corrosion rate and penetration index values*

Sample code	Time	Weight difference	Penetration index	Group of resistance	Note of appreciation
	[day]	[g]	[mm/year]		
Witness sample	3	0.0017	0.431	medium resistant	6
	4	0.0018	0.336	medium resistant	6
	5	0.0021	0.241	medium resistant	6
	6	0.0029	0.207	medium resistant	6
	7	0.0033	0.199	medium resistant	6
Lacquer coated sample	3	0.0004	0.08	resistant	5
	4	0.0008	0.18	resistant	5
	5	0.0010	0.22	resistant	5
	6	0.0013	0.29	resistant	5
	7	0.0014	0.37	resistant	5

As shown in Table 8, the penetration index values are much smaller for witness samples than for lacquer coated samples. It also notes that have uncovered evidence of assessment notice and samples coated with varnish resists corrosion better note with appreciation 5.

Macro structural analysis

Macro structural analysis of the samples before and after corrosion is shown in Figures 5-10.

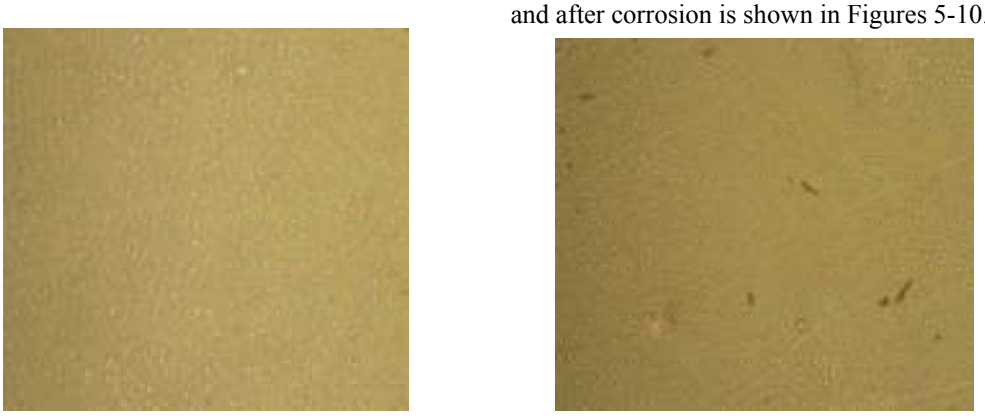

a) *b)*

Fig. 5. *Macrostructure surface: optical aspect of coated samples before corrosion: a) x 200; b) x 400.*

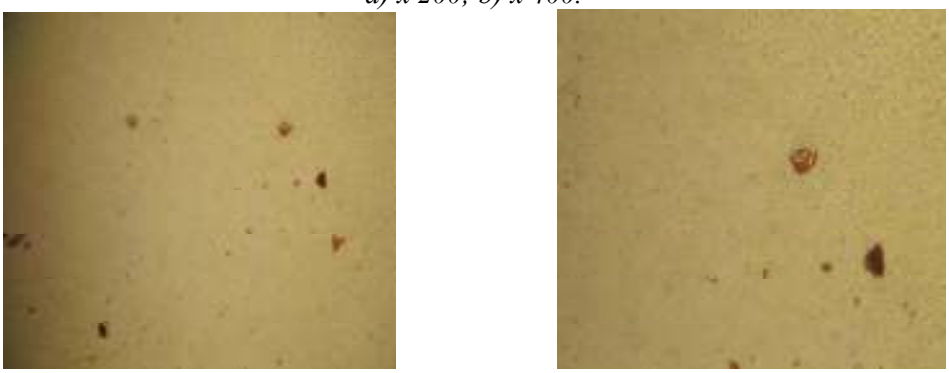

a) *b)*

Fig. 6. *Macrostructure surface: optical aspect of coated samples after 3-day keeping in salt spray: a) x 200; b) x 400.*

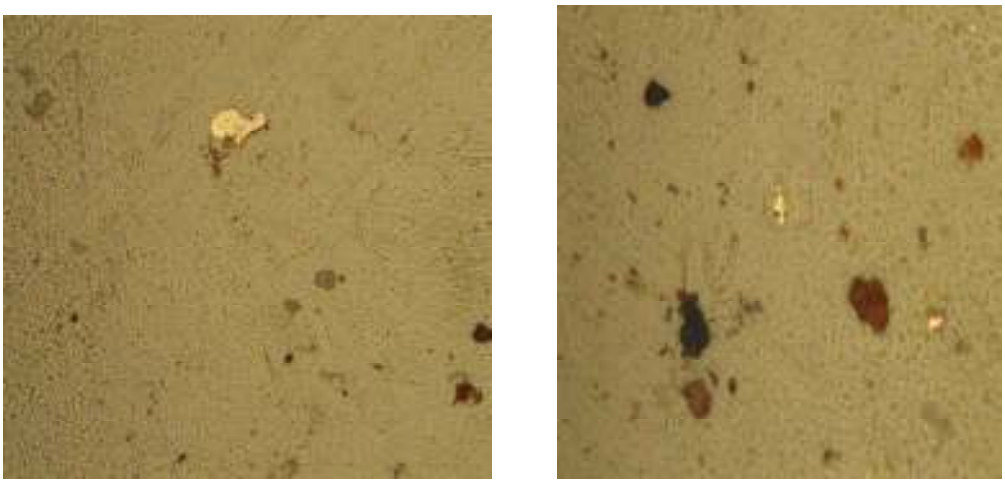

a) *b)*

Fig. 7. *Macrostructure surface: optical aspect of coated samples after 4-day keeping in salt spray: a) x 200; b) x 400.*

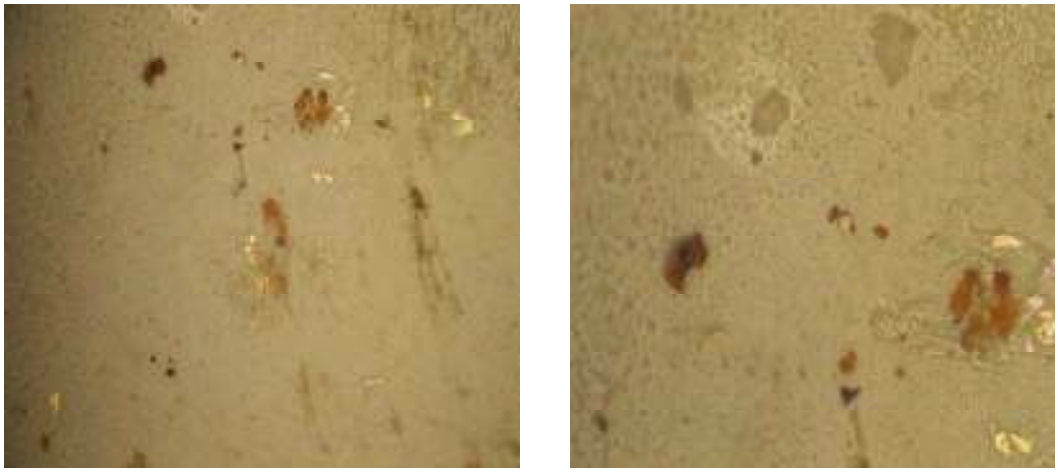

a) *b)*

Fig. 8. *Macrostructure surface: optical aspect of coated samples after 5-day keeping in salt spray: a) x 200; b) x 400.*

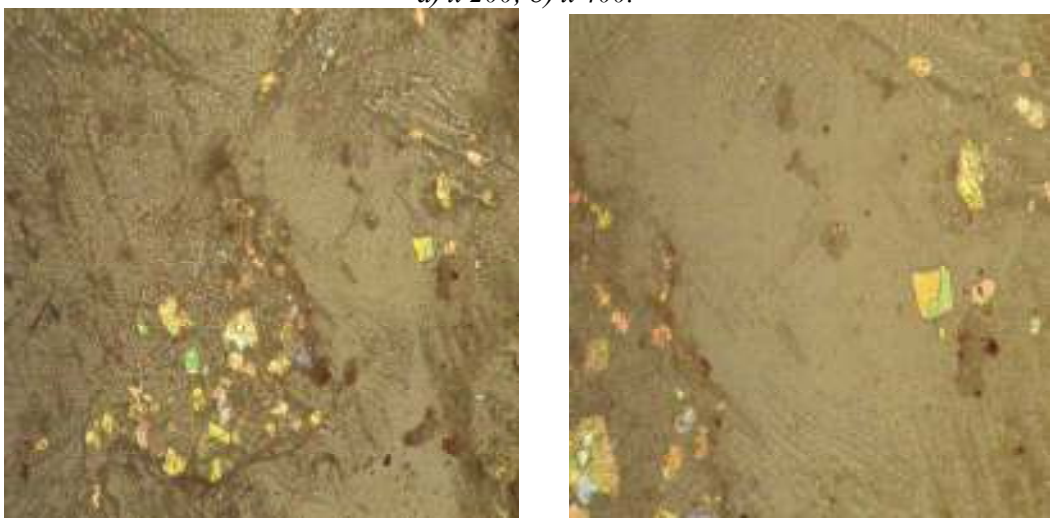

Fig. 9. *Macrostructure surface: optical aspect of coated samples after 6-day keeping in salt spray: a) x 200; b) x 400.*

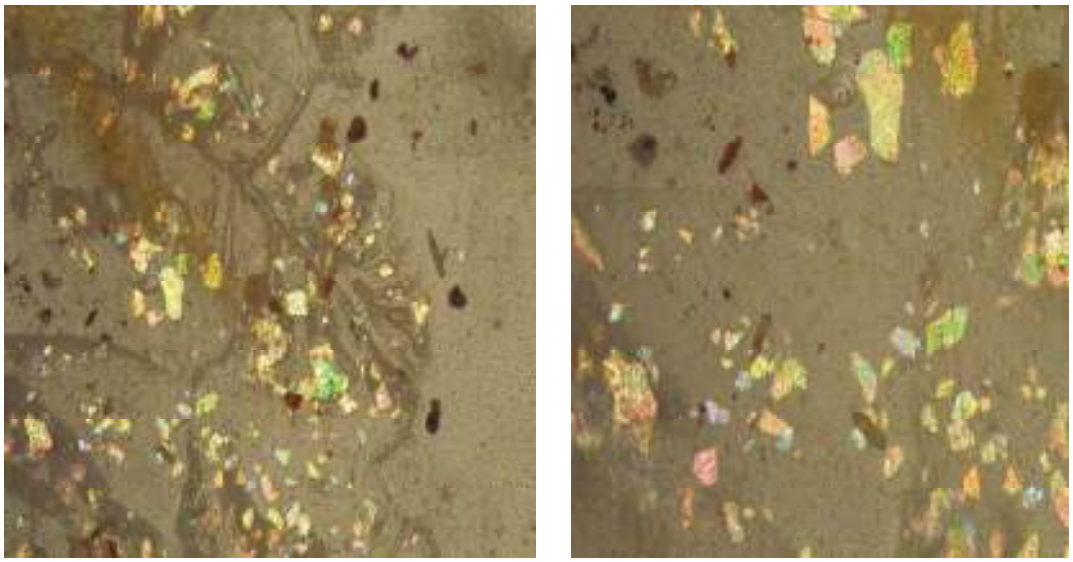

Fig. 10. *Macrostructure surface: optical aspect of coated samples after 7-day keeping in salt spray: a) x 200; b) x 400.*

As shown in Figure 5, after three days, slight traces of corrosion appeared on Interfine 979 and Intershield 300, whereas Intergard 269 was not challenged. In Figures 6 and 7, after four and five days, respectively, we see spots of corrosion, Interfine 979 and Intershield 300 being attacked again while lake Intergard 269 resisted corrosion. After six days (Figure 8), all three coats were corroded, and on the seventh day, corrosion came up at the base, Fig. 9.

4. Conclusions

- The corrosion rate of the varnish coated samples is lower than that of the uncoated samples.
- The penetration index values are much smaller for witness samples than for lacquer coated samples.
- Samples were coated average corrosion resistance, notice of assessment in June and samples are coated with varnish resistant, notice of assessment in May.
- After three days, there were slight traces of corrosion, lakes Intersheild 300 and Interfine 979 having been attacked, while Intergard 269 was not challenged. After four and five days, respectively, spots of corrosion could be observed on Interfine 979 and Intersheild 300, while Intergard 269 resisted corrosion. After six days, all three coats were corroded and on the seventh, it came up at the base.

References

[1]. M.Constantinescu, T. Badea - *Coroziune şi protecţie anticorosivă,* Ed. Didactică şi Pedagogică, Bucureşti, 1987
[2]. L. Oniciu, E.Constantinescu - *Electrochimie şi coroziune,* Ed. Didactică şi Pedagogică, Bucureşti, 1987
[3]. A.J. Bard, Faulkner - Electrochemical Methods*:* Fundamentals and Applications*,* New York, 1980
[4]. Electrochemical Techniques for Corrosion*,* edited by R. Baboian, National Association for Corrosion Engineers, Houston, Texas, 1977, 1-10
[5]. A. Marinescu, Gh. Andronianţ, E. Bay - *Tehnologii electrochimice şi chimice de protecţie a materialelor metalice*, Editura Academiei, Bucureşti 1972
[6]. T. Bradea, M.V.Popa, M.Nicola - *Stiinta si ingineria coroziunii*, Ed. Academiei Romane, Bucuresti, 2004
[7]. Dragomir, I. - *Teoria proceselor siderurgice* - Editura Didactică şi Pedagogică, Bucureşti, 1985.
[8]. Constantin, N. - *Procedee neconvenţionale de obţinere a materialelor feroase*, Editura Printech, Bucureşti, 2002.

THE ANNALS OF "DUNAREA DE JOS" UNIVERSITY OF GALATI.
FASCICLE IX. METALLURGY AND MATERIALS SCIENCE
N^0. 2 – 2011, ISSN 1453 – 083X

THE INFLUENCE OF BOTH FUNCTIONING TIME AND THE SERVICE TEMPERATURE ON THE MECHANIC CHARACTERISTICS AND METALLOGRAPHIC STRUCTURE OF SOME STEELS

D. MIHAI[1], S. MACUTA[2]
[1]"Gh. Asachi" Technical University, Faculty of Mechanical Engineering,
Strength of Materials Department, Iasi
[2]"Dunarea de Jos" University of Galati, Faculty of Mechanical Engineering
email: Silviu.Macuta@ugal.ro

ABSTRACT

The paper determines the influence of both functioning time and the service temperature on mechanic characteristics of 12H1MF steel. In this purpose, the results of mechanical tests, performed at temperatures ranging from 510 to 590^{0}C, have been correlated with those of the optical microscopy analysis.

Due to the prolonged exposure to high temperatures, a slight degradation of the mechanical behaviour has been noticed that has been ascribed to the structural changes produced during functioning. The microstructural study of the steel has emphasized that after prolonged functioning several irreversible changes have occurred such as the increase of the ferrite grains, the dispersion of pearlite areas as well as the precipitation and coalescence of carbides. Yet, since neither decarburation nor network formation tendencies for the precipitated carbides have been observed, it has been concluded the 12H1MF steel can be kept in service even after more than 71000 functioning hours in live steam, at temperatures of 570^{0}C and pressures of 155 atmospheres.

KEYWORDS: low alloy steel, metallurgical degradation, irreversible structural phenomena

1. Introduction

It is well known that, with increasing the temperature and the functioning time at elevated temperatures, structural changes occur within the metallic materials that alter their mechanic and elastic characteristics [1]. The present paper aims to derive the influence of both the functioning time and the service temperature on the mechanic and elastic characteristics of 12H1MF steel. In this purpose, the structural changes will be analyzed in the above steel when used in the steam pipes of the kettles from thermal power stations. In addition, the functioning time of the piping will be predicted under safe service conditions.

2. Experimental part

The specimens were taken from longitudinal and transversal sections of 12H1MF steel pipes that initially had the following dimensions: 865-mm length, 273-mm diameter and 36 mm wall thickness. The service temperature and pressure of the piping from which samples have been taken were: T = 540^{0}C and p = 155 atmospheres, respectively. The specimens have been analyzed after three different functioning periods: 0 functioning hours, 29867 functioning hours and 71409 functioning hours. The experiments consisted in mechanical tests and metallographic analyses.

The mechanical tests comprised tensile tests, dynamic shock tests and Brinell hardness tests.

Tensile tests were performed on a VEB 500KN tensile testing machine, at the following temperatures: 20^{0}C, 510^{0}C, 540^{0}C, 560^{0}C, 565^{0}C, 570^{0}C, 580^{0}C. The main tensile mechanical characteristics are: the yield stress ($R_{p0.2}$) and ultimate stress (R_m)

Dynamic shock tests were performed on MK30 Amsler pendulum, in order to determine the toughness designated by KCU30/2/10, at the following test temperatures: 20^{0}C, 510^{0}C, 540^{0}C, 560^{0}C, 565^{0}C, 570^{0}C, 580^{0}C.

These tests allowed observing the macroscopic structural aspect of the material.

The results are merely qualitative since they did not reveal any quantitative information related to the purpose of the paper.

Brinell hardness, designated by HB 300/10/15, has been determined at the same test temperatures as above, by means of a universal hardness tester type AB-1.

All the three testing apparatus were equipped with heating chamber able to automatically adjust the temperature.

3. Results and discussion

The experimental results of the mechanical tests are listed in Tables 1, 2 and 3 that contain the values of ultimate stress (R_m), yield stress ($R_{p0.2}$) and Brinell hardness (HB), respectively [2]. In the tables the symbols specify whether the values are taken from standards (S) or are experimentally determined (E) and whether the specimens were taken from longitudinal (L) or transversal (T) sections.

Table 1. *The standard and experimental values of the ultimate stress*

Functioning hours	Source of data	Position	R_m [MPa] Test temperature [ºC] 20	510	540	560	565	570	580
	S	T	min 450	190 at 500ºC	110 at 550ºC				85 at 575ºC
		L	min 450						
0	E	T	594	403.6	357.9	347.5	350.8	335.4	321.1
		L	600.1	387.9	365.4	355.8	341.4	338.9	325
29867	E	T	501.3	285.6	275.8	254.6	248.9	230.6	225.1
		L	515.6	301.2	295.6	275.8	265.6	245.9	215.8
71409	E	T	465.9	255.6	245.8	238.9	225.6	215.6	201.9
		L	470.2	260.2	258.9	239.2	235.6	231.2	226.4

Table 2. *The standard and experimental values of the yield stress*

Functioning hours	Source of data	Position	$R_{p0.2}$ [MPa] Test temperature (ºC) 20	510	540	560	565	570	580
	S	T	min 250	110				65 at 575ºC	
		L	min 260						
0	E	T	380.6	323.6	312.2	312.8	299.9	284.5	273.2
		L	399.4	316	313.6	309.7	303.3	295.7	268.4
29867	E	T	345.8	248.5	235.2	225.8	216.9	195.3	187.2
		L	355.6	250.6	240.6	238.3	225.6	224.8	206.9
71409	E	T	301.4	175.6	165.3	161.2	159.6	143.4	131.2
		L	315.8	180.1	170.2	169.3	161.5	148.9	135.6

Table 3. *The experimental values of the Brinell hardness*

Functioning hours	Source of data	Position	HB [MPa] Test temperature (ºC) 20	510	540	560	565	570	580
0	E	T	1584	1462	1409	1405	1329	1318	1200
		L	1612	1514	1461	1385	1313	1301	1205
29867	E	T	1426	1170	1145	1101	995	896	805
		L	1461	1191	1160	1109	997	875	853
71409	E	T	1368	1045	1001	976	896	848	746
		L	1376	1099	1036	1021	946	935	902

The metallographic analysis revealed that 12H1MF steel has a ferrite-pearlite structure [3]. The ferrite grains have uniform sizes and pearlite is mostly located on the boundaries of ferrite grains. Along the wall thickness, no variations of the grain size have been noticed. Both in longitudinal and transversal

sections the grain size has been determined as N3-4 according to the standard GOST-10801-64. The decarburation process is not metallographically noticeable either in the interior or at the exterior of the wall thickness. On the micrographs recorded at the magnifications 500:1 and 1000:1 a slight precipitation of carbidic islets has been observed both inside the grains and along the grain boundaries. The carbides show a very reduced tendency to form a network. The results of the mechanical tests are summarized in Fig. 1, 2 and 3 that show the evolution of ultimate stress (R_m), yield stress ($R_{p0.2}$) and Brinell hardness (HB), respectively, with the test temperature and the functioning period. The curves have been plotted by the interpolation of the data found in the above three tables. Here again the symbols t and l designate transversal and longitudinal sections, respectively.

The study of the variations of the mechanical properties with temperature emphasizes a behaviour that agrees well with the general tendencies of high temperature low alloy steels.

As compared to the data found in standards it is obvious that the material has a large reserve regarding the ultimate stress R_m. For all the tests, the spreading of the partial values is very low for the same test conditions.

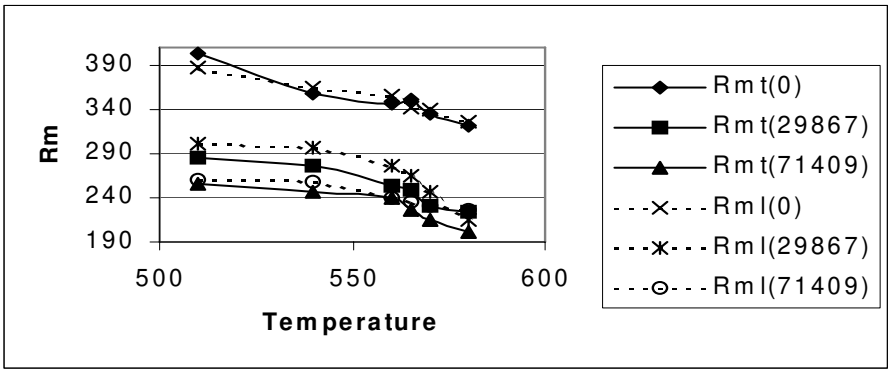

Fig.1. *Evolution tendency of the ultimate stress with test temperature and functioning period.*

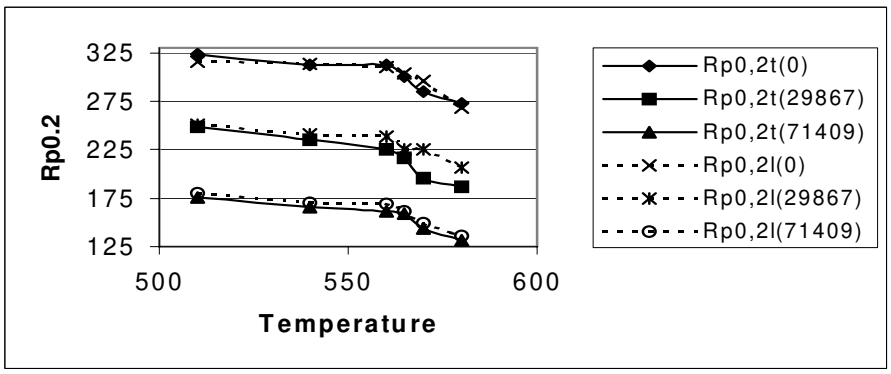

Fig.2. *Evolution tendency of the yield stress with test temperature and functioning period.*

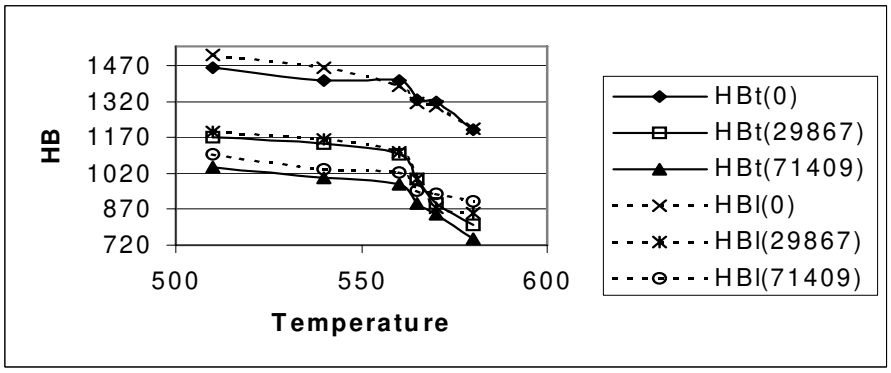

Fig.3. *Evolution tendency of the Brinell hardness with test temperature and functioning period.*

4. Conclusions

1. Based on the values determined for the mechanical characteristics in the case of the pipe under study, it may be concluded that the material is suitable for continuing the service and has marked resistance reserves. These reserves are explained by the absence of both the grain boundary decarburation process and the carbide network.

2. Based on the interpolated variation tendencies of the mechanical characteristics R_m, $R_{p0,2}$ and HB as a function of temperature, the functioning time under safe service conditions, of the piping from thermal power plants, can be predicted with high enough accuracy.

3. The structural changes that have been produced during functioning represent the cause for the alteration of mechanical characteristics. The microstructural study of the steel has emphasized that after prolonged functioning at high temperatures, metallurgical degradation has occurred comprising the increase of the ferrite grains, the dispersion of pearlite areas as well as the precipitation and coalescence of carbides.

References

[1]. Ailincai, G. and Mihai, D. – *Studies on the structural transformation stage of the steam piping materials of the kettles from thermal power stations* (in Romanian), Research contract no. 821-84. Beneficiary: CIPEET Bucuresti

[2]. Baciu.C. and Mihai, D. – *Studies on the structural transformation stage of the steam piping materials of the kettles from thermal power stations* (in Romanian), Research contract no. 49/2206-89. Beneficiary: ICEMENERG Bucuresti

[3]. *** Romanian standard STAS 2883/3-88 – Steels for high temperature pipes. Grades and technical quality conditions.

THE ANNALS OF "DUNAREA DE JOS" UNIVERSITY OF GALATI.
FASCICLE IX. METALLURGY AND MATERIALS SCIENCE
N^0. 2 – 2011, ISSN 1453 – 083X

STUDY OF THERMAL CONDUCTIVITY VARIATION DEPENDING OF THE HEAT TREATMENT FOR TOOL STEELS

Manuela Cristina PERJU, Carmen NEJNERU, Dragoş Cristian ACHIŢEI, Anca Elena LĂRGEANU, Roxana Gabriela STEFĂNICĂ
Technical University "Gheorghe Asachi" of Iaşi
email: cryss_ela@yahoo.com

ABSTRACT

This paper studied the influence of quenching and tempering steel structures on the thermal conductivity for OSC 11 steel. For the experiment we used samples that were subjected to heat treatment quenching and tempering at 200˚C and at 500˚C. To emphasize the structure and structural changes in both the sample and the untreated samples, micrographs and photos were made by scanning electron microscopy. Measured conductivity results were presented graphically and studied to highlight their influence on the hardening structure.

KEYWORDS: thermal conductivity, heat treatment, steel, structure

1. Introduction

Thermal energy if found in metallic materials with privileged propagation medium. Thus, metallic materials have the property to transport thermal energy. An energy flow appears from the warmer part to the colder one into a material out of its thermal equilibrium. Heat propagation phenomenon into the mass of a metallic material is thermal conductivity, [1]. Thermal conductivity influences mechanical functioning of parts, because running mechanical coupling heat-up and expand. Heating depends of friction coefficient of the mobile parts, of internal friction, of the type of the metallic materials lattice, of material homogeneity and the discontinuities present within the lattice, such as lamellar metallographic component, point, linear and volume defects, [4].

Metallic materials have the highest thermal conductivity. Thermal conductivity for steels depends of the type of alloying elements and their percentage. Carbon percentage has a special influence. The alloying elements and their percentage in steel creates defects in the crystalline lattice of the material, and, conclusively thermal barriers.

2. Experimental results

Tool steel was used for the experiment as well as some standard test specimens were subjected to heat treatments to modify their properties. They were tested for impact bending resistance. The structure was after fracture with scanning electron microscope. Thermal conductivity tests were made for the tool steel as annealed, cold-worked, after quenching and low tempering and graphics for comparative analysis of thermal conductivity were made, too.

2.1. The analysis of the tool steel

The tool steed used for the experiment is OSC 11, STAS 1700-98, a type of Fe-C-Mn-Cr-Si alloy, which corresponds to the equilibrium structures from thermal diagrams. According to these, the structure contains pearlite, cementite and complex carbides of manganese and chromium, [2, 3, 5].

OSC 11 steel is used for tools, such as: punch, dies, milling tools, drills, tools for wood processing, screwdrivers, files, scissors for sheet, block cutters, gauges, saws for metal. This material has the chemical composition presented in Table 1 and it was established as means of a mass spectrometer (Foundry Masters) tests.

Table 1. *Chemical composition, %*

Fe	C	Si	Mn	S	Cr	Cu
96.7	1.19	0.11	0.61	0.12	0.7	0.32

The specimens were subjected to martensitic quenching. Technological parameters were as follows:

- heating temperature 820°C;
- holding period ¼ hours;
- oil cooling at 50°C.

Two kinds of tempering were achieved after martensitic quenching:

- low tempering – heating at 200°C, holding for 1 hour in the furnace and air cooling for obtaining a structure with reduced great hardness relatively;
- high tempering – heating at 550°C, holding for 1 hour in the furnace and air cooling for obtaining a structure with a good resilience.

2.2. Microstructure analysis

Microstructure analysis was achieved by means of VEGA II LSH scanning electron microscope and was realized in fracture, after impact bending test. The resilience test was made on Charpy impact machine, [7].

2.2.1. Microstructure analysis of the untreated specimen

The untreated sample (in phase of equilibrium state) has a pearlite and cementite structure. Studying the micrography notices a fragile fracture with edgy well-defined grains. The small area of plastic deformation concentrates mainly on the edges of the grains. Figure 1 presents cleavage areas and sharp areas that characterize an intercrystalline fracture with crystallographic plans prominence. The EDX analysis of fracture surface, scale 50 µm, was measured at a concentration of 96.82% Fe, 1.008% C, 1.2% Cr and 0.96% Mn. The breakage area has a grainy, bright and shiny crystalline aspect.

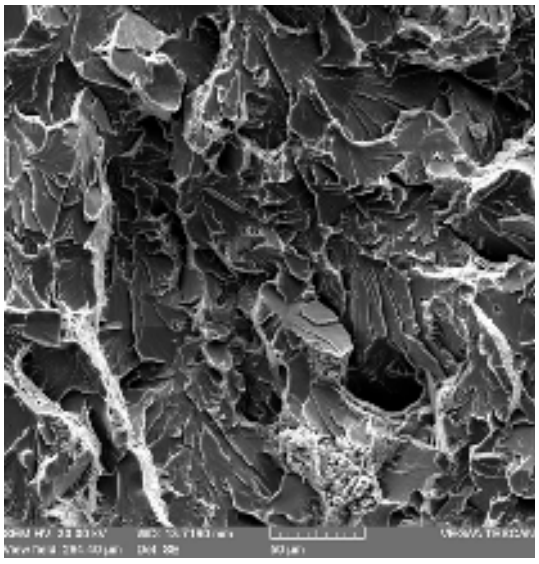

Fig. 1. *Fractography of the untreated sample, after breakage, order of magnitude 2500 x*

Table 2 presents the chemical composition of the studied area.

Table 2. *Chemical composition on the distribution area of the elements*

Bruker AXS Microanalysis GmbH. Germany. 22/04/2010		
Element	[norm. wt.%]	[norm. at.%]
Iron	95.15078	88.39028
Carbon	2.059743	8.896639
Chromium	1.477005	1.473683
Manganese	1.312477	1.239398

2.2.2. Microstructure analysis of the heat-treated sample martensitic quenching and tempering at 200˚C

The sample has a structure like tempering martensite and bainite. The breakage area has a crystalline, grainy aspect with hard formations.

Analyzing the structure with scanning electron microscope, it is noticed a brittle structure with an intercrystalline fracture. Table 3 presents the chemical composition of the studied section, with quantitative values of the elements both in mass percentages and in atomic ones.

Table 3*. The chemical composition of the elements on the studied section*

Element	[norm. wt.%]	[norm. at.%]
Iron	96.8221	93.29203
Chromium	1.209581	1.2518
Carbon	1.007881	4.515438
Manganese	0.960439	0.940733

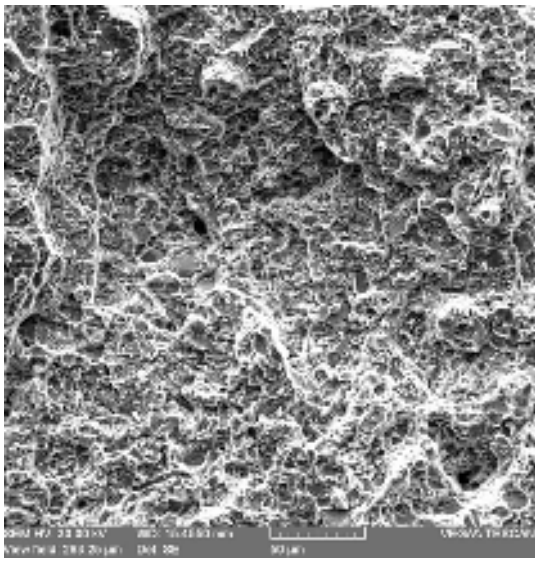

Fig. 2. *Fractography of the heat-treated sample by martensitic quenching and tempering at 200˚C, after breakage; order of magnitude 2500 x*

Hard microformations distinguish between the types of iron, chromium and manganese complex carbides.

2.2.2. Microstructure analysis of the heat-treated sample through martensitic quenching and tempering at 550˚C

The material has a sorbite structure corresponding to high tempering. Breakage structure is semi fragile and there are areas with lattice cementite. For disappearing of the lattice cementite, a special treatment must be done and it consists in heating hypereutectoid steels over A_{ccem}, followed by water or oil cooling (quenching). Then it will be done a heating over A_{c1} with 20-50°C, the sample is hold in the furnace and then air-cooled. The sample presents a partially tough structure, partially brittle with intercrystalline breakages so that the grains edges are evident (especially in the area with lattice cementite). Chromium carbides of hexagonal shape are well distinguished.

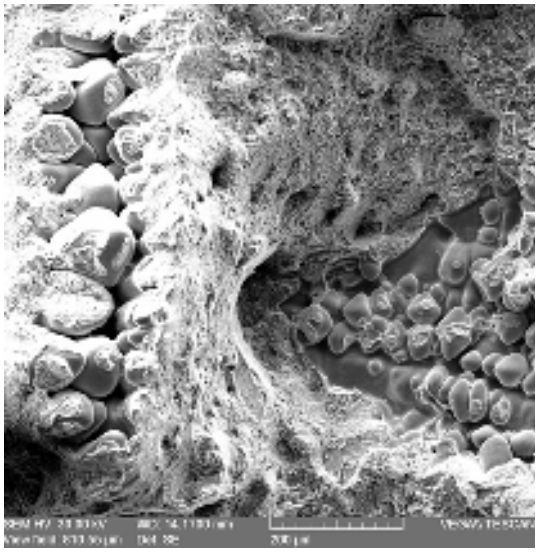

Fig. 3. *Fractography of the heat-treated sample through martensite quenching and tempering at 550˚C, after breakage, order of magnitude 300 x*

Table 4. *Chemical composition in point*

Element	[norm. wt.%]	[norm. at.%]
Iron	86.94674	73.80106
Chromium	5.418011	4.939456
Carbon	2.925038	11.54414
Manganese	2.019162	1.742238

At point analysis by means of EDX it can also be distinguished an area with complex carbides of Fe, Cr, Mn with percentages of 45.89% Mn, 28.83% Fe, 18.65% Cr and 6.64% C.

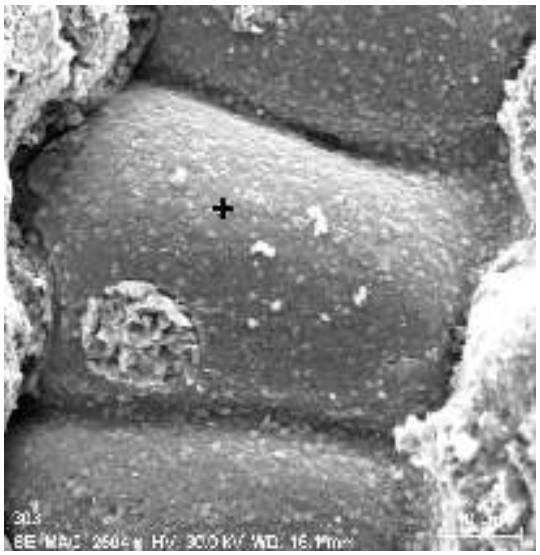

Fig. 4. *Point analysis, order of magnitude 2500 x*

2.3. Analysis of thermal conductivity

The analysis of thermal conductivity is realized by means of Mathis TCI apparatus, [6]. In order to determine thermal conductivity, a series of ten tests for an average of the final value will be done. By means of TCI system, thermal conductivity of the material is directly taken but diffusivity is achieved by applying the following relation

$$a = \frac{\lambda}{\rho \times C_p} \quad (1)$$

$$C_p = \frac{e^2}{\lambda \times \rho} \quad (2)$$

where λ = thermal conductivity, C_p = caloric capacity, ρ = density, a = thermal diffusivity , e = thermal inertia (effusivity).

Table 5. *Values obtained for OSC 11 steel*

Heat treatment	λ $[w/mk]$	**e** $\left[wS^{\frac{1}{2}}/m^2k\right]$	$\mathbf{C}_p$ $[J/kgk]$	$\mathbf{a}\times10^{-6}$ [m^2/S]
cold-worked	8.82	5381.3	421.6	2.69
annealed	11.6	6203.6	425.8	3.50
quenched and tempered 200°C	7.49	4969.1	423.2	2.27
quenched and tempered 550°C	8.18	5185.3	422.3	2.48

Thermal conductivity is influenced by quenching due to structural transformations that appear (transformation $A \rightarrow M$) being accompanied by the increase of defects quantity per unit volume. Thermal conductivity decreases if residual stresses and lattice defects appear which represent barriers and thermal blockages.

At low tempering (200°C) when the structure is made of tempering martensite and bainite, a part of the lattice stresses are loosening a part of the defects disappear and thermal conductivity has a slight decrease.

At high tempering (550°C) the structure of the material is sorbite and because of the transformations within, the structure, is more approached of equilibrium state so that, there are few lattice defects and, consequently, few thermal blockages and thermal conductivity is more increased than at low tempering.

From the graph of comparative analysis of the thermal conductivity, it notices that the biggest value is 11,615 [W/m K] and corresponds to phase equilibrium state of the material (annealed state).

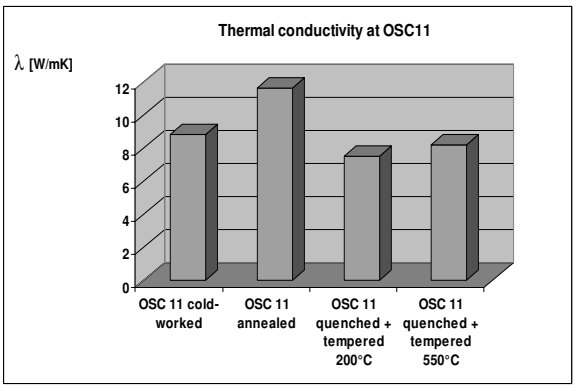

Fig. 5. *Variation graph of thermal conductivity at OSC 11*

In mechanical cold-worked state, thermal conductivity decreases because of increased the number of defects of the crystalline lattice per unit volume. These defects can be: point defects (vacancies, interstitial atoms etc), linear defects (supplementary reticular plans, dislocations) and volume defects (cylindrical defects).

The bigger number of defects corresponds at the more blockage situations of the dislocations and the number of thermal blockages and thermal barriers increases.

Conclusions

1. For OSC 11 steel, phase equilibrium state (annealed state) corresponds to a maximum value of conductivity, this is justified by the minimum number of defects and dislocations in the lattice per unit volume.

2. For the heat-treated OSC 11 steel, heat treatment, which consists in martensitic quenching, followed by low tempering, where the structural constituent is bainite, thermal conductivity has a lower value. This happens because of the phasic cold hardening, introduced after quenching is present after low tempering too.

3. For high tempering, where sorbite is the main constituent, the material approaches the equilibrium state of the material by achieving a decrease in the number of lattice defects per unit volume.

4. In case of mechanical cold hardening (resilience), it is noticed a decrease of thermal conductivity the increased number of dislocations and due to increased lattice defects. Lattice defects appear by the shifting of the reticular plans on atomic distances according to the theory of plastic deformation.

References

[1]. Bădărău Gheorghe - *Proprietăţile materialelor metalice*, Note de curs, 2007-2008.
[2]. Hopulele Ion, Alexandru Ion, Găluşcă Dan-Gelu - *Tratamente termice şi termochimice*, vol I, 1983.
[3]. Hopulele Ion, Alexandru Ion, Găluşcă Dan-Gelu - *Tratamente termice şi termochimice*, vol II, 1984.
[4]. Leinhard IV, J.H., Leinhard V, J.H. - *A Heat Transfer Textbook*, Editura Phlogiston Press, Cambridge.
[5]. Mitilea Ion, Budău Victor - *Studiul metalelor* - Editura Falca, Timişoara, 1987.
[6]. Ştefan Mihai, Vizureanu Petrică, Bejinariu Costică, Bădărău Gheorghe, Manole Vasile - *Studiul proprietăţilor termice ale materialelor*, Editura Tehnopress, Iaşi, 2008, ISBN 978-973-702-566-1.
[7]. Zaharia Luchian - *Teoria deformării plastice*, Editura „Gh.Asachi", Iaşi, 2001.

THE ANNALS OF "DUNAREA DE JOS" UNIVERSITY OF GALATI.
FASCICLE IX. METALLURGY AND MATERIALS SCIENCE
N^0. 2 – 2011, ISSN 1453 – 083X

THE INFLUENCE OF FRICTION FORCES IN METAL POWDERS COMPACTION PROCESS OF STAINLESS STEEL 316L

Monica SAS-BOCA, Luciana RUS, Marius TINTELECAN, Ionuţ MARIAN, Liviu NISTOR
Technical University of Cluj-Napoca
e-mail: Monica.Sas.Boca@ipm.utcluj.ro

ABSTRACT

The purpose of this study is to determine as precisely the influence of friction in the compaction of powders, and "conversion" of it, increasing densification.

The process is intended to be used in the compaction of hard deformable materials, which increased to approximately 90% densification required very high compaction pressures. These pressures are high, significant wear of the tools produce the compaction and thereby increasing production costs of finished parts from metal powders.

KEYWORDS: friction forces, "conversion", compaction, metal powder

1. Introduction

Technological processes that use pressure to achieve plastic deformation state are common element of friction forces. These forces can be active or resistive character depending on the context of their occurrence as: desirable or undesirable phenomenon in engineering.

Whatever the process of compaction, it involves a complex: factors, material and process variables. The ability to understand all the factors that influence individual particles are in a compact area of fundamental interest both for carrying out theoretical models and practical applications of these models. One of the factors specific to the compaction process is friction [2].

If for materials "full" (cast, forged, rolled), the force of friction depends on the type of contact (ie. a single type of contact throughout the deformation) and it causes one type of motion (sliding, rolling, the spin or the impact or combinations thereof), where powder densification of P/M can be no succession or simultaneously all types of motion caused by contact kinematics, during the process [3].

Types of friction in different stages of densification of powders are:

- Friction that occurs between two or more powder particles in contact between them, called static friction - friction contact (τ). It is given by the normal tension (σ_n) on the contact surface (Fig. 1) and coefficient of friction (μ).

- Friction that occurs when starting the pressing, the particles tumble while some others besides occupying vacancies - rolling friction (Fig. 1 b).

At this stage the powder particles are not deformed, the contact between them resumed at one point. As a result of the existence of gaps, because of its filling, the particles will move to these areas (least resistance) under the action of deformation tools.

Friction is in turn influenced by: the relative kinematics of contact, geometrical surface, the nature of the materials that form the coupling, the chemical composition of the body deformed and the deformation tool, the presence of impurities and a third coupling material, forming pressure (degree of deformation), deformation temperature, the relative speed of sliding contact surface.

Rolling friction is a complex phenomenon and is dependent on mechanical factors, physical and chemical. This type of friction can be classified:

- Rolling with high shear forces;

- Rolling with small tangential forces of friction is called "roll off".

- Friction that occurs at the start of deformation of particles, the elastic deformation - we call intermittent friction ("stick-slip") figure 1 c) [3, 4]. Particles have no where to move, can only rotate and deform (elastic deformation), thereby increasing the contact area between particles and between particles and walls tool.

- Friction that occurs between particles during the compaction effect, in which plastic deformation predominates.

At this stage the particles are in intimate contact (Fig. 1 d), so the entire surface of the particle is in contact with other particles or walls of the pressing tool. We call this type of friction sliding friction.

The same type of friction is found in contact with the walls of the powder forming tool at this stage of densification.

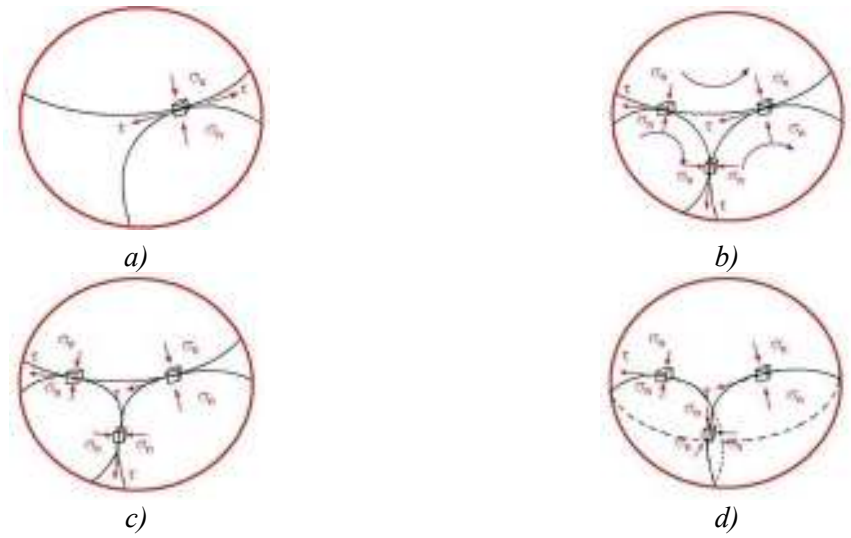

Fig. 1. *Powder compaction:*
a) powders are brought into contact by filling the die, b) early stage of deformation there is still pressing the powder particles, the particles stick to each other, spinning and tumbling vacancies
c) compaction beginning: the emergence elastic strain at the contact between particles,
d) effective compaction, material flow occurrence at the contact between particle and particle-surface tools.

- Ejection friction of green compacts process. This type of friction occurs between green compact and forming tools. In this phase may bring about a new compaction is the result of an improvement densification, or surface quality of green compacts. This friction is similar to the friction between blank and tools for solid materials.

The direction of this frictional force is the opposite movement of the material. Friction between particles of powders and between powder and tooling plays a major role during densification of PM parts. As a result there is a densification of green edges compacts.

2. Experimental procedure

Material. In this paper was used stainless steel powder 316L produced by gas atomization, with a particle size < 120 μm.

Cold compaction with assisted friction. Before compaction the powder was mixed with zinc stearate in a ratio of 0.5%.

Green compacts have been carried out on an tensile-compression test installation (Heckert) with maximum force of 200 kN, driven by a hydraulic cylinder located at the bottom.

The proposed process consists in moving the mold during the pressing, die movement in the same direction with a given speed (fig. 2). As a result, the frictional forces acting in the same direction as the punch achieving a better distribution of powder flow during compaction process.

Activation of friction [1, 5], plastic deformation processes, create a peripheral flow which causes the material in the central and peripheral axial-flow direction (deformation) (fig. 2,b)). Material from these two regions are moving simultaneously in the mold resulting in reduction of strains and increase their uniformity, strain, working speed and the degree of deformation. Thus, this procedure creates additional opportunities to reduce deformation due to flow uniformity and standardization of their right under certain conditions.

Sintering. Green compacts were sintered in a vacuum furnace room is equipped with an electric heater and temperature control, so they were maintained in vacuum (10-4 bar) at a temperature of 1200 °C for 60 minutes.

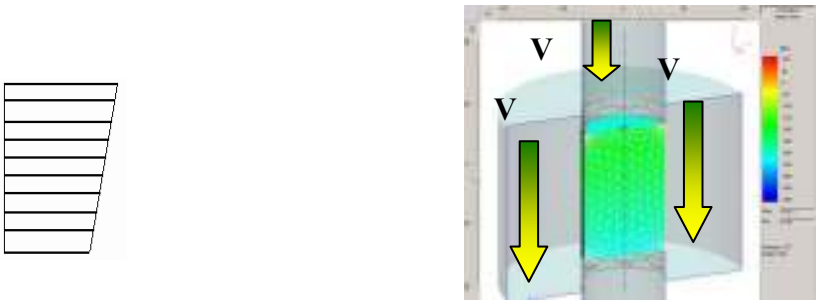

a) b)

Fig. 2. *Friction assisted compaction of 316L stainless steel powder*
a) density distribution, b) compaction process $V_m > V_p$

3. Results and discussion

Cylindrical green compacts were made of 6.5 grams and 10.5 grams with classical friction assisted compaction at a pressure of 600 MPa and 700 MPa. The inner diameter of the die is 11.12 mm, compacts obtained with varying heights depending on the weight, pressure and compaction process.

Table 1. *Densities obtained in the process of compaction*

No	Compaction process	Pressure [MPa]	Weight [gr]	Green density [gr/cm^3]	Density [gr/cm^3]
1	with assisted friction	600	10.5	6.29	6.49
2		700		6.50	6.67
3	classical	600		6.60	6.76
4		700		6.76	6.92
5	with assisted friction	600	6.5	6.45	6.61
6		700		6.60	6.69
7	classical	600		6.60	6.79
8		700		6.76	6.97

Densities were obtained after sintering fig. 3 between 82% and 89%, in line with the literature [4] (to 1240°C value obtained is 90% of theoretical density), taking into account the conditions of sintering.

Density gradient was determined by removing the turning of 1 millimeter of material in radial section. Height density distribution reported in parts was determined by Archimedes method. Comparison of density gradient was performed for both processes at different compaction pressures (600 MPa and 700 MPa).

As can be seen, in fig. 3 a) and c) we obtained a uniform density distribution for samples of 10.5 grams with assisted compaction achieved by friction, but with lower values 1% ÷3% for samples compacted classic. The results obtained on samples of 6.5 grams comply with the trend to uniform density, which leads to the conclusion that the activation of friction produces densities with 1% ÷ 3% lower, but earn more by getting a better gradient. As a consequence, the fill height of the die is no longer conditioned to 3x height of compact. These results are applicable for parts with large lengths.

In what follows (fig. 4) presents microstructures in the process of sintering compacts in a vacuum. Metallographic samples were prepared as follows: longitudinal were polished with abrasive paper of 500-1200 grit, then polished with alumina and were etched with royal water (HCl 33%, 66% HNO_3).

It is noted that the material was sintered well. The resulting structure is similar to a molten metal, is observed grains (crystallites - white areas) with polygonal boundaries clearly outlined. The microstructures presented for both classical and assisted compaction processes are very similar. In both, approaches can be distinguished macles in specific grain austenitic steels and fine carbides (small black dots on grains), due to alloying elements, the basic blend of grain weight.

10.5 gr *6.5 gr*

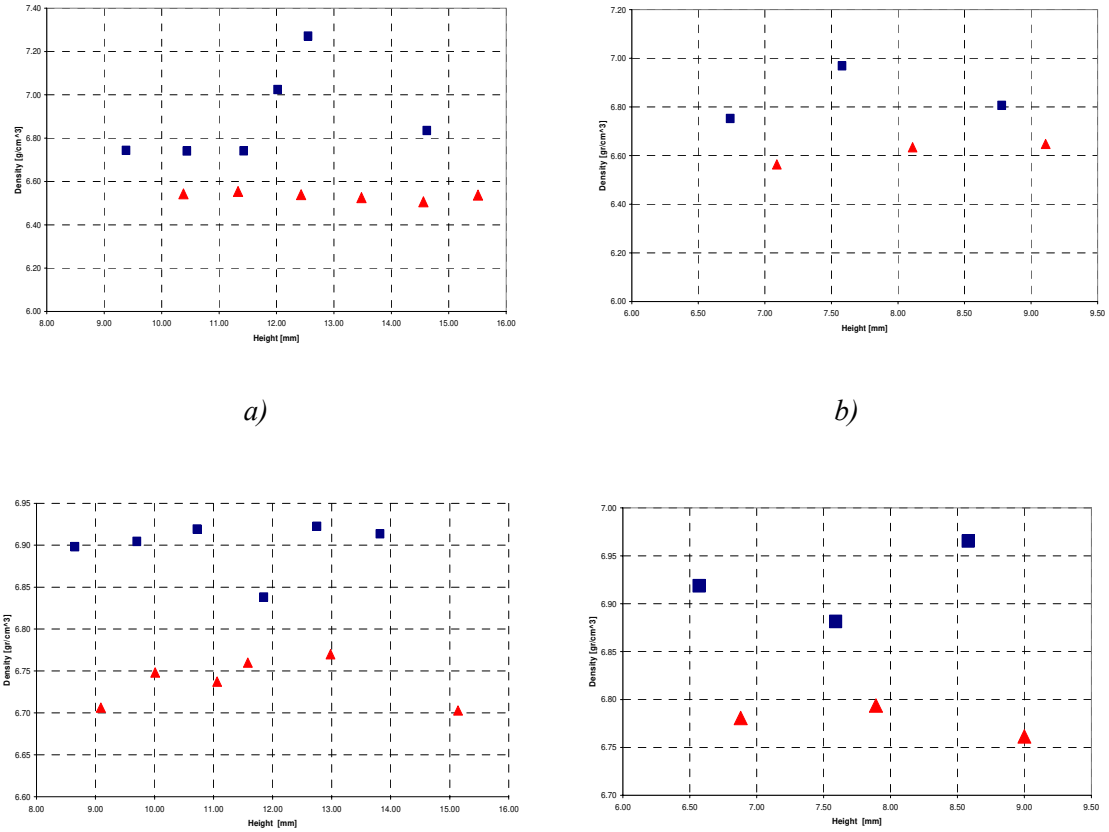

a) *b)*

c) *d)*

■ *classical compaction* ▲ *friction assisted compaction*

Fig. 3. *Density gradient of stainless steel powder, 316L*
a), b) pressure at 600 MPa; c), d) pressure at 700 MPa.

So, if compact 6.5 grams, fig. 4, 5 a), b) and for those of 10.5 grams, fig. 4, 5 c), d), we see a greater number of grains in the microstructures obtained at compaction with friction assisted fig. 4 b), d). This is due to the presence of friction assisted, given that the same conditions were observed in compaction.

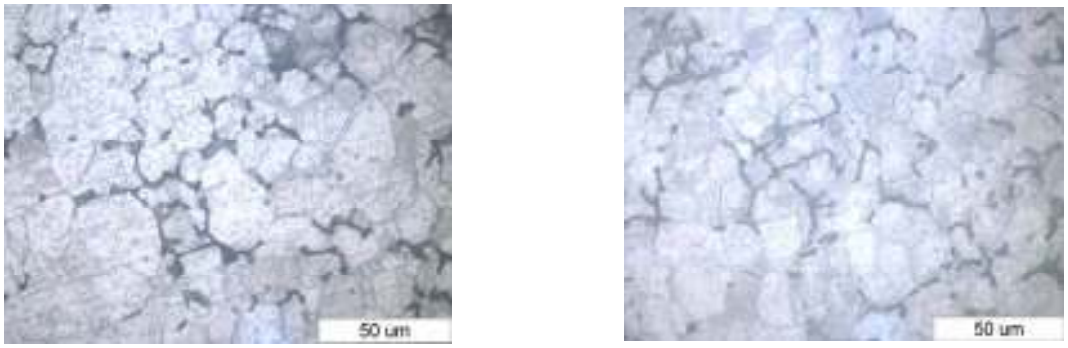

a) *b)*

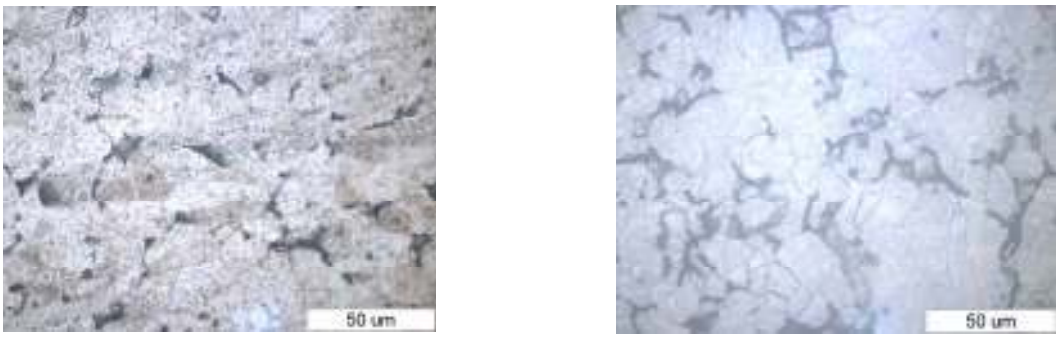

c) *d)*

Fig. 4. *Microstructures of 316L stainless steel samples compacted at pressure of 600 MPa: a) classical compaction of 6.5 g samples, b) with friction assisted compaction of 6.5 g samples, c) classic compaction samples of 10.5 g d) compaction with friction assisted samples 10.5 gr.*

It can be seen in the microstructure, the presence of an amount of pores (dark areas), this fact it is specific sintered structures. Porosity decreases according to the method of compaction, compaction pressure and sintering temperature.

The explanation for the existence of an increased amount of pores, or pore size may result from the dependence of compaction speed. A too rapid compaction (low height for samples) can be achieved without the grain to find the most advantageous positions of green compact volume.

The boundaries between grains are well defined and can be seen present carbides in the grain.

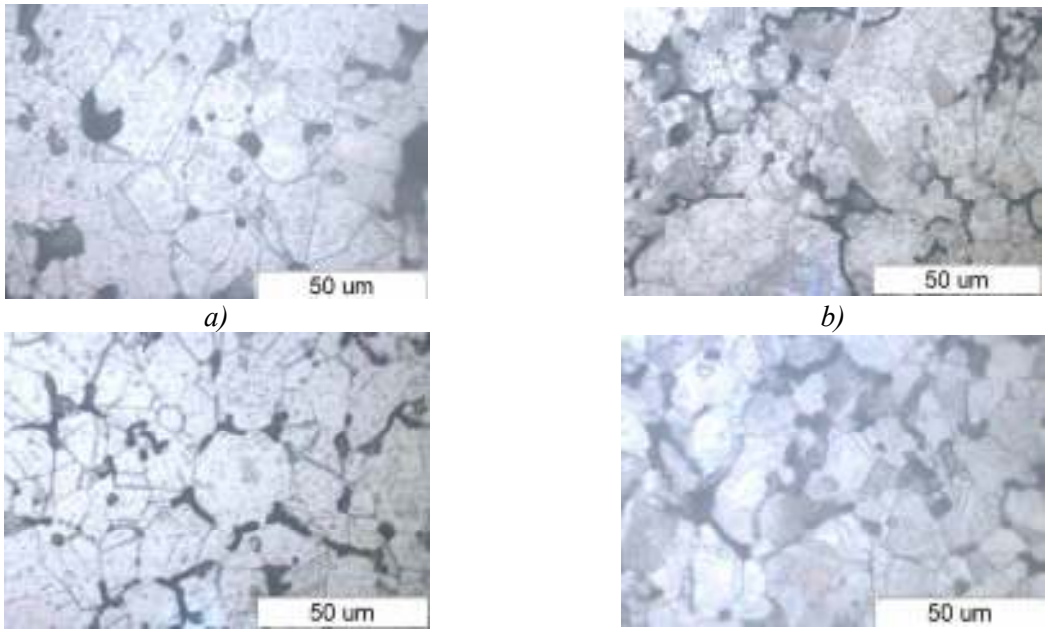

a) *b)*

c) *d)*

Fig. 5. *Microstructures of 316L stainless steel samples compacted at pressure of 700 MPa: a) classical compaction of 6.5 g samples, b) with friction assisted compaction of 6.5 g samples; c) classical compactness samples of 10.5 g d) compaction with friction assisted samples of 10.5 grams.*

Conclusions

It was comparatively studied in this paper, two methods of densification of powders, classic - bilaterally and with friction assisted. Differences between classical and assisted friction compaction is relatively low, due to the small size of samples. The compact with longer lengths could be more relevant results.

The main difference between the two processes is given by the influence of frictional forces between particles, powders and tools.

Advantages:

- uniform density distribution of the green compact height
- removal of the neutral zone
- low density in the case of the classical-bilateral compaction
- unconditional height filling of compact height
- activation of friction between the container and the powder effecting in the reduction of the pressing force applied to the die
- minimum implementation costs in industry, concerning only the movement of the mobile device for driving the mold
- long time suitability of friction assisted compaction for resistive deformable materials.

Disadvantages:

- compact density reduction by 1% ÷ 3%
- implementation costs of the appropriate process
- location of the training devices on the existing press.

References

[1]. V. Lazăr, L. Nistor, I. M. Sas-Boca *Optimizarea parametrilor de compactizare-sinterizare în procesarea pulberilor din oţel inoxidabil*, Metalurgia nr. 5-2008, pag 36-49.

[2]. Sh. Keshavarz, A.R. Khoei, A.R. Khaloo *Contact friction simulation in powder compaction process based on the penalty approach*, Materials and Design 29 (2008) 1199–1211.

[3]. A. Khoei *Computational Plasticity in Powder Forming Processes*, Great Britain, 2005.

[4]. N. Kurgan, R. Varol, *Mechanical properties of P/M 316L stainless steel materials*, Powder Technology 201 (2010) 242–247.

[5]. I.M Sas-Boca., T. Canta, D. Frunza *Pressing Powder with Friction Assisted Compaction for HS Tool Steels*, Proceedings of 3-rt Internatioan Conference on Powder Metallurgy, RoPM 2005, pag 640-648.

THE ANNALS OF "DUNAREA DE JOS" UNIVERSITY OF GALATI.
FASCICLE IX. METALLURGY AND MATERIALS SCIENCE
N^0. 4 – 2011, ISSN 1453 – 083X

A NEW CONFIGURATION FOR CAST BEARING SUPPORT FROM THE WORK ROLL AS PART OF A THICK SHEET ROLLING MILL

Stefan DRAGOMIR, Georgeta DRAGOMIR, Marian BORDEI
"Dunărea de Jos" University of Galaţi
email: Stefan.Dragomir@ugal.ro

ABSTRACT

In this work is made an optimization of configuration for casting bearing support of backup rolls, with Finite Element Method. This program is used for configuration of parts or subassemblies realized from cast iron. The deformation and displacement of bearing support are configured by using the "Finite Elements Method". In this study is shown too, an approval on the behavior of bearing support material (hardness, resistance and elongation).

KEYWORDS: backup roll, bearing support, thick sheet, shape, hydraulic installation

1. Introduction

The optimization of configuration for casting bearing support of backup rolls is made because the old configuration has some damage like: in the zone of corner and welded joint are produced – after a short functioning – some cracks because of the premature fatigue of material.

For the first time it is the bearing structure is checked and we take account of the tensions that deformed this part.

At the next stage, for obtaining the optimal configuration it is necessary to consider the force of lamination, other stresses, their direction, the masses which loaded the bearing and the type of bearing which was chosen.

In the FEM, (FINITE ELEMENT METHOD) the structural system –a back-up roll body-is modeled by a set of appropriate **finite elements** interconnected at points called nodes. Elements may have physical properties such as thickness, coefficient of thermal expansion, d, Young's modulus, shear modulus. Some common element types are listed below:

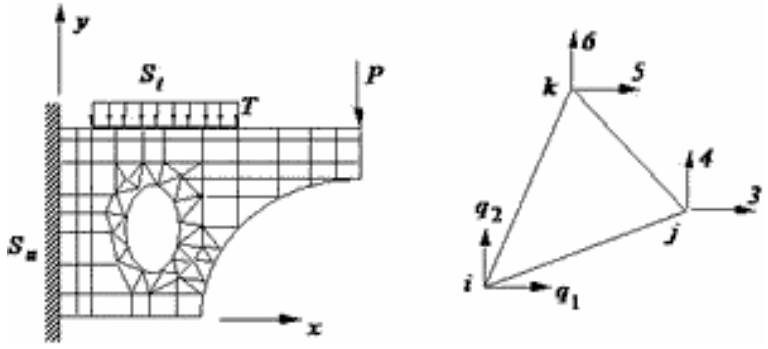

***Fig.1.** Mesh (shape with triangular and rectangular elements) for the upper of back up work roll.*

Straight or curved one-dimensional elements are endowed with physical properties such as axial, bending, and torsion stiffness'. This type of elements is suitable for modeling cables, braces, trusses, beams, stiffeners, grids and frames. Straight elements usually have two nodes, one at each end, while curved elements will need at least three nodes including the end-nodes. The elements are positioned at the central axis of the actual members.

Two-dimensional elements are used for membrane action (plane stress, plane strain) and/or bending action (plates and shells).

They may have a variety of shapes such as flat or curved triangles and quadrilaterals. Nodes are

usually placed at the element corners and, if needed for higher accuracy, additional nodes can be placed along the element edges or even inside the element.

Three-dimensional elements for modeling 3-D solids such as machine components, or solid masses are required to use different element shapes that can include tetrahedral and hexahedral forms.

Nodes are placed at the vertexes and possibly in the element faces or within the element.

The elements are interconnected only at the exterior nodes, and altogether they should cover the entire domain as accurately as possible.

Nodes will have nodal (vector) displacements or degrees of freedom which may include translations, rotations, and for special applications, higher order derivatives of displacements.

When the nodes displace, they will drag the elements along in a certain manner dictated by the element formulation.

In other words, displacements of any points in the element will be interpolated from the nodal displacements, and these are individual elements.

This is the crucial step where we will need displacement functions written only for the main reason to approximate the nature of the solution.

For obtain a good simulation, it is important to consider the next rules:

-symmetry or anti-symmetry conditions are exploited in order to reduce the size of the domain;

-displacement of finite elements, including any required discontinuity, is ensured at the nodes, and preferably, along the element edges as well, particularly when adjacent elements are of different types, material or thickness;

- compatibility of displacements of many nodes can usually be imposed via constraint relations.

When such a feature is not available in the software package, a physical model that imposes the constraints may be used instead;

-elements' behaviors capture as the dominant actions of the actual system, both locally and globally.

-the element mesh is sufficiently fine in order to have acceptable accuracy. To assess accuracy, the mesh is refined until the important results show little change. For higher accuracy, the elements should be as close to unity as possible and smaller elements are used over the parts of higher stress gradient;

-proper support constraints are imposed with special attention paid to nodes on symmetry axes.

While the theory of FEM can be presented in different perspectives or emphases, its development for structural analysis follows the more traditional approach via the virtual work principle or the minimum total potential energy principle.

The virtual work principle approach is more general as it is applicable to both linear and non-linear material behaviors.

The virtual internal work in the right-hand-side of the above equation may be found by summing the virtual work in the analyzed structure.

The principle of virtual displacement for structural system has the expression - equation (Hook) in the subsequent sections:

$$\sigma = E \cdot з \quad (1)$$

$$R=Kr + R^0 \quad (2)$$

where:

R - vector of nodal forces, representing external forces applied to the system's nodes.

r - vector of system's nodal displacements, which will, by interpolation, yield displacements at any point of the finite element mesh.

R^0 – is vector of equivalent nodal forces, representing all external effects other than the nodal forces which are already included in the preceding nodal force vector **R**.

These external effects may include distributed or concentrated surface forces, body forces, thermal effects, initial stresses and strains.

K= system stiffness matrix, which will be established by *assembling* the *elements' stiffness matrices*: K^e.

Once the supports' constraints are accounted for, the nodal displacements are found by solving the system of linear equations (2), symbolically:

$$R= k^{-1} (R – R^0) \quad (3)$$

Subsequently, the strains and stresses in individual elements may be found as follows:

$$з =B.q \quad (4)$$

$$\sigma = E \cdot (з - з^0) + \sigma^0 \quad (5)$$

where:

q-vector of element's nodal displacements--a subset of the system displacement vector **r** that pertains to the element under consideration.

B- strain-displacement matrix that transforms nodal displacements **q** to strains at any point in the element.

K- system stiffness matrix, which will be established by *assembling* the *elements' stiffness matrices*: K^e.

Once the supports' constraints are accounted for, the nodal displacements are found by solving the system of linear strains and stresses in individual elements may be found by using equation (4).

E- elasticity matrix that transforms effective strains to stresses at any point in the element and 3^0 is vector of initial strains in the element.

The strain-displacement matrix has the possibility to transforms nodal displacements **q** to strains at any point in the element.

σ^0= vector of initial stresses in the element.

We can apply the virtual work equation to the system and we can establish the element matrices **B** and K^e. The computer program can assembly the system matrices $\mathbf{R}^0$ and K. Other matrices Parameters such as ε^0, σ^o, **R** and **E** can be directly set up from data input.

2. Interpolation and shape functions

If we consider that q is the vector of nodal displacements of a typical element. The displacements at any point of the element may be found by interpolation functions such as:

$$U = \mathbf{N} \cdot q \quad (6a)$$

where:

u= vector of displacements at any point {x, y, z} of the element.

N= matrix of *shape function* serving as interpolation functions.

Equation (6) gives rise to other quantities of great interest:

Virtual displacements consistent with virtual nodal displacements:

$$\delta u = \mathbf{N}.\delta q \quad (6b)$$

Strains in the elements:

$$\varepsilon = \mathbf{D}.u \quad (7)$$

where: **D** is matrix of differential operators that convert displacements to strains using linear elasticity theory. Equation (7) shows that matrix **B** in (4) is:

$$\mathbf{B}=\mathbf{D}.\mathbf{N} \quad (8)$$

Virtual strains consistent with element's virtual nodal displacements:

$$\delta\varepsilon = \mathbf{B}.\delta q \quad (9)$$

The shape of the bearing support is shown in Figure 2.

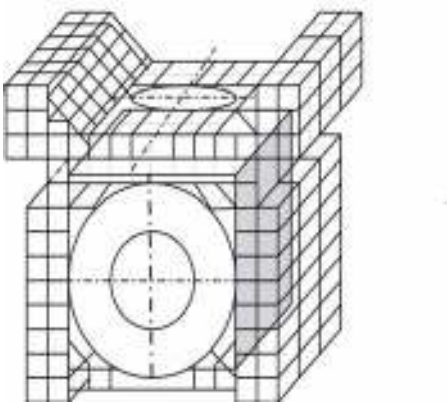

Fig.2. *The configuration of support bearing with finite elements.*

For determining the tensions which loaded the bearing support, the following stages must be included:

-the determination of the exterior and interior tensions applied on this part;

-the measurement of torques, forces and displacement;

-the configuration of the bearing support model and the Finite Elements Method should be applied on this shape;

-the calculus of torques, forces and displacement made by the program and the verification of this structure.

3. Experiments and results

In the experimental phases are recorded the maximum load of $54x10^3$ kN and the displacement of 0.002 mm.

Based on this registered measurement is made a computer simulation.

There were selected five representative models from 476 different experimental measurement and is made a modal analysis by using the IDEAS-Program. The regression-active model is shown in Fig. 3.

The IDEAS program establishes the types of finites elements, their number, arranges the mesh on the shape and shows in dark colour the most tensioned zones and in light colour the less tensioned zones.

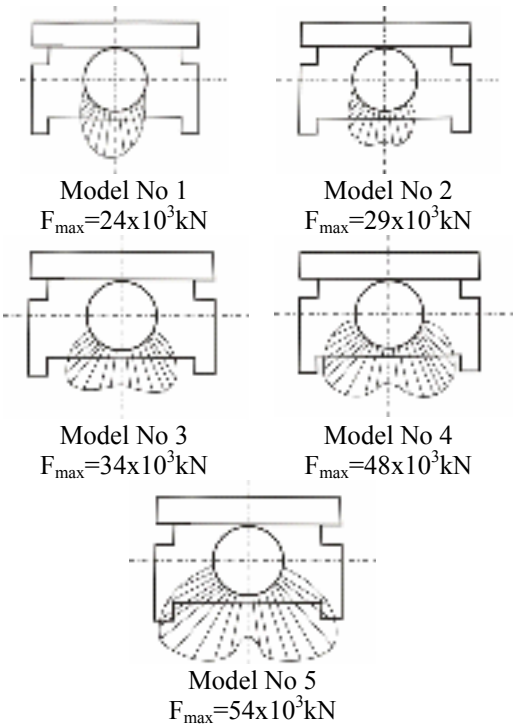

Fig.3. *The five most important loads on the bearing support.*

After the verification of the resistance of this part, it is chosen the optimal shape for the bearing support.

The ideal shape of the cast bearing support was chosen by following the line of model number 4 (Fig. 3) because it supports the maximum of tensions and deformations: $F_{max} = 48x10^3$ kN and the displacement 0.0187 mm.

3. Material

The material choice for the bearing support was nodular graphite irons Fgn700-2. This material supports (after the experiment) the maximum force of $48x10^3$kN and the less deformation in work.

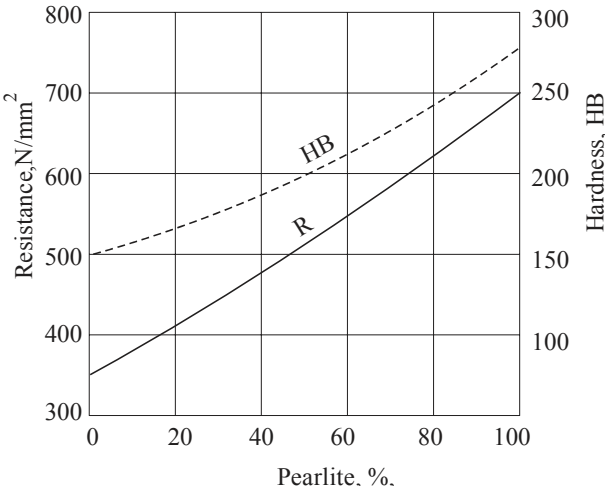

Fig.4. *The characteristics of hardness resistance and elongation for the material Fgn 700-2.*

The growing of pearlite inside the structure determines the increase of cast bearing resistance (R) and the hardness (HB) like in Figure 4.

By using this material is registered the low value for the deformation of the cast bearing support. The equipment used was crucible induction furnace. Like separation plans was chosen the middle of the bearing support and the cast is made in the middle of the bearing shape.

4. Conclusion and result

The modern proceeding for stress and tensions analysis is important for obtaining an optimal shape and a new material for the cast bearing support.

The support model takes account of the tensions, the torques and the dynamics coupling in the functioning time.

It is necessary to chosen the rationally cinematic scheme with a real number of masses and the gap between the bearing and its support.

This part is made from Fgn 700-2 and we chosen iron with nodular graphite because its support the greatest effort at the less deformation.

It must consider the less deformations because in functioning time, a great deformation of bearing support determines the variations of the thick sheet rolling.

References

[1]. Dragomir S. - *Utilaje, agregate, echipamente pentru fabricarea produselor carbonice,* Ed. Universitatii „Dunarea de Jos".

[2]. Dragomir St., Tudor B., *Research about the actionnary system at the continnous discharge heating furnace at ISPAT-SIDEX S.A.* Conferința Internațională de tribologie. Galați. ROTRIB'03, PAG.167, 2003,

[3]. Dragomir St., *Monitoring of iron sheet deformation in the rolling mill process by using CVC system, published at*: the-XII International Metallurgy Materials Congress, Istambul, Turkie, pag.843 – 847, 2005.

[4]. Cao, J.G., Qi, J.B., Zhang, J., et al. - *Backup roll contour for edge drop control technology in tandem cold rolling mill.* Journal of Central South University (Science and Technology), Vol.39, No. 5: 1011-1016, 2008.

[5]. Cao, J.G., Mao, N., Zhang, J., et al. - *Study on shifting mathematical model of edge drop control in tandem cold rolling mill.* Iron and Steel, Vol.43, No.8: 57-60, 2008

[6]. Campas, J.J., Terreaux, S., Roches, L.V D, et al. - *New on-line gage for edge drop measurement and effect of tapered work rolls.* Iron and Steel Engineer, Vol.72, No.12:27-32, 1995.

[7]. Wang, J.S., Zhao, Q.L., Jiao, Z.J., et al. - *The research on the principle and application for T-WRS&C cold mill*. Heavy Machinery, No.6:8-11, 2001.

MANUSCRISELE, CĂRŢILE ŞI REVISTELE PENTRU SCHIMB, PRECUM ŞI ORICE CORESPONDENŢE SE VOR TRIMITE PE ADRESA:

MANUSCRIPTS, REVIEWS AND BOOKS FOR EXCHANGE COOPERATION, AS WELL AS ANY CORRESPONDANCE WILL BE MAILED TO:

LES MANUSCRIPTS, LES REVUES ET LES LIVRES POUR L'ECHANGE, TOUT AUSSI QUE LA CORRESPONDANCE SERONT ENVOYES A L'ADRESSE:

MANUSCKRIPTEN, ZIETSCHRITFTEN UND BUCHER FUR AUSTAUCH SOWIE DIE KORRESPONDENZ SID AN FOLGENDE ANSCHRIFT ZU SEDEN:

After the latest evaluation of the journals achieved by National Center for the Science and Scientometry Politics (**CENAPOSS**), as recognition of its quality and impact at national level, the journal is included in B^+ category, 215 code (http://www.cncsis.ro/2006_evaluare_rev.php).

The journal is indexed in Cambridge Scientific Abstract

http://www.cncsis.ro/userfiles/file/CENAPOSS/B+feb_2011(9).pdf

The papers published in this journal can be visualized on the "Dunarea de Jos" University of Galati site, the Faculty of Metallurgy, Material Science and Environment, page: www.fmsm.ugal.ro.

Publisher's Name and Address:
Contact person: Prof. Dr. Eng. Elena MEREUTA
Galati University Press - GUP
47 Domneasca St., 800008 - Galati, Romania
Phone:+40 336 130103, Fax: +40 236 461353
Email: elena.mereuta@ugal.ro

Editor's Name and Address:
Prof. Dr. Eng. Marian BORDEI
Dunarea de Jos University of Galati, Faculty of Metallurgy, Materials Science and Environment
111 Domneasca St., 800201 - Galati, Romania
Phone: +40 336 130223, Phone/Fax: +40 236 460750
Email: mbordei@ugal.ro

AFFILIATED WITH:

- *ROMANIAN SOCIETY FOR METALLURGY*
- *ROMANIAN SOCIETY FOR CHEMISTRY*
- *ROMANIAN SOCIETY FOR BIOMATERIALS*
- *ROMANIAN TECHNICAL FOUNDRY SOCIETY*
- *THE MATERIALS INFORMATION SOCIETY (ASM INTERNATIONAL)*

Annual subscription (4 issues per year)

Edited under the care of
Faculty of
METALLURGY, MATERIALS SCIENCE AND ENVIRONMENT

Edited date: 30.06.2011
Issues number: 200
Printed by
Galati University Press
accredited CNCSIS
47 Domnească Street, 800036
Galati, Romania